An Investigation into the Reliability of Thermosonics for Aero Engine Turbine Blade Inspection

Gabriel Nnamdi Bolu

Submitted in May 2013

for the degree of Doctor of Engineering

Centre for Ultrasonic Engineering

Department of Electronic and Electrical Engineering

University of Strathclyde

204 George Street, Glasgow,

G1 1XW, Scotland, UK

Copyright

Abstract

Turbine blades in gas turbine engines are liable to fatigue cracking due to the harsh conditions in which they operate. The current non-destructive testing (NDT) method for inspecting these blades for cracks is Fluorescent Penetrant Inspection (FPI). However, extensive chemical cleaning of the blades is required for FPI to be effective. This pre-inspection cleaning process is expensive and time-consuming. A reliable and rapid NDT screening method that could detect cracked blades prior to cleaning would reduce the number of blades going through the mandatory cleaning and FPI inspection, thus saving cleaning and inspection costs.

Thermosonics has been proposed as a suitable candidate for this NDT screening. In thermosonics, an ultrasonic horn is used to vibrate a component, and if a crack is present, the vibrating crack generates heat which is detected by an observing infra-red (IR) camera. Although thermosonics is capable of detecting defects in several types of components, its reliability remains uncertain due to lack of repeatability of the excitation and the non-uniform nature of the vibration field excited in the component.

This Thesis investigates the reliability of thermosonics as a rapid screening technique on Rolls-Royce turbine blades. First, an empirical study was conducted to optimise the thermosonic technique developed for this project, after which the reliability of the technique was assessed on a large set of turbine blades with known cracks. The

developed technique was shown to be robust and capable of detecting cracks in the blades. However, the non-repeatability of the excitation was evident in the empirical study. Researchers at Imperial College have proposed a vibration monitoring tool called the Heating Index (HI) to mitigate the non-repeatability issue with the excitation. The HI was assessed in this Thesis to determine its reliability on turbine blade thermosonic inspection. The HI was found to be useful for cases where a crack was known to be present, but not for a realistic case where the presence of a crack is unknown. An alternative vibration monitoring parameter (A^2) was proposed and found to compare favourably with the HI parameter. Importantly, the A^2 parameter can be used without prior knowledge of the presence of a defect. Finally, a methodology was proposed to simulate the full-field vibrational response of a turbine blade under thermosonic excitation. The results from this work demonstrated the non-uniformity and complex vibrational energy field excited in a typical thermosonic test. In addition, the vibrational energy distribution across a blade for a typical thermosonic test is presented.

Acknowledgements

Firstly, I would like to thank the Almighty God for His grace in completing this Thesis.

I am extremely grateful to my academic supervisors, Tony Gachagan and Gareth Pierce for guidance and support over the last four years. I am also grateful to my industrial supervisors, Gerald Harvey and Tim Barden, for their support throughout my stay in Rolls-Royce. A special thanks to Tony Dunhill for his encouragement and support throughout the EngD programme.

I would like to thank Darryl Almond and the Bath University team (i.e. Ben, Simon and Umberto) for lending their technical support to my project and also use of their equipment. Similarly, I would like to acknowledge Peter Cawley and the Imperial College team (i.e. Marco and Bu Byoung) for their support. I am grateful to the RCNDE family – Chris Scruby, Peter Thayer, Keith Newton and Nina Hancock for their support.

Special thanks to my Dad (Christian Bolu) and friend (Michael Arumemi-Ikhide) for inspiring me to pursue an EngD. Finally, I would like to thank my wife, Ebiere Bolu, for her love and support over the last four years. In that time, we got married and had a wonderful son, Chinonso Bolu.

Dedication

I dedicate this Thesis to my wife, Ebiere, for her unwavering belief in me. Love you darling!

Table of Contents

List of Figures

List of Symbols

A^2	Total energy content of a vibration waveform
b	Regression coefficient
CI	Confidence Interval
e	Percentage error
E	Young's modulus
EI	Energy Index
f	Frequency
F	Vector of nodal forces
g	Filtered image
G	Shear modulus
h	Original image
HI	Heating Index
k	Heating Index decay constant
K	Element stiffness matrix
N	Shape function
P	Power dissipated at crack
r	Correlation coefficient
t	Time

$t_{(\ )}$	Critical t-distribution value
T	Temperature
ΔT	Temperature variation
u	Displacement vector
$U`$	Maximum strain energy
$\Delta U`$	Strain energy dissipated per cycle
$v(t)$	Vibration waveform
w	Filter mask
X	Independent variable
Y	Dependent variable
$\hat{Y}$	Predicted value of dependent variable
ψ	Specific damping capacity
τ	Time
σ	Vibration amplitude
ε	Strain
ν	Poisson's ratio
ρ	Density

Chapter 1

Introduction

1.1 Background

Gas turbine engines are the power plants of an aircraft that provide the necessary thrust for propulsion [1]. Key to their operation are aerofoil blades experiencing high rotary velocities and loads, and for the blades in the turbine section, high temperatures (> 1600°C). In these harsh conditions, turbine blades are susceptible to fatigue cracks, creep or corrosion, which are detrimental to their life. In this respect, these blades are removed from the engines at pre-designated times (i.e. overhaul) for inspection, and possibly repair, to maintain the engines reliability and performance.

Figure 1-1 (a) shows the current inspection process for turbine blades in Rolls-Royce (RR). The blades are first booked in to register their part numbers, after which they go through an extensive chemical cleaning process prior to crack testing with Fluorescent Penetrant Inspection (FPI). FPI is the accepted and mandatory method used to inspect turbine blades for surface-breaking cracks [2, 3]. Surface preparation is important as it removes any contaminant that may hinder the infiltration of penetrant into a crack. However, removal of contaminants such as debris, dirt, corrosion or grease that can accumulate on the surface of a blade while in-service, is not trivial, and in most cases requires a time-consuming and expensive cleaning process.

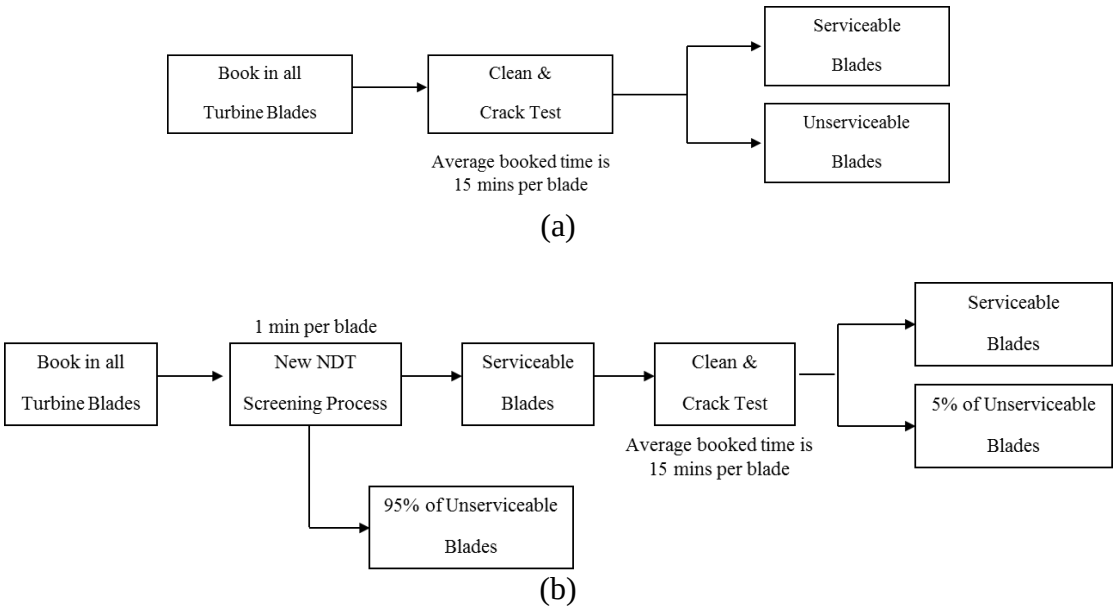

Figure 1-1 (a) Current inspection process (b) proposed inspection process.

In the current inspection process shown in Figure 1-1 (a), both serviceable and unserviceable blades go through the clean and crack test process. However, cleaning and inspecting unserviceable blades is a non-value-added process, costing time and money. At present, approximately 11% of RR turbine blades (civil large engine) are classed as unserviceable (due to cracking) after the clean and crack test. Therefore, a reliable and rapid NDT method that can filter unserviceable blades at the pre-cleaning stage is desirable. This will reduce the number of blades going through the mandatory cleaning and FPI process, thereby saving cleaning and inspection costs, and time.

Figure 1-1 (b) shows the proposed inspection process which includes an additional NDT method prior to clean and crack test. However, for this additional NDT method to

generate meaningful cost savings, the following criterion must be met: reliability of at least 95% in detecting cracks and an inspection time of less than 1 minute. This criterion was established in a business case produced by RR personnel prior to the start of this EngD project. Note that the remaining 5% of cracked blades not detected by the additional NDT method will be later detected at the FPI inspect stage. Figure 1-2 shows the effect of the inspection time of the additional NDT method on the potential cost savings over 5 years. This Figure shows estimated savings of at least £327 k over 5 years with an inspection time of less than 1 minute (and 95% reliability), while an inspection time over 1.6 minutes results in additional costs to the inspection process. Note that Figure 1-2 was produced by RR personnel as part of the business case for this project.

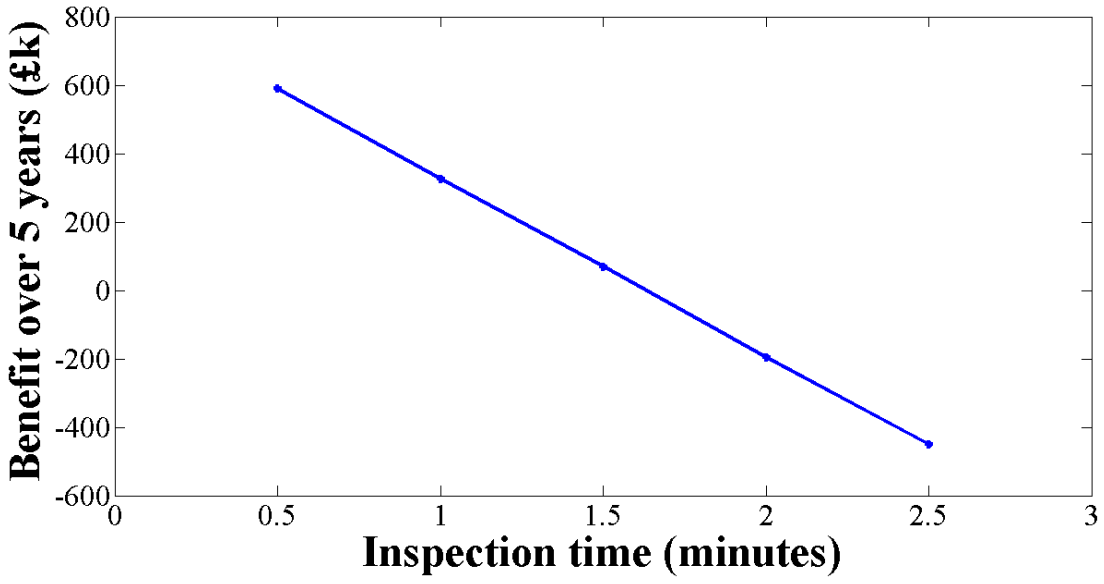

Figure 1-2 Effect of inspection time of additional NDT method on cost benefit over 5 years (Rolls-Royce).

Prior to the start of this EngD project, three NDT methods were identified as potential techniques capable of detecting cracks in engine-run turbine blades. These methods were laser shearography, X-ray Computer Tomography (CT) and thermosonics. However, after careful evaluation of the three techniques, thermosonics was selected as the most viable technique to achieve the desired business benefit. Laser shearography is capable of detecting cracks in turbine blades [4]; however, expert knowledge is required for interpreting results [4], making this method unsuitable as a rapid screening technique. Similarly, X-ray CT has been shown in a trial study [5] to be capable of detecting cracks in turbine blades, although at a slow inspection speed (~10 minutes per blade) [5]. In addition, X-ray CT has poor sensitivity to tight cracks and the cost of equipment is relatively high.

Thermosonics was considered to have the strongest potential in achieving the inspection objectives, particularly the one minute inspection time. Figure 1-3 shows a simple thermosonics setup, comprising an ultrasonic exciter (welding horn) and an infra-red (IR) camera. In a typical test, the component is excited with a short pulse (typically less than 1 second) of high-power ultrasound to generate a vibration field across the component. The vibration causes defect faces to rub (or clap) and generate heat, which is imaged by the IR camera. The heat generated by the vibrating defect appears as a bright 'hot' spot against a dark background. The frequency rating of the ultrasonic exciter typically used in thermosonics is 20 kHz or 40 kHz. However, the frequency excited in

the test-piece is highly non-linear and this is caused by the non-linear hammering action of the exciter against the test-piece. The advantages of thermosonics include: rapid inspection, suited to closed defects and no requirement for rigorous surface preparation, while the drawbacks include: poor defect sizing, potential damage to the component surface and poor repeatability. Poor defect sizing is not considered a disadvantage for this project as thermosonics is only required as a screening technique. Surface damage which is a potential issue can be mitigated using a soft coupling material between exciter and component, or in some cases, reducing the power of the excitation system. The lack of repeatability refers to the excitation, which has been shown to differ from test-to-test on a component, potentially leading to non-detection of a defect. This is a major concern with the thermosonic technique and hence, is addressed in this Thesis.

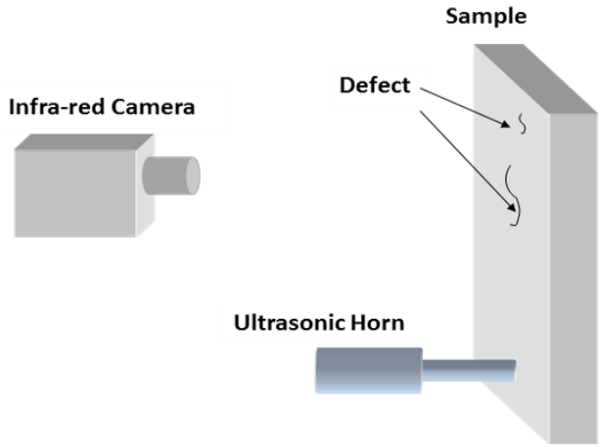

Figure 1-3 Typical thermosonic setup.

1.2 Aims and contributions of Thesis

1.2.1 Aims of Thesis

The aim of this Thesis is to assess the reliability of thermosonics as a rapid screening technique for cracks in Rolls-Royce turbine blades. Findings from this research work will contribute to the decision making process of whether or not thermosonics can be employed in the Rolls-Royce overhaul process to realise meaningful cost savings. The following were carried out to achieve the aim of this Thesis:

- Conduct an empirical investigation of thermosonics that highlights the capability, limitations and reliability issues concerned with the technique.
- Investigate procedures for ensuring a thermosonic test is carried out reliably given the poor repeatability of the excitation. This will increase confidence of the technique.
- Use Finite Element Analysis to simulate the full-field vibrational response of a turbine blade under thermosonic excitation. This will provide valuable insight of the vibrational energy distribution across a turbine blade for a typical thermosonic inspection.

1.2.2 Contributions to knowledge in the field of Thermosonics

The research work described in this Thesis contributes to the understanding of the capability and reliability of thermosonics on aero engine turbine blades.

- The work presented in this Thesis involves the inspection of a large set of turbine blades. Thermosonics is shown to be capable of detecting a wide range of crack sizes, including sub-millimetre cracks, in multiple locations of a blade. In addition, multiple cracks, up to four in some cases, on a single blade were detected in a single inspection. These results demonstrate the potential of using thermosonics for crack detection in complex components such as turbine blades.

- Electrical insulating tape, which has not yet been reported in literature, is shown to fare better than commonly used coupling materials. The use of electrical insulating tape was one of the factors that ensured a high probability of detection (POD) seen throughout this Thesis. In addition, this material was shown to be durable for at least 15 consecutive inspections, compared to other commonly used coupling materials which degrade considerably after fewer inspections.

- A repeatability study was carried out to assess the repeatability of results and robustness of the experimental process in repeated tests. This study demonstrated that the inherent excitation variability and also changes to the experimental

setup, such as component clamping and renewal of coupling material, do not necessarily affect the outcome of an inspection. This finding is important because in a real inspection scenario, component clamping and coupling material will vary between inspections on a component or between identical components.

- This Thesis further validates the Heating Index (HI) study carried out by Morbidini et al. [6] on aero engine turbine blades. The strength of linear correlation seen between the HI computed from a high frequency microphone and crack temperature rise in this Thesis compared favourably to Morbidini et al.'s results. The strength of linear correlation from vibration measurements captured by a laser vibrometer and strain gauge were also presented in this Thesis. The superior linear correlation between the HI and crack temperature rise when using a laser vibrometer was highlighted. In addition, this Thesis demonstrated the poor linear correlation when using the strain gauge in a practical context i.e. attached to the blade clamp as opposed to the blade itself.

- This Thesis found the application of the HI technique limited to cases where there is prior knowledge of the presence of a crack in the test-piece. This is because computation of the HI and subsequent determination of a reliable HI threshold, requires prior knowledge of crack behaviour. However, approximately 90% of blades to be inspected in a real inspection scenario will be crack free.

- An alternative vibration monitoring parameter to the HI is proposed in this Thesis. The proposed parameter, called the A^2 parameter, was shown to compare favourably with the HI in terms of the strength of linear correlation with crack temperature rise. However, the A^2 can be used without prior knowledge of the presence of a defect whereas the HI requires prior knowledge.

- This Thesis proposed a new methodology for simulating the full-field vibrational energy within a turbine blade under thermosonic excitation. This work highlighted the distribution of vibrational energy across all parts of a turbine blade for a typical thermosonic inspection. This proposed methodology would be most useful prior to the introduction of a new blade or component to a thermosonic process. It can potentially highlight the inspection dead zones where relatively little or insufficient vibrational energy will be excited in the component. Thus, a judgement as to whether to inspect a component or a change to the inspection setup can be made at an early stage.

1.2.3 Publications to date arising as a result of Thesis

Journal Publications

G. Bolu, A. Gachagan and G. Pierce "Reliable thermosonic inspection of aero engine turbine blades" Insight Nondestructive Testing and Condition Monitoring, vol. 52, 9, pp. 488 - 493, 2010.

G. Bolu, A. Gachagan, G. Pierce, T. Barden, G. Harvey "Investigations into the vibrational response of an aero-engine turbine blade under thermosonic excitation" Key Engineering Materials, vol. 518, 184 – 192, 2012.

Conference Publications

G. Bolu, A. Gachagan, G. Pierce and G. Harvey "Reliable crack detection in turbine blades using thermosonics: an empirical study" Review of Progress in Quantitative Nondestructive Evaluation, vol. 29, pp. 474 - 481, 2010.

G. Bolu, A. Gachagan, G. Pierce and G. Harvey "Monitoring crack propagation in turbine blades caused by thermosonic inspection" Review of Progress in Quantitative Nondestructive Evaluation, vol. 29, pp. 1654 - 1661, 2010.

G. Bolu, A. Gachagan, G. Pierce and T. Barden "A comparison of methods used to predict the vibrational energy required for a reliable thermosonic inspection" BINDT NDT2010 Conference Proceedings, 2010.

G. Bolu, A. Gachagan, G. Pierce and T. Barden "The application of finite element analysis to investigate the vibrational response of a turbine blade under thermosonic excitation" Review of Progress in Quantitative Nondestructive Evaluation vol. 32, pp. 510 - 517, 2012.

1.2.4 Conference presentations not resulting in publications

G. Bolu, A. Gachagan, G. Pierce and G. Harvey "Reliable thermosonic inspection of turbine blades: an empirical study" Non-Destructive Testing Conference, Blackpool, 15th - 17th September 2009.

G. Bolu, A. Gachagan, G. Pierce and G. Harvey "An investigation into crack propagation in turbine blades caused by thermosonics" Non-Destructive Testing Conference, Blackpool, 15th - 17th September 2009.

G. Bolu, A. Gachagan, G. Pierce and T. Barden "Simulation of the vibrational response of a turbine blade under thermosonic excitation" Review of Progress in Quantitative Nondestructive Evaluation, University of Vermont, Burlington, 17th – 22nd July 2011.

G. Bolu, A. Gachagan, G. Pierce and T. Barden "The vibration response of a turbine blade under thermosonic excitation" 18th World Conference on NDT, South Africa, 16th – 20th April 2012.

1.3 Overview of Thesis

Chapter 2: Literature review: Thermosonics

Chapter 2 presents a review of thermosonics and the reliability issues concerning the technique. The origins of the technique and the underlying heat generation mechanisms are introduced. Next, the advantages and disadvantages of the different excitation methods currently associated with thermosonics are reviewed. The reliability issues concerned with the excitation method adopted for this Thesis are then presented. Finally, a review of current thermosonic literature on turbine blade is discussed.

Chapter 3: Assessing the reliability of thermosonics on aero engine turbine blades

Chapter 3 describes an empirical study carried out on 60 identical turbine blades with known cracks. The aim of this study was to first optimise a newly developed thermosonic technique and then assess the reliability of the developed technique on the set of 60 blades. First, the excitation parameters known to influence the temperature rise generated by a crack were investigated to establish optimal setup parameters. Next, a repeatability study was carried out a subset of the 60 blades to evaluate the robustness of the experimental process. Finally, all 60 blades were inspected with the developed thermosonic technique.

Chapter 4: Validation of the Heating Index for a reliable thermosonic inspection

The Heating Index (HI) is a reference parameter that can be used to monitor the sufficiency of the vibration excited in a component. This reference parameter is useful because it correlates linearly with the temperature rise from a crack. This Chapter evaluates the linear correlation between the computed HI from three different vibration measurement systems and the measured temperature rise from a crack. First, the basis and theory of the HI are presented, after which the methodology for computing the HI is described. Finally, the strength of the linear relationship seen in the results of some tests and also the performance of the three vibration measurement devices are evaluated.

Chapter 5: An alternative vibration monitoring parameter for a reliable thermosonic inspection

Chapter 5 presents an alternative parameter to the HI for monitoring the vibration applied to a blade during a thermosonic test. The proposed parameter, called the A^2, was evaluated to validate its linear relationship with the temperature rise generated by a crack. This validation exercise involved the use of a set of blades with single and multiple cracks, and a high-frequency microphone to capture vibration. Furthermore, a comparison between the strength of linear correlation for the A^2 and HI is reported. Validation of the A^2 parameter and comparison with the HI was performed to assess its applicability as a reliable alternative to the HI for turbine blade thermosonic inspection.

Chapter 6: Simulation of the full-field vibrational response of a turbine blade under thermosonic excitation

Chapter 6 describes a methodology involving vibration measurements and finite element analysis (FEA) to simulate the full-field vibrational energy excited in a turbine blade under a typical thermosonic excitation. First, a laser vibrometer was used to capture the steady-state vibrational response of several points on a blade. Next, these measured vibrational responses were used to determine an input excitation function for the FEA approach. After validating the input excitation function, the vibrational response across the whole blade was simulated. Finally, the predicted displacement field was used to determine the vibrational energy at every point on the blade. This information can be overlaid onto a CAD representation of the blade to interrogate the suitability of the thermosonic excitation excited across the entire surface of the blade.

Chapter 2

Literature review: Thermosonics

2.1 Thermography NDE

Thermography is a non-contact imaging technique used for measuring infrared (IR) radiation emitted from the surface of an object. In NDE, thermography may be used to inspect for subsurface defects, measure coating thickness, or image hidden features within a structure [7]. This is achieved using an IR camera to observe the temperature differential of the structure's surface. There are two forms of thermography: passive thermography and active thermography [8, 9]. Passive thermography simply involves pointing an IR camera at a structure to measure a temperature profile of its surface [9]. This form of thermography is widely used in power stations for detecting leaks in lagged pipes and overheating in electrical components [10]. Conversely, active thermography involves application of an external stimulus to the component to generate a temperature differential between defective and non-defective regions in the component [9, 11].

There are several active thermography techniques used in NDE. These techniques are broadly defined by the type of external stimulus applied to the component, which include: optical, inductive and mechanical excitation [11]. Optical thermography techniques include pulsed thermography, lock-in thermography and laser-spot thermography [10]. In optical thermography, heat is applied to the surface of the

component and the transient temperature of the surface is monitored by an IR camera [7, 11]. A defect present in the component blocks the propagating heat in the material causing a temperature contrast between the surface above defective and non-defective areas of the component. Lock-in thermography is similar in principle to pulsed thermography except that different methods are used to apply heat to the component surface. In pulsed thermography a flash lamp is typically used to apply a heat pulse [7, 11], while for lock-in thermography, periodic modulated heating is used [11]. Laser-spot thermography is performed by scanning a laser-spot over the surface of a component. The laser-spot provides a localized heat-spot that generates a lateral heat flow in the component surface. When the laser-spot is placed closed to a crack, the lateral heat flow is disturbed by the crack and this disturbance is detected by an IR camera [12].

Optical thermography, particularly pulsed and lock-in thermography, are the most widely used form of active thermography due to their ease of implementation, fast inspection time and wide area inspection capability [7, 13]. Laser-spot thermography is however a relatively new thermal NDE technique, which is primarily used for detecting surface-breaking cracks in metals [14]. However, one of its main disadvantages, compared to pulse and lock-in thermography, is the point-to-point scanning of the laser-spot over the component surface [12]. This restricts the technique to small components if a rapid inspection is required.

Inductive thermography, also known as pulsed eddy current thermography (PECT), uses the principle of electromagnetic induction to generate eddy currents in a component [15, 16]. A defect present within the component disturbs the current flow in the component, leading to a change in the current density and heating around the defect vicinity [15, 16]. Inductive thermography has several advantages such as: fast inspection time (seconds), minimal surface preparation, suitable for complex geometries and detection of cracks under coatings [10, 17]. However, the main disadvantage with the technique is its limitation to electrically conductive materials.

Finally, mechanical excited thermography involves application of mechanical oscillations to a component to generate a vibration field in the component. If a defect is present, such as crack in a metal or delamination in a composite, the excited vibration causes the defect faces to rub and generate heat due to friction. This internally generated heat diffuses to the component surface and is detected by the observing IR camera [18, 19]. The most common form of mechanically excited thermography is thermosonics, also called vibrothermography or sonic IR. Typically, a high-power ultrasonic horn is applied to a point on the component to generate the vibration field. Compared to other active thermography techniques, no external heat is applied to the component surface. Instead, the heat observed by the IR camera in a thermosonic test is generated by the vibrating defect and therefore localised to the defect area. In addition, thermosonics is a

quicker technique, and capable of detecting perpendicular defects which can be difficult to detect using pulsed thermography [12].

2.2 Origins of thermosonics

Thermosonics has its origins from earlier research in vibro-thermal NDE techniques carried out in the late 1970's and early 1980's. This early research was carried out by Henneke et al. [20, 21], Mignogna et al. [22] and Pye and Adams [23, 24], although their excitation methods and test-pieces differed. Nevertheless, most of the research at the time focused on the detection of defects in composite materials with fewer studies on metals. Henneke et al. described a new NDT technique called vibrothermography which combined mechanical vibrations and real-time video thermography for detecting delaminations in composites [21]. Mignogna et al. [22] investigated the heating of metals using high-power ultrasound generated by a 20 kHz ultrasonic horn. Their excitation method is similar to the method currently used in thermosonics, except it uses much longer excitation times (20 to 30 seconds), generating temperature increases of up to 200 °C in the metal specimens [22]. More importantly, Mignogna et al. observed localized temperature increases at fatigue cracks, induced defects and grain boundaries.

Pye and Adams [23, 24] described a new NDT technique for composite structures that used oscillating stresses in a component to cause frictional heating at crack faces. Their excitation method relied on exciting the resonances (tens of Hz) of the component

because of the high cyclic stresses that can be generated from a small input force. This avoided the need for large and heavy testing machines for generating the same level of oscillating stresses [23, 24]. The sensitivity of the IR cameras used by Henneke et al., Mignogna et al. and Pye and Adams were in the order of 0.2 and 0.3 °C. This level of sensitivity and the general state of IR camera technology at the time was a limiting factor for the advancement of vibro-thermal NDT techniques. This meant these vibro-thermal NDT techniques were not widely used until the early 2000's [25].

In the early 2000's, Thomas et al. [26] from Wayne State University (WSU) revived interest in vibrothermography, which is now commonly referred to as sonic-IR or thermosonics. This revival was in part due to the advancement of IR cameras which now have much higher temperature sensitivities (~0.02 °C) and frame rates. The advancement in IR camera technology has also lead to more focus on application to metallic components. The method employed by the research group at WSU is similar to that of Mignogna et al. [22], except their excitation uses a short pulse (100 ms – 1 s) of ultrasound (20 – 40 kHz) generated by a high-powered ultrasonic welding horn. WSU have since made valuable contributions to the advancement of thermosonics in the form of published papers and patents [18, 19, 27-51]. Other research groups that have made significant contributions to the field of thermosonics include groups from Iowa State University [25, 52-67], Imperial College London [6, 68-75] and Bath University [10, 14, 76-79].

2.3 Heat generation mechanism in thermosonics

The vibration-induced heat generated by a defect has been attributed to three physical mechanisms: friction, plastic deformation and viscoelasticity [21, 58, 80]. Frictional heating occurs when opposing defect faces rub or move in relation to each other. Heating due to plastic deformation occurs at the plastic zone around the crack tip during crack propagation, while viscoelastic-induced heating is typically seen in polymer-based materials and relates to energy losses in the bulk material, although additional heating has also been observed in high stress-concentration regions [21, 58, 80]. Research carried out by Henneke et al. [21] indicated friction and viscoelasticity as the dominant heat generation mechanisms in composite materials. In addition, the authors reported plastic deformation as another efficient source of heat generation, particularly in metals. Since the work of Henneke et al., other researchers [58, 80] have also come to the same conclusion through similar experiments, albeit with more advanced IR cameras and different excitation sources.

Renshaw et al. [58] has provided experimental verification of the three different heat generation mechanisms using metallic and composite specimens. For frictional heating, it was reported that regions of heat generation along the crack correlated with crack surface damage (or wear) when the crack was opened [58]. Evidence of plasticity-induced heating was shown by propagating a crack in an aluminium specimen with high vibration stresses from an ultrasonic welder. As expected, heat was detected in the

plastic zone around the crack tip, although the authors believe a small proportion of the heat around the crack tip was from frictional rubbing. Evidence of viscoelastic heating was shown using a CFRP sample with a series of drilled holes to generate regions of stress concentrations. The sample was then excited with low vibration stresses to avoid plastic deformation. As discovered earlier by Henneke et al. [21], additional heating was found in high stress concentration areas around the defect. Of all the three heat generation mechanisms, frictional rubbing is generally accepted as the major contributor to the heat generated by a defect. However, the amount of the heat generated by this mechanism is fundamentally related to the area of the crack surfaces in contact [10, 47, 66].

2.4 Chaotic and resonance excitation

There are currently two main forms of excitation employed in thermosonics: chaotic and resonance excitation. Chaotic excitation, popularized by researchers at WSU, is the more commonly used excitation method. [45, 46]. The chaotic vibration of a test-piece is evident by the audible noise generated in testing, but more importantly, is seen in the spectral content of the component vibrations. Typically, the spectral content contains harmonics and fractions of the excitation frequency of the ultrasonic horn device [45]. The chaotic vibration seen in a component has been attributed to the non-linear coupling between the excitation source (i.e. ultrasonic welding horn) and the component under

test [45, 46]. However, this non-controllable excitation method has been shown to enhance the heat generated by a crack [81].

The increased defect detectability from chaotic excitation is because of the interactions of multiple frequencies excited in the component [46, 81]. This ensures the defect responds to at least one or several of the frequencies, increasing its heat generation capacity and thus its probability of detection [46]. This frequency dependence of defect detectability was investigated by Henneke and his colleagues in the 1980's [21]. Henneke et al. [21] used simulated and artificial delaminations in composites to demonstrate the different heating patterns generated by different resonance frequencies. Evidence of this frequency dependence of crack heating can also be seen in Holland's study [65], where a complex geometry (aero engine stator vane) with multiple cracks was excited at different discrete frequencies with a bespoke broadband piezoelectric transducer. Results from Holland's study showed different cracks only generating heat at certain frequencies; however all the cracks were detected when a broadband excitation was used. This frequency dependence associated with defect heating is why an ultrasonic horn that generates chaotic excitation is widely used. However, one of the key concerns with this form of excitation is poor repeatability, which leads to different vibration field conditions excited in a component in different tests [55].

The other form of excitation typically used in thermosonics (i.e. resonance excitation) has been extensively utilized by researchers at Iowa State University (ISU). Their excitation system uses a low power, broadband piezoelectric stack transducer capable of exciting a wide range of frequencies, 0.1 kHz to 32 kHz [25, 65]. This excitation source is used to excite components by either tuning the piezoelectric stack to a single component resonance or sweeping through a range of frequencies that coincide with several resonances of the component. This method of excitation is similar to that used by Henneke et al. and Pye et al., as it relies primarily on the resonance coupling energy into the component more efficiently.

ISU has shown resonant excitation to be repeatable and more importantly, successful in detecting defects in metals and composites. However, this form of excitation requires prior knowledge of the resonances of the test-piece, which for complex geometries may be difficult and time-consuming to measure, especially in an industrial environment. Furthermore, knowledge of just a few resonances is not sufficient; rather, knowledge of the modes that can excite a crack to generate sufficient heat is required. Determining the most effective resonances for a single component may be feasible; however, this would be more challenging for a batch of similar components as their resonances will differ due to slight differences in dimensions and mass.

Researchers at ISU have shown their low power broadband exciter to be more effective when using a frequency sweep as opposed to single mode excitation [65]. This approach ensures that one of the resonances of the component coincides with the resonance of the exciter and therefore, less reliance on knowledge of the modes that generate sufficient heat for detection. However, this is only useful if the component resonances that generate sufficient strain across the component are within the bandwidth of the exciter, which in the case of the ISU exciter is between 0.1 kHz and 32 kHz. Conversely, chaotic excitation relies on high amplitude forced vibrations at a much higher and wider range of frequencies (up to 250 kHz) [45, 51, 75]. This is important because the higher frequencies are beneficial as they increase the rate of energy dissipation at a defect, causing a higher temperature rise [75, 82]. The main issue however with chaotic excitation is non-repeatability, which can potentially lead to a crack going undetected if sufficient heat is not generated for the IR camera to detect.

2.5 Heating Index

The poor repeatability of the excitation when using a high-power ultrasonic welding horn has been observed by several researchers [55, 75, 81, 83]. Furthermore, this poor repeatability has been described as one of the main reliability issues preventing the technique from being utilized in industry as a reliable NDT method [75, 84]. To address this repeatability issue, Morbidini et al. [75] have developed a calibration method to

ensure the vibration excited in a component is sufficiently high to detect any defect of interest.

The fundamental basis of Morbidini et al.'s method is the increased heating at a defect caused by the extra damping introduced by the defect. Similar to Pye et al. [24], Morbidini et al. [70] investigated the prediction of temperature rise from a vibrating crack, based on the extra-damping introduced by the crack. Results from this work showed some correlation between the predicted and measured temperature rise from a crack, with disagreements in some cases. Although desirable, the prediction approach proposed by Morbidini et al. was impractical in a situation where information such as damping is unavailable. In this respect, Morbidini et al. [75] proposed a new parameter called the Heating Index (HI) which does not require damping information. The HI is computed from the measured vibration in a test and can be used to determine whether the vibration is sufficient to detect a crack of a certain size. The HI has been shown to correlate linearly with the measured temperature rise of a vibrating defect, thus allowing a threshold vibration level sufficient for crack detection to be determined.

First, a threshold HI is obtained from a series of inspections on representative cracked and uncracked specimens. Using the same calibration setup and specimens, real inspections can be carried out with the HI computed for the test and then compared against the threshold HI. If the computed HI for the test is below the threshold, the test is

repeated until the threshold is surpassed. Results from Morbidini et al.'s works show the reliability of the HI to be excellent for cracks in simple geometries such as beams [75], although poorer for cracks in complex turbine blades [6]. Part of the research carried out in this Thesis involves investigating the HI as a reliable vibration monitoring parameter in turbine blade inspection. This research extends the work of Morbidini et al., using different blade geometry and also blades with multiple cracks. In addition, this Thesis focused on three different vibration devices (strain gauge, microphone and laser vibriometer) that may be used to capture the vibration required to compute the HI. Kang [85] has compared the HI profiles computed from these three vibration measurement devices; however, a comparison of the linear relationship of HI and crack temperature rise when using these three different vibration measurement devices has not been reported in literature. This result is important because the linear relationship between the HI and crack temperature rise is what forms the basis for determining a threshold vibration level for a reliable inspection. This focus was important for this Thesis as it assesses the practicality of using the HI in an industrial context.

2.6 Non-uniform vibration coverage

Another reliability issue concerning thermosonics is the non-uniform vibration field generated across a component, particularly in complex components such as a turbine blade [6, 25, 85]. Non-uniform vibration coverage results in different parts of the component being excited with different amounts of vibrational energy. This may lead to

defects going undetected if sufficient vibration energy is not excited in some parts of the component.

Rothenfusser et al. [86] have developed a calibration method for assessing the vibrational energy excited across a component for a typical thermosonic test. The method involves measuring the thermal response of a material attached to the component. Materials such as adhesive tapes are used as they are responsive to acoustic vibrational energy [86]. In a typical calibration, several pieces of the thermal responsive tape are attached to various locations of the component. Next, vibrational excitation is applied to the component and the thermal responses of the individual tapes are measured from the captured IR image. The captured images give an indication of the level of vibrational energy excited at different points on the component. Rothenfusser et al.'s calibration method has been used on several components including aero engine turbine blades and rotating discs [86, 87]. This calibration method has been shown to be useful; however, achieving consistent attachment of the thermal responsive tape across a component remains a reliability issue.

Renshaw [25] investigated vibration coverage on components under thermosonic excitation. The author's study involved two different specimens: a rectangular beam and an aero engine stator vane, each with viscous material-filled synthetic defects [25]. The rectangular beam had an array of 21 × 3 drilled holes of 1.18 mm diameter and 1 mm

depth. Each hole was filled with honey, which is a highly viscous material that generates heat under vibration. The holes were covered with an emissive coating to trap the honey and also increase the emissivity of the component. A similar process was used for the stator vane, but using the stator vane cooling holes instead of drilled holes. The beam was excited at a single known resonance while the stator vane was excited with four known resonances separately. For the beam, the honey-filled defects located at the vibrational anti-node positions generated significant heat, while those at the nodes generated little or no heat. Although this was expected, the result produced a good image of vibration coverage across the simple beam for a single frequency. The results for the stator vane were however more interesting with each excitation frequency generating a different heating pattern across the stator vane. Three resonances generated heat in only a few, but different regions, while the fourth resonance generated heat across a larger area of the component. This result demonstrated the non-uniform heat generation resulting from a multi-frequency vibration field. One aspect not investigated in Renshaw's study was the chaotic excitation case, where many more frequencies are simultaneously excited in the component. This case is important to understand as chaotic excitation is the more common excitation method utilized for thermosonic inspection. This Thesis later presents a different methodology for assessing the full-field vibrational response of a real component under a typical thermosonic inspection with chaotic excitation.

2.7 Thermosonic excitation parameters

The temperature rise generated by a defect is a strong function of the excitation parameters. These parameters include: horn static force, coupling material, vibration amplitude and excitation time. The horn static force is the coupling force between the horn and the component prior to excitation. This coupling force is typically applied by mechanically pressing the horn tip against the component surface using a pneumatic cylinder [59, 88, 89] or a spring system attached to the ultrasonic horn [10, 30, 75, 78]. Force levels between 50 – 290 N have been used in various studies [77, 90-93]; however, the force chosen for an inspection is mostly dependent on the size and material of the test-piece. In general, higher forces are used for metallic structures [91, 93] compared to composite structures [77]. This is because high horn tip forces can cause damage to the surface of a composite [77]. Of all the excitation parameters, the horn static force is generally regarded to have the most effect on the heat generated by a crack [50, 90, 94]. This is because a higher coupling force leads to more non-linear vibration, which is known to enhance the heat generated by a crack [72].

The coupling material is a piece of material placed between the test-piece and the exciter. Its purpose is to prevent surface damage on the component and also efficiently couple energy into the component [45, 77]. At present, there is not one accepted coupling material; rather, a variety of coupling materials has been proposed through various studies. Materials such as duct tape [31, 44, 75, 85, 95], leather [31, 96], paper

[19], soft copper [85], Teflon [76, 77] and business cards [44, 50] have all been reported. Han and Yu [31], under the same experimental conditions, conducted a comparison study between leather and duct tape to determine which material generated the higher temperature rise from a crack. Duct tape was found to generate a higher crack temperature rise. Another similar study by Yu and Han [31] and Han et al. [44], but this time comparing duct tape, laminated business card and a non-laminated business card, also showed duct tape to be the most efficient, closely followed by the laminated card. The reason for the non-laminated business card not generating as much heat compared to the other two materials was attributed to the non-chaotic vibration observed when using non-laminated business card. For the other two materials, their respective vibration was chaotic. A more comprehensive study involving a larger set of coupling materials is required to get a better understanding of the effect of coupling materials on crack detectability and also to propose the most effective material for thermosonic applications.

The vibration amplitude here refers to the displacement of the vibrating horn tip. For most ultrasonic horn systems, the horn tip displacement may be varied between 20% and 100% of the maximum horn tip displacement [91, 97-99]. The maximum displacement of a horn device is a function of the horn design. The variation of the horn tip displacement is usually controlled via the power amplifier connected to the horn. The horn tip displacement affects the amplitude of vibration excited in the test-piece and

thus the amount of heat generated by a defect [75]. Finally, the excitation time is the length of time the horn excitation is active. It is also controlled via the power amplifier, and the length of time may be varied depending on the test-piece. Barden et al. showed long-pulse excitation (10 - 15 secs) with reduced vibration amplitude was sufficient for detecting impact damage in composites and at the same time prevents surface damage [77]. However, short-pulse excitation (i.e. < 1 sec) using high amplitude vibration is more effective on metals due to their high thermal diffusivity [18, 75, 81].

Mayton [100] carried out a comprehensive study to characterize and optimize thermosonics for inspecting several US Air-Force aircraft components with known cracks. The aim of Mayton's study was to determine a set of optimal excitation parameters for inspecting these components. The author concluded that generally, the heat signal generated from the known cracks increased as the settings of the vibration amplitude, horn static force and pulse time length increased. However, the heat signals did not scale linearly with crack size, which is not surprising as the heat signal generated by a crack also depends on other factors such as crack morphology. Various thermosonic studies presented in literature, including Mayton's study, all show different experimental setups and test-pieces, and also different excitation parameter settings. This suggests that the optimum excitation parameters must be determined empirically, using the parameter settings seen in literature only as a guide. The first part of this Thesis presents a study investigating the optimum parameter settings required for inspecting certain types of

Rolls-Royce turbine blades. In addition, the effect of these parameter settings on the reliability of the technique was also investigated.

2.8 Thermosonic studies on turbine blades

Published thermosonic studies involving turbine blades are relatively few in number [6, 85, 92, 100, 101] compared to studies on simple geometries such as rectangular bars and beams [14, 19, 27, 32, 52, 75, 90, 94, 95, 102]. The use of simple geometries is important in investigating the capability of an NDT technique; however, it is difficult to use results from such geometries to fully determine the capability of thermosonics on complex components such as turbine blades. This is because the heat generated by a crack is dependent on several crack and component specific factors such as: crack morphology, crack location, component material, component geometry, and the local vibration at the crack [10, 47, 66, 85, 92]. It must be noted that majority of cracks seen in bars and beams are typically laboratory-induced cracks, compared to the service-induced cracks seen in turbine blades. Manufacturing cracks similar to those seen in real components is difficult, if not impossible.

Thermosonics has attracted huge interest from several turbine blade manufacturers who mainly operate gas and steam turbine engines. Their primary interest in thermosonics is its potential to improve inspection quality or reduce inspection costs [95]. Some of these manufacturers include Rolls-Royce, Siemens, npower, General Electric and Pratt &

Whitney (P&W) [10, 60, 97]. Thermosonics has been mentioned as a potential replacement for FPI [84, 95, 103], which is the currently accepted and mandated method for inspecting turbines blades [3]. The advantages thermosonics has over FPI include: faster inspection time, minimal surface preparation (no chemical clean, no coating removal), better suitability to tight cracks, insensitive to rough surfaces, easier interpretation of results, operator independent, smaller floor space requirement and environmentally friendly (no chemical cleaning) [84, 95, 100]. Industrial interest in thermosonics is important as it provides the necessary funding and impetus in further investigating the capability and reliability of the technique. This will not only benefit the turbine blade manufacturers but also other industries that rely on NDE for assessing the reliability of their products.

Guo and Ruhge [92] compared the capability of thermosonics and FPI on turbine blades using generated probability of detection (POD) curves. Their POD study used a signal response approach on a set of 50 turbine blades containing 146 cracks. The number of cracks used in this study was well in excess of the 30 flaws generally recommended for a signal response POD study [104]. The thermosonic tests were carried out by a Level 2 IR operator (ASNT-SNT-TC-1A), while the FPI inspections were carried out by a Level 2 FPI certified inspector [92]. The POD for thermosonics in Guo and Ruhge study was approximately 89% and for FPI, approximately 77%. Furthermore, the minimum crack size detected with 90% POD (with 95% confidence) was ~2.6 mm and ~5.8 mm for

thermosonics and FPI respectively. The results in Guo and Ruhge study is in agreement with DiMambro et al.'s study [95] which also showed thermosonics with a better crack detection capability than FPI, although DiMambro et al.'s study was on bars. The results of Guo and Ruhge [92] and DiMambro et al. [95] clearly demonstrates the potential of thermosonics as NDT technique for detecting cracks in components currently inspected with FPI.

DiMambro carried out a different thermosonic study on turbine blades [101]. This study was carried out in conjunction with researchers at Wayne State University (WSU) to assess the capability of thermosonics in detecting cracks in components commonly inspected with Fluorescent Penetrant Inspection (FPI) and Magnetic Particle Inspection (MPI). The blades used for this study were 2^{nd} and 4^{th} stage turbine blades from a P&W aero engine [101]. The authors were able to detect several fatigue cracks which were not detected optically. Similar to DiMambro et al.'s [101] study, Mayton [100] found thermosonics was able to detect cracks in turbine blades missed by FPI. Another interesting observation in Mayton's study was that cracks in the aerofoil section of the blade were easier to detect than cracks in the shroud area. For the aerofoil section, lower excitation levels were required and setup excitation parameters did not have to be accurate, whereas, cracks in the shroud required higher excitation levels and more effort in determining optimal excitation parameters.

Kang [85] investigated the vibration characteristics of a turbine blade under a variety of thermosonic experimental configurations. Kang demonstrated the advantage of using a clamp attached to the root of the blade as the excitation point, as opposed to exciting the blade directly. This approach reduces the possibility of surface damage, but also allows permanent attachment of a strain gauge for monitoring the vibration of the blade. Kang showed that a minimum clamping torque of 10 Nm between the clamp and blade ensured consistent transfer of vibration to the blade. Kang showed that the exciter (i.e. horn) can either be coupled to the clamp by simply pressing against the clamp or by coupling the horn to the clamp via a stud. The former is the conventional method, while the latter has been used by fewer researchers [10, 85], although it has been shown to generate a higher vibrational response than the former [85]. Furthermore, with the horn attached to the clamp via a stud, Kang achieved an even higher vibrational response when the excitation frequency coincided with the resonances of the system (i.e. horn, clamp and blade). This higher response was achieved by employing a chirp input signal (to the horn) over a frequency range centred on the system resonance frequency [72, 85]. Kang's work on turbine blades demonstrated several experimental configurations that may be used to achieve higher vibrational response and thus, increased probability of crack detection.

One application of thermosonics that will significantly benefit turbine blade manufacturers is crack detection in coated components, particularly blades that require

proprietary coating for thermal protection (e.g. thermal barrier coating (TBC)). Inspecting such components is time-consuming and expensive as it requires stripping the coatings off prior to inspection with FPI. To date, there has been practically no quantitative study into detection of cracks under coating using thermosonics, except that of Weekes [10]. Weekes investigated the feasibility of using thermosonic for detecting cracks in an Inconel substrate under a full TBC system. The TBC system comprised of a metallic bond coat (MCrAlY) first applied on the substrate and then a ceramic top coat (YSZ) applied on the metallic bond coat. Four Inconel specimens with a total of five cracks were used in the study. The thickness of the bond coat and top coat were typical of the thickness used in the power generation and aerospace industries. The specimens were tested before and after application of the bond and top coats. The cracks were detected in all cases, although the crack heat signal gradually reduced with successive application of the coatings. The results from Weekes study are significant as it demonstrates the potential of inspecting ceramic coated blades for cracks in the base metal.

2.9 Review of chapter

This section has reviewed the thermosonic literature relating to its origin, heat generation mechanisms, typical excitation methods, reliability issues, excitation parameters and related literature on turbine blades. The review found that chaotic excitation, the more popular excitation method, was non-repeatable, which can

potentially lead to a crack being missed if sufficient vibrational energy is not excited in the test-piece. The non-repeatability of the excitation may be mitigated using a method that ensures the vibration in a test is sufficient to detect the defect of interest. The Heating Index (HI), developed by Imperial College [75], was described as a potentially suitable vibration monitoring parameter. However, it was shown that more work on assessing the reliability of the Heating Index on turbine blades with single and multiple cracks is required, and therefore is investigated in this Thesis.

Non-uniform vibration was also discussed as a potential reliability issue. This area of thermosonics has not been extensively researched and therefore more knowledge is required. Part of the work carried out in this Thesis aims to contribute to this area of thermosonics. The review of excitation parameters used in thermosonics highlighted not only their importance in the effect they have on the heat generated by a defect, but also the need to empirically determine the optimum excitation settings for a specific application. In this respect, an empirical study is presented later in this Thesis with focus on determining the optimal settings for the excitation parameters required for crack detection in RR turbine blades. Finally, a review of thermosonic research relating to turbine blades was discussed. This review showed only a handful of published literature on turbine blades, yet potentially significant benefits that may arise from using thermosonics on these components.

Chapter 3

Assessing the reliability of thermosonics on aero engine turbine blades

3.1 Introduction

Thermosonics is a non-destructive testing (NDT) technique capable of detecting defects in metallic and composite components [19, 30, 42]. The component is excited at a single point with a high-power (0.4 – 3 kW) ultrasonic horn for a short time (~ 1 second or less) and observed with an IR camera [19]. The vibration field generated in the component causes defect faces to rub or clap and generate heat, which is detected by the observing IR camera. The aim of this Chapter was to assess the reliability of thermosonics as a screening technique for detecting cracks on Rolls-Royce turbine blades. The assessment involved the inspection of 60 turbine blades (same engine type) with known cracks. However, a study of the excitation parameters was first conducted to maximize the temperature rise generated from a crack. Next, a repeatability study was carried out on a subset of the 60 blades to evaluate the robustness of the experimental process. Finally, all 60 blades set out for this study were inspected.

3.2 Methodology

3.2.1 Specimens

Figure 3-1 shows a representation of the blades used in this study. This blade is made of high-strength nickel alloy and is approximately 70 mm in height and 27 mm at the widest point. The blades were all in a clean condition having been through the routine cleaning and FPI process, during which cracks were detected at the shroud, as indicated in Figure 3-2. The cracks on all 60 blades were visible and their lengths measured using a calibrated optical microscope/CCD camera (Leica MZ8/ JENOPTIK ProgRes® C12). The crack lengths ranged between 0.3 mm and 6.0 mm. Figure 3-3 shows a frequency distribution of the crack lengths, which shows a relatively consistent distribution of crack lengths between 1 mm and 6 mm. In addition, the accepted minimum detectable crack size (~0.75 mm) using the current method (i.e. FPI) for inspecting these blades is represented in the range of crack lengths set out for this study.

Figure 3-1 Turbine blade used in empirical study.

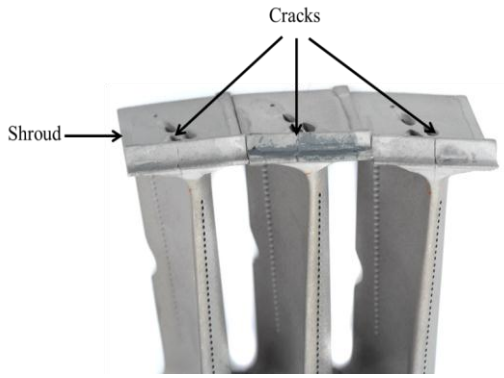

Figure 3-2 Crack location (shroud) on turbine blade.

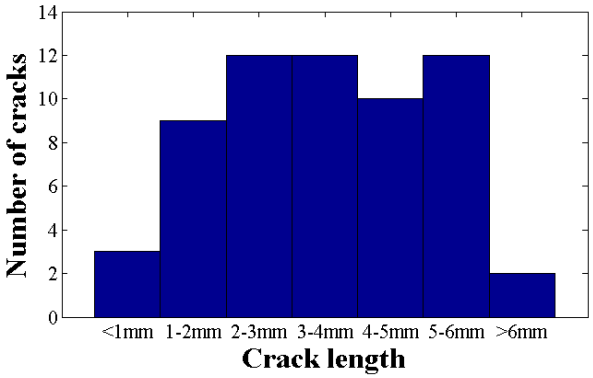

Figure 3-3 Frequency distribution of crack length in set of 60 turbine blades.

An important material property to consider when using a thermographic technique is emissivity. Emissivity is a measure of how effectively an object emits infrared energy. The emissivity of the blades used in this study was considered low because of their clean and polished-like condition. However, this was not detrimental to this study, because thermosonics uniquely relies on localised heating at cracks [10, 105], as opposed to bulk heating of the component as seen in other thermography techniques such as pulse

thermography. For techniques such as pulse thermography, painting the whole surface of the component with high emissivity black paint improves reliability of inspection [7].

3.2.2 Experimental setup

The experimental setup used in this study is shown in Figure 3-4. The ultrasonic excitation source was a Sonotronic welding system, comprising a 40 kHz ultrasonic horn driven by a 400 W ultrasonic generator (USG400-40) [106]. The horn tip was spring-loaded to the root of the blade with a measured horn static force. The blade root was chosen as the point of excitation on the blade because its flat surface allowed for good alignment with the flat surface of the horn tip. This ensured efficient coupling of energy into the blade. The blade was secured in a holder made of cork material, and then both blade and holder secured between the jaws of the metal clamp. The cork material between the blade and metal clamp acted as a vibration isolation material, minimizing leakage of the acoustic energy excited in the blade to the metal clamp and other parts of the experimental fixture [90, 94]. Perez et al. [94] demonstrated a vibration isolation material such as cork can enhance the heat generated by a crack compared to metal to metal clamping.

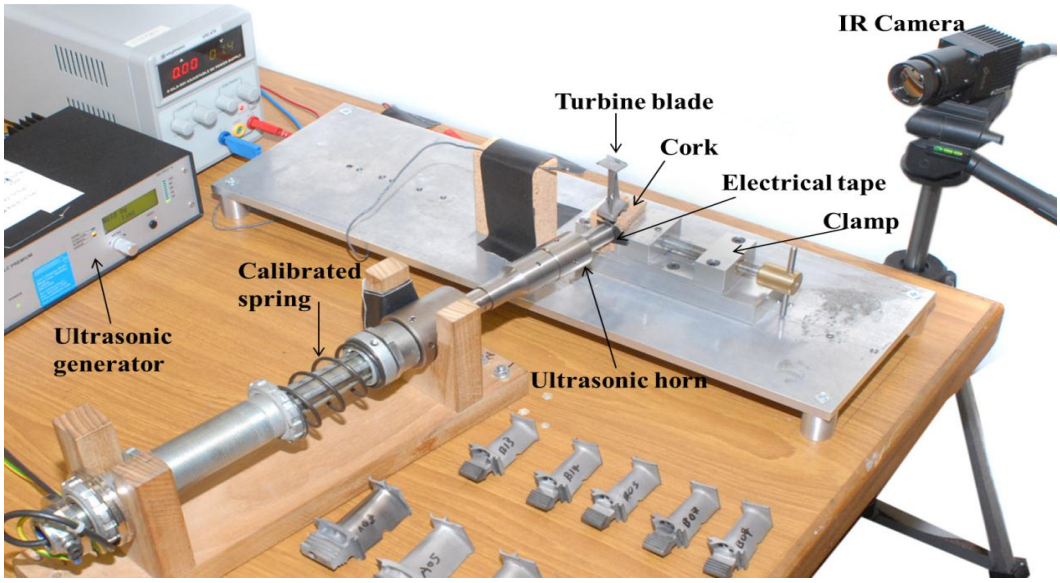

Figure 3-4 Experimental setup for thermosonic inspection of turbine blades.

Typically, a layer of soft material such as paper, copper sheet, Teflon® and duct tape is placed between the horn tip and component [6, 18, 19, 27, 75, 77, 81, 95, 105]. Such material prevents damage to the component surface, which could arise from the high horn tip forces during vibration [19, 27, 75, 77, 105]. However, in this work, electrical insulating tape was used and compared with several materials such as paper and duct tape and was found to generate more heat for the same setup (i.e. crack and experimental setup). The result of this comparison work is presented later in this Chapter.

The IR camera shown in Figure 3-4 is a Thermoteknix 'uncooled' microbolometer (Miricle 110K-35), with a detector array of 384 x 288 pixels, a temperature sensitivity of ≤ 50 mK, a 50 Hz frame rate and a spectral response between 8 μm – 12 μm. Cooled

cameras are commonly used in thermosonic studies because of their higher temperature sensitivity when compared to uncooled cameras [18, 47, 64, 70, 75, 77, 95]. However, uncooled cameras are smaller and more cost-effective than their cooled counterparts [18, 27, 107]. For example a high specification uncooled camera, such as that used in this study, can cost between £15,000 and £25,000, while its cooled counterpart can cost between £75,000 and £200,000, depending on the specification. For this research work, an uncooled camera was chosen primarily because of its relatively lower cost and also is demonstrated capability of detecting the cracks in various thermal NDT applications [18, 27, 34, 107, 108]. However, for a production system, cooled cameras (e.g. FLIR SC5000) will be utilized to ensure the best possible detection capability.

3.2.3 Thermosonic inspection

3.2.3.1 Excitation and imaging

The thermosonic inspection of a blade involved three operations: excitation, thermal imaging and image processing. The first two were programmed for simultaneous operation via National Instruments (NI) Labview software, while the image processing was carried out in MATLAB. Figure 3-5 shows an image of the graphical user interface (GUI) of the software developed in Labview for operating the excitation source and IR camera. The software has a multi-image window display for live video, background image and multiple image acquisition. The software can also perform simple image

processing techniques and export captured image data to MATLAB for further processing.

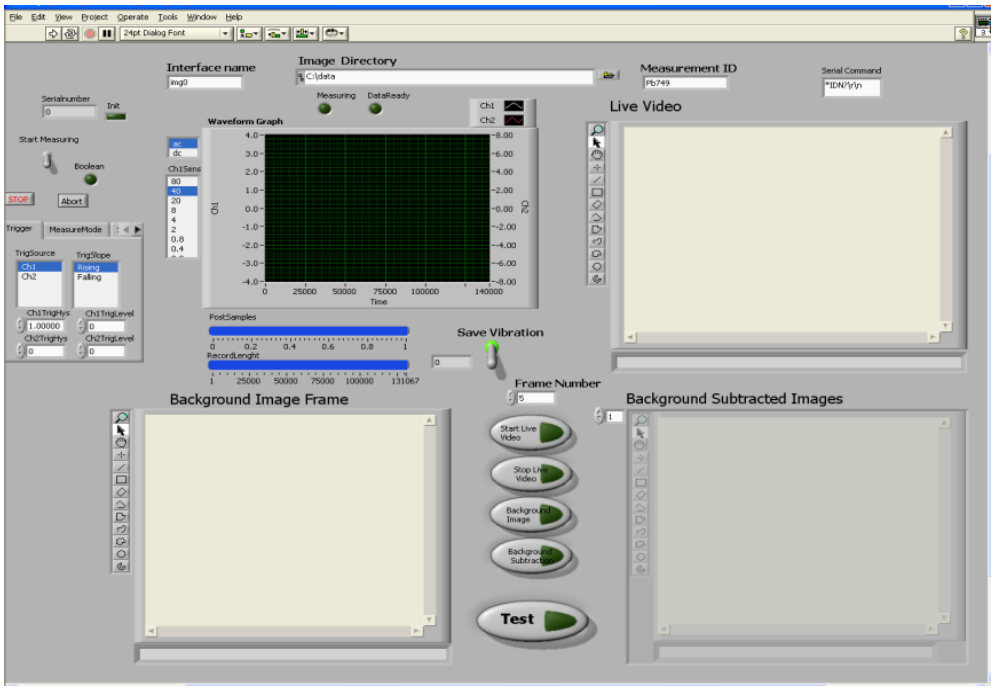

Figure 3-5 Graphical user interface (GUI) of bespoke software for operation of excitation source and IR camera.

Prior to the start of an inspection, a single background image of the blade was captured and stored on the PC. Next, the ultrasonic excitation was turned on between 0.4 seconds and 1 second in different tests, while the IR camera simultaneously captured 75 images at a maximum possible frame rate of 50 frames per second (fps). This number of images (i.e. 75) was specifically chosen to ensure images were captured during excitation and also for some time after the excitation was turned off. Due to the background noise

present in the images, the heat signal generated by a crack was not evident in the raw thermal images and therefore post-processing was utilised to enhance any potential crack indication.

3.2.3.2 Image processing

The following image processing techniques were coded in MATLAB and used in this specific order: background subtraction, linear filtering (convolution) and averaging. Background subtraction is a simple and popular image processing technique used in thermosonics [47, 75, 81]. It involved subtracting the captured background image (acquired before excitation) from each of the 75 images acquired during and post excitation. This technique removed the unwanted background/artefacts, highlighting only the heat signal generated by the crack during excitation. However, for some inspections in this study, background subtraction was not sufficient in highlighting the crack heat signal. Figure 3-6 shows an example of such an image, with the crack location indicated. The crack heat signal generated in this image is comparable to the background noise level, making discrimination between the crack signal and background difficult. Therefore, further image processing was performed to increase the heat signal-to-noise ratio.

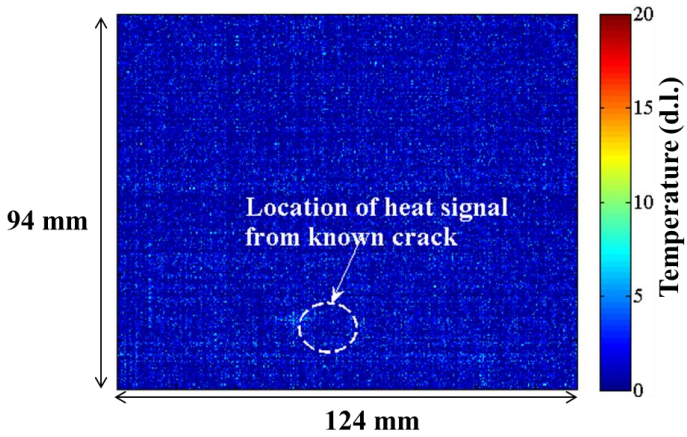

Figure 3-6 Example of a difficult to interpret background subtracted image.

The noise in images obtained from an IR camera can either be random noise or 'salt-and-pepper' noise [109]. Two filters commonly used for reducing such noise are linear filters (convolution) and median filters [109]. Both approaches were evaluated with the convolution method producing better discrimination of the defect location in the processed images. The convolution method replaces each pixel value in an image by a weighted average of itself and its neighbourhood pixels using a 2D array (i.e. filter mask) of known integer weights [109]. The random noise pixels are reduced because of the contributions of the non-random image pixel values from the neighbourhood pixels. For an image h of size $M \times N$ with a filter mask w of size $m \times n$, the linear filtering operation can be expressed by Equation 3.1 [109]. In Equation 3.1, $a = (m-1)/2$; $b = (n-1)/2$; $x = 0,1,2.....,M-1$; $y = 0,1,2.....,N-1$ and $g(x,y)$ is the filtered image.

$$g(x,y) = \sum_{s=-a}^{a} \sum_{t=-b}^{b} w(s,t)h(x+s,y+t) \qquad (3.1)$$

One drawback of using this type of filter for noise reduction is image blurring [109]. However, this did not adversely influence the interpretation of the imaging results obtained in this work. A 9 x 9 filter mask with a weighting of one in all locations was found to enhance the crack heat signal and allow for easier interpretation. This is illustrated in Figure 3-7 where the heat signal from the crack (red spot) is clearly discernible from the rest of the background. The image in Figure 3-7 was a result of applying a linear filter to the background subtracted image shown in Figure 3-6.

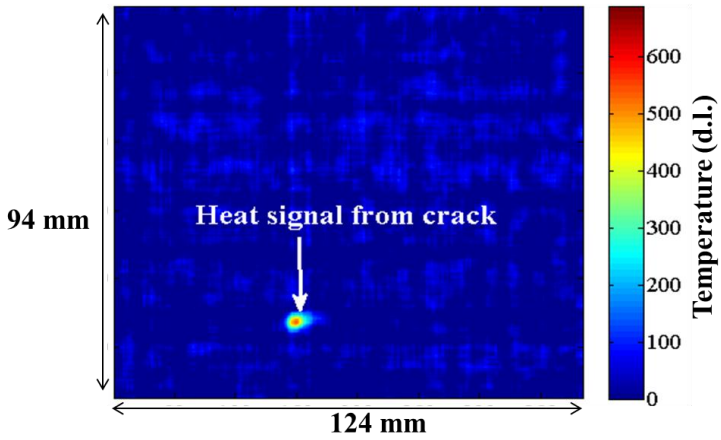

Figure 3-7 Improved imaging result after applying a linear filter to the background subtracted image shown in Figure 3-6.

For each blade inspection, the filtering operation was applied to all 75 background-subtracted images. A combination of these images provides a video sequence that shows the transient heat signal from the crack over the inspection period. However useful,

studying individual images in the video sequence can be time-consuming, especially with the high number of frames captured in a typical inspection. Reducing the video sequence to a single image is a better and much faster way of presenting the result. In this study, averaging the filtered images captured during the excitation period was used to obtain the single image for representing the result of an inspection. This type of averaging is generally referred to as temporal averaging [109], as it involves averaging images captured over a finite period. This image processing method also gives the additional benefit of potentially increasing the heat signal-to-noise ratio by reducing temporal noise [109].

3.2.4 Thermosonic excitation parameter study

Prior to inspecting the 60 blades set out for this study, it was important to understand how the different excitation parameters affect crack detection in the turbine blades. The excitation parameters investigated included: horn static force, coupling material, vibration amplitude and excitation time. These parameters are fundamental in carrying out a thermosonic test and have been shown by several researchers to affect the vibration excited at a crack or the resultant heat generated by the crack [91, 100]. In this study, the optimum parameter settings were determined using an initial set of settings known to generate a detectable heat signal. These initial settings were: horn static force (70 N); coupling material (electrical tape); vibration amplitude (100% on generator) and excitation time (one second). The effect of each parameter was investigated by varying

the parameter, while keeping the values of the other three parameters constant (i.e. initial settings). For each parameter, five tests were conducted and the coupling material renewed after the set of tests. One blade was considered sufficient for this study because it was representative in geometry and crack position. The maximum temperature rise from the crack was the difference between the average of the ten hottest pixels around the crack and an averaged background area in the image.

3.2.5 Repeatability study

After establishing the excitation parameter settings, a repeatability study was carried out to assess the consistency of results in repeated tests and the robustness of the experimental process. This study was important mainly to understand how the inherent inconsistency of the excitation affects results in repeated tests. Repeatability of results was measured by the number of positive or negative (hit/miss) crack detections in 300 repeated inspections on four blades. The hit/miss approach was chosen because thermosonics is generally recognised as a screening technique for detecting the presence or absence of defects [75, 78, 93, 97, 110]. Therefore, in this study, absolute temperature was not important, but rather, that the temperature rise associated with a crack was above the background noise level, which ensures its detection in the final thermosonic image.

Apart from the inconsistency of the excitation generated by the ultrasonic horn, two other variations that can influence the excitation generated in a blade in repeated inspections were introduced to the experimental procedure. The variations were reclamping the blade and renewing the coupling material after a specific number of repeated inspections. It was important to determine the influence of these two experimental variables because blade clamping can vary between components or in-between inspections on the same component [80], while renewing the coupling material after a certain number of inspections is an inevitable part of thermosonic inspection process. Studies have shown that a change in the coupling material conditions can influence the characteristics of the excitation, and hence the resulting temperature rise generated by a crack [31, 44, 50]. Reclamping a blade in this study involved taking the blade out of the clamping system and then clamping back immediately. The blades were not reclamped to the same torque but reclamped only to ensure the blade was secure between the jaws of the clamp. The reason for not using precise torque measurements was the permanent deformation of the cork material during every clamping process, which meant that consistent torque was not achievable during reclamping of the blade.

The variations to the experimental process described above were included in 300 inspections carried out on the four blades. These 300 inspections were divided into five separate sets of inspections, comprising 50 or 100 inspections on each blade. Table 3-1 shows the five sets of inspections. This Table details the number of inspections carried

out before a blade was reclamped and the coupling material renewed. The inspections were split into batches to avoid exposing one blade/crack to more than 100 inspections. This maximum of 100 inspections was arbitrarily chosen and the effect of exposing the blade/crack to this level of excitation is uncertain. However, after the 50 or 100 inspections, there was no visual evidence of surface damage to the blade root or obvious propagation of the crack. It must be noted that in a real inspection scenario, turbine blades will not be exposed to this high level of ultrasonic excitation.

Table 3-1 Experimental procedure split into five separate sets of repeated inspections on the four turbine blades.

Blade	Total number of inspections	Excitation time (seconds)	Number of inspections before reclamping	Number of inspections before replacing coupling material
B1	100	0.6	50	10
B2	50	0.6	10	5
B3	50	0.6	10	5
B4	50	1	1	1
	50	1	5	5

It was impractical to show all 300 imaging results in this Thesis. Instead, the results are illustrated using the temperature rise profile of the heat generated by a crack and a boxplot that illustrates the variability caused by the variations introduced to the experimental process. Figure 3-8 shows an example of the temperature rise profile of a crack for one inspection. This Figure illustrates crack heating during excitation and after the excitation is turned off at approximately 0.4 seconds. The x-axis represents the excitation time, while the y-axis, the temperature rise of the crack. The temperature rise,

represented in digital levels (d.l.), was computed as the contrast between an average pixel intensity of a specified region of interest around the crack and an average of a background area elsewhere in the image. Furthermore, the red dashed line in Figure 3-8 represents the chosen detection threshold, which was set at three times the background noise level. Any heat signal above this threshold was discernible in the final thermosonic image.

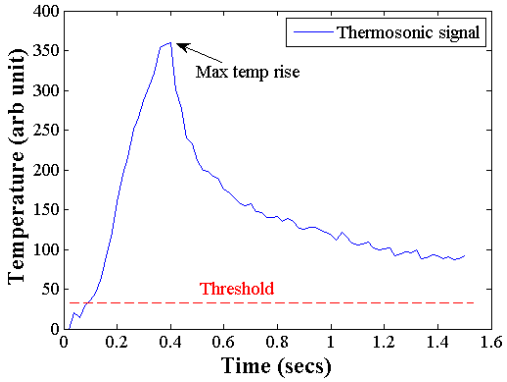

Figure 3-8 Temperature rise profile of a crack heat signal.

It is worth noting that for uncooled IR cameras the digital level for a corresponding temperature can vary slightly. This variation is due to changes to the temperature of the internal camera body or changes to the ambient temperature of the scene. This is typical of uncooled cameras and it is because the temperature of their detectors are not precisely controlled, as in the case of a cooled camera [111]. This is however the main reason why uncooled cameras are smaller and less expensive. In this work, variation of the camera's digital levels was mitigated by carrying out inspections after a period when the internal

temperature of the camera was deemed to be stable and with the ambient temperature of the surrounding environment also stable. This stability was verified prior to carrying out this study by measuring the temperature of a stationary scene over a period of time. Furthermore, the temperature rise generated by the cracks was not large enough to distort the digital levels of the camera. Nevertheless, it must be noted that absolute temperature was not important in this study, but rather that the temperature was above the specified threshold level.

3.2.6 Reliability study

The objective of this study was to assess the reliability of the developed thermosonic technique on 60 cracked turbine blades. Three consecutive inspections were carried out on each blade, taking approximately two minutes to complete, and this included blade clamping, excitation, image processing and interpretation of results. The coupling material was changed for each set of three inspections on a blade. Three inspections were conducted per blade to improve the reliability of the inspection technique. These additional inspections did not adversely extend the inspection time window for each blade, but importantly could provide additional information about the reliability of the technique. Reliability was assessed in terms of whether or not the known crack in each blade generated a discernible heat signal in all three thermosonic inspections.

3.3 Results

3.3.1 Thermosonic excitation parameter study

Figure 3-9 shows the effect on crack temperature rise when the four different excitation parameters are varied. Figure 3-9 (a) shows the result for the horn static force, (b) coupling material, (c) vibration amplitude and (d) excitation time. All five tests for each parameter setting produced a detectable heat signal from the crack. Furthermore, the crack temperature rise for the five different tests of each parameter setting is represented by a box plot, as shown in Figure 3-9. The box-plots show the median and quartiles of the five different tests, while the whiskers show the maximum and minimum data points. The horn static force was varied using the spring support system attached to the rear of the ultrasonic horn shown in Figure 3-4. Ten force levels between 22 N and 107 N were used. Figure 3-9 (a) shows a general increase in crack temperature rise as the horn static force increases. This increase in crack heating at higher horn forces was also seen in a similar study carried out by Perez et al. [94]. This increase in crack detectability may be attributed to the increased chaos in the excitation as the horn force increases [72, 81]. Evidence of this increased chaos can also be seen in the increased variability of the crack temperature rise of the five tests (i.e. box plot), particularly at 98 N and 107 N.

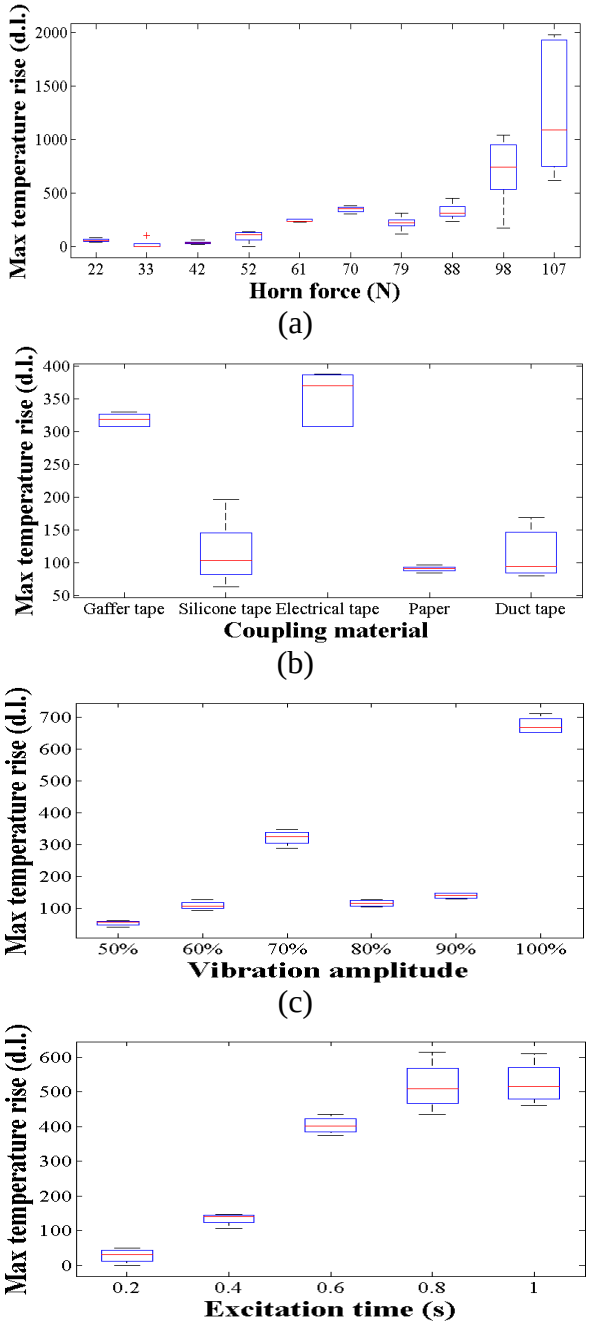

Figure 3-9 Crack temperature rise with varying (a) horn static force (b) coupling material (c) vibration amplitude (d) excitation time. Note: the box-plots show the median (red line) and quartiles (blue line) of the five different tests, while the whiskers show the maximum and minimum data points (black lines).

Five different coupling materials were investigated in this study: gaffer tape, silicone tape, electrical insulating tape, duct tape and paper. Duct tape has been used in several other studies [31, 44, 75] while paper has been mentioned as a suitable material [96, 112]. However, the other three coupling materials had not been reported in literature. Figure 3-9 (b) shows electrical tape with the highest average crack temperature rise, closely followed by gaffer tape. Duct tape which is commonly used had a much lower crack temperature rise, along with silicone tape and paper. However, paper had the lowest variability between the five tests.

The next parameter investigated was the vibration amplitude and the result is shown in Figure 3-9 (c). The vibration amplitude of the horn tip was controlled by the ultrasonic generator between 50 - 100% of the maximum amplitude. The maximum amplitude (i.e. 100%) of the horn tip, with no loading, was 6.7 μm. The crack temperature rise was highest at 100% amplitude; however, the temperature rise at 80% and 90% deviated from the increasing trend between 50% and 70%. The reason for this deviation is presently unclear. It has been speculated that it is related to the configuration of the ultrasonic generator at those two settings, although this hypothesis is unsubstantiated.

Finally, Figure 3-9 (d) shows the result for the excitation time, varied between 0.2 and 1 second. This time range was considered reasonable to investigate as the excitation in time used in most thermosonic tests in literature fall within this range [45, 50, 72, 75, 94,

113]. Figure 3-9 (d) shows an increase in the crack temperature rise as the excitation time increased, although the temperature rise at 0.8 and 1 second were identical. This study has shown that the crack temperature rise does vary with variation of the parameter settings. To ensure the highest probability of crack detection on the blade type set out for this study (i.e. 60 blades), the following parameter settings that achieved the highest crack temperature rise were used;

- Horn static force - 107 N
- Coupling material - electrical tape
- Vibration amplitude - 100%
- Excitation time - 1 second

The excitation parameter settings shown above are the same as the baseline settings except for the horn static force which is now 107 N as opposed to 70 N.

3.3.2 Repeatability study

The results of this study are illustrated in Figure 3-10 - Figure 3-14. Each Figure has two parts: (a) shows the temperature rise profiles of the crack heat signal for each set of 50 or 100 inspections, while (b) further illustrates the variability of the maximum temperature rise due to reclamping and renewal of coupling material. It is important to note that for each set of 50 or 100 repeated inspections, a 15 second delay was allowed between inspections to ensure any residual heat at the crack completely dissipated. This was to

avoid any build-up of heat in consecutive tests, which would distort the measured temperature rise.

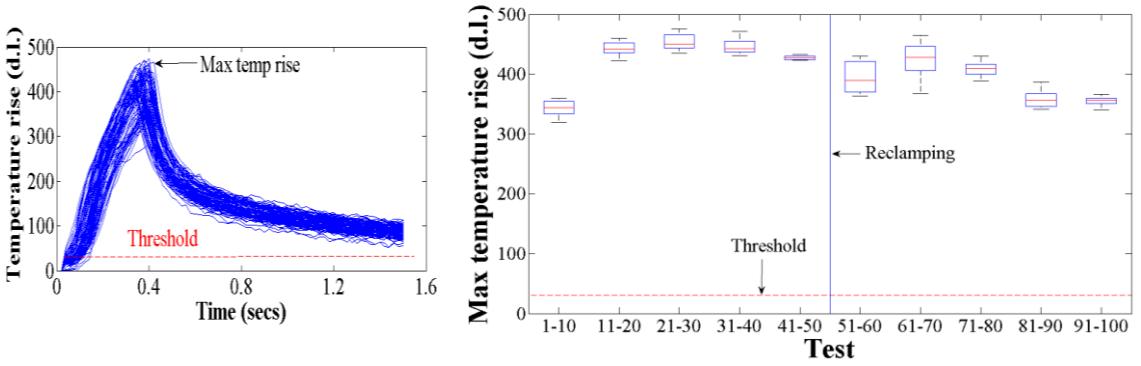

(a) (b)

Figure 3-10 (a) Temperature rise profile of 100 inspections on blade B1 with reclamping after 50 inspections and coupling material renewed after 10 inspections.

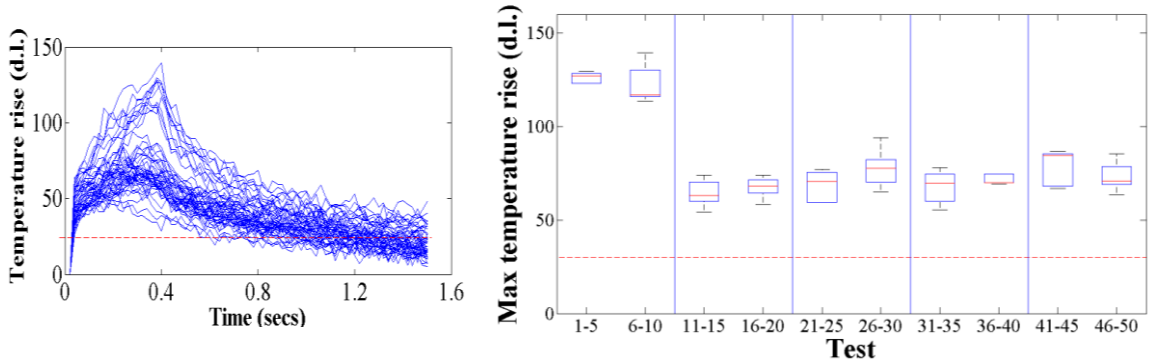

(a) (b)

Figure 3-11 Temperature rise profile of 50 inspections on blade B2 with reclamping after 10 inspections and coupling material renewed after 5 inspections.

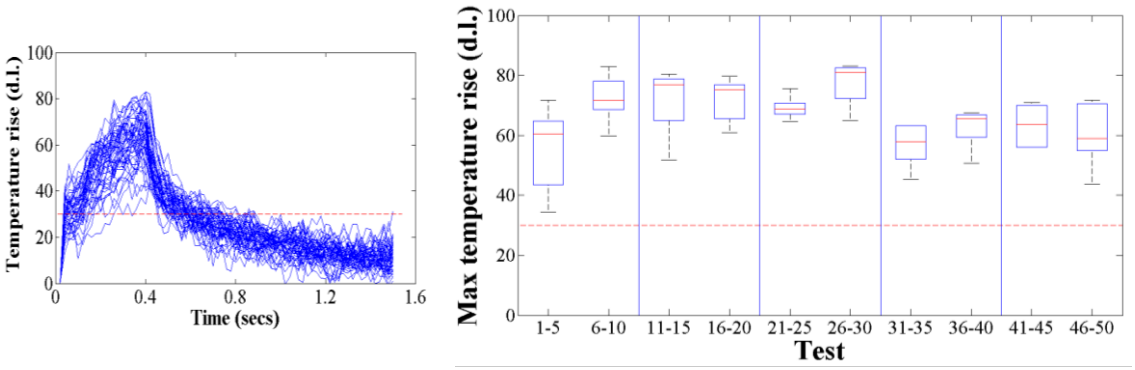

(a) (b)

Figure 3-12 Temperature rise profile of 50 inspections on blade B3 with reclamping after 10 inspections and coupling material renewed after 5 inspections.

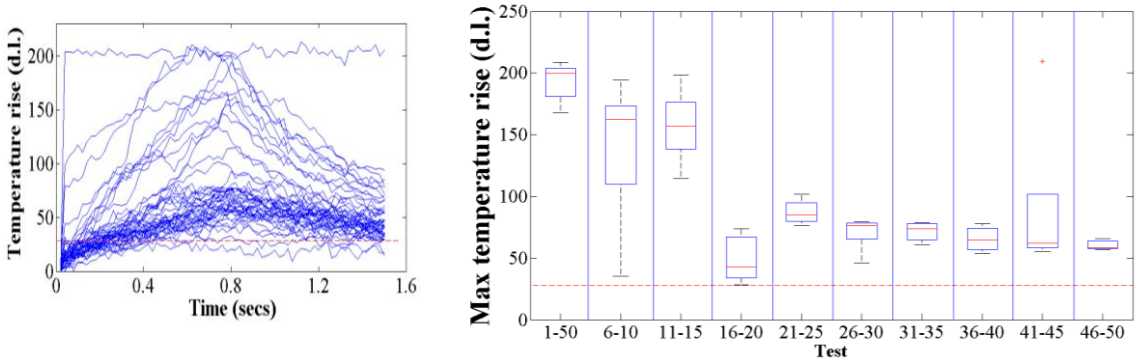

(a) (b)

Figure 3-13 Temperature rise profile of 50 inspections on blade B4 with reclamping after 5 inspections and coupling material renewed after 5 inspections.

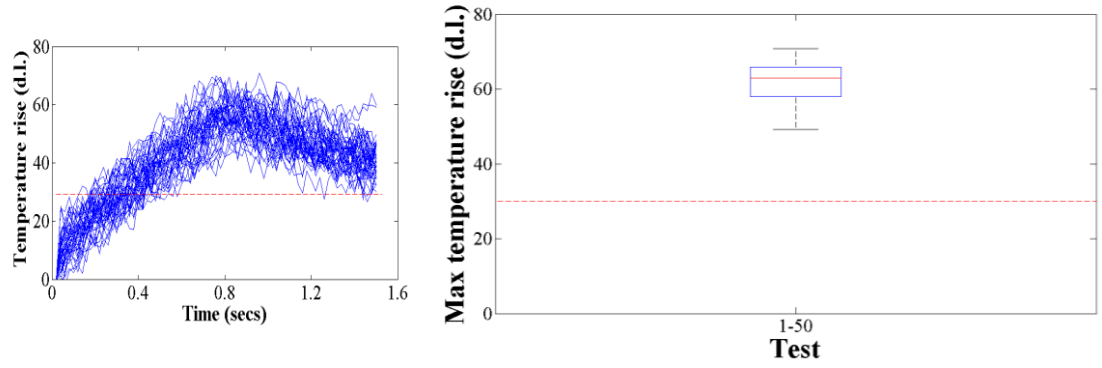

(a) (b)

Figure 3-14 Temperature rise profile of 50 inspections for blade B4 with both variations included after one inspection.

In Figure 3-10 (a) - Figure 3-14 (a), the shape of the temperature rise profiles within each set of inspections show a similar trend, in terms of the initial temperature rise and subsequent decay. However, some variation in the amplitude of the temperature rise profiles can be seen, with the most significant variation seen in the set of 50 inspections in Figure 3-13 (a). Firstly, the variation between the temperature rise profiles in Figure 3-10 (a) - Figure 3-14 (a) is primarily as a result of the differences in the respective crack characteristics (i.e. morphology) and the excitation applied at the cracks. The significant variation seen in the set of 50 inspections in Figure 3-13 (a) may be as a result of a greater change in the clamping conditions during the inspection intervals, compared to the other sets of repeated inspections on that blade. Although Figure 3-10 (a) - Figure 3-14 (a) gives an overall view of the temperature rise variation for each set of inspection, it does not highlight the variation caused by the change in clamping conditions or coupling material.

Figure 3-10 (b) - Figure 3-14 (b) presents a boxplot illustrating the variation of the maximum temperature rise due to the change in clamping conditions and coupling material. In these Figures, a new boxplot represents a change in coupling material, the solid vertical blue line represents a change in clamping condition and the dashed horizontal red line indicates the detection threshold. First thing to note in Figure 3-10 (b) - Figure 3-14 (b) is the variability of the temperature rise within each box plot, which is when the experimental process is unchanged (i.e. same coupling material and clamping

conditions). This variability was expected given the inherent non-repeatability of the excitation. However, more interesting was the effect caused by changes to the experimental process in repeated tests. For each set of inspections, the level of variability differed between a change in coupling material or clamping. In a few cases the change in the temperature rise range (between maximum and minimum) is significant, such as after test 10 in Figure 3-11 and after test 15 in Figure 3-13. However, in most cases, the change in the temperature rise range was not as significant and are of similar magnitude to the range seen when the experimental process is kept constant.

Despite the variations in the temperature rise generated by the respective cracks in repeated tests, the maximum temperature rise in all 300 inspections was above the specified threshold. This means the crack in every inspection was detected, irrespective of the inherent variability of the excitation or changes in experimental process. This set of results demonstrated the repeatability and robustness of the thermosonic technique developed in this study.

3.3.3 Reliability study

After establishing a robust inspection process, all 60 cracked turbine blades were inspected. The known cracks in 52 blades generated a heat signal in all three inspections completed for each blade, while the cracks in 5 blades generated a heat signal in only one inspection and no discernible heat signal was seen for the remaining 3 blades. As

mentioned in Section 3.2.6, the reliability of the thermosonic technique developed in this study was to be assessed in terms of whether the crack was detected in all three inspections. This approach gives a more accurate measure of the reliability of the technique on this set of blades. Therefore, it can be concluded that the technique developed in this work was reliable for detecting the cracks in 52 out of the 60 turbine blades (i.e. POD of ~86%) .

Figure 3-15 (a) and (b) respectively show images of a positive and negative detection case. This Figure highlights the total area of the image covered by the blade, which is relatively small. The field of view (FOV) of the camera, with the blade in focus, was approximately 200 mm x 150 mm (i.e. Horizontal x Vertical). This FOV was large compared to the size of the blade in the image. Nevertheless, the heat signal generated by the crack was still visible in the image as shown in Figure 3-15 (a). In Figure 3-15 (a), the crack heat signal in red (hotter) is distinguishable from the rest of the blade area, which mostly appear blue (colder). This level of contrast between the known crack location and other parts of the image allowed for easy interpretation of the results, and this was typical of the positive detection cases. However, for the negative detection case shown in Figure 3-15 (b), the heat signal shown in the vicinity of the known crack location appears colder than the rest of the blade which is crack free. This indicates that the crack generated little or no heat. The heat distribution seen across the blade area is simply due to the vibration of the material.

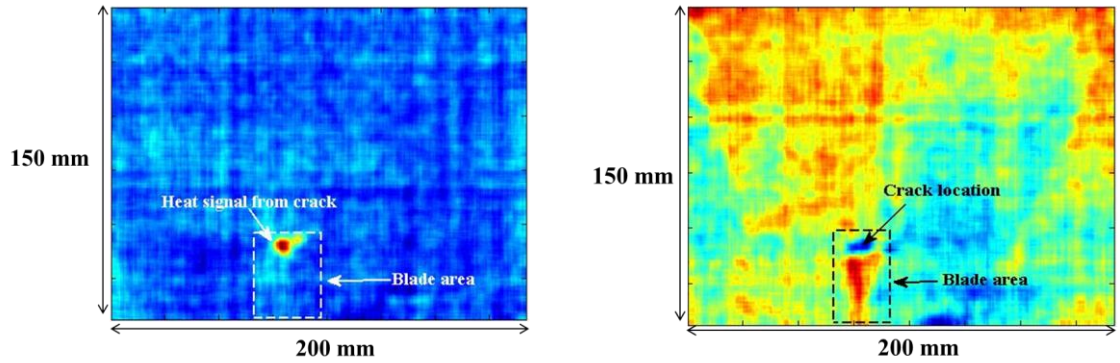

(a) (b)

Figure 3-15 Thermosonic image result (a) crack generated a discernible heat signal (b) no heat signal generated by crack.

The three cracks not detected may be attributed to either the local vibration excited at crack or the noise floor of the IR camera. The characteristics of the local vibration at the crack play an important role in activating the rubbing or clapping motion of the crack faces that generates heat [55, 65, 80]. If the vibration modes that produce this rubbing action are not excited or the vibration amplitude is not sufficient, then little or no heat will be generated and the crack may go undetected. However, if heat is generated, but significantly below the IR camera noise floor level, the crack may go undetected, irrespective of image processing. It is difficult to ascertain whether the non-detection of the three cracks was due to the excitation or the IR camera used in this study. However, one way to eliminate the possibility of the latter is to use more sensitive IR camera, such as a cooled camera.

3.4 Discussion

The aim of the work presented in this Chapter was to assess the reliability of thermosonics as a screening technique on a large set of turbine blades with real fatigue cracks. Results from this work demonstrated a robust experimental process that produced a high degree of repeatability and a high POD. The high POD compares favourably with the results in a similar study carried out by Guo and Ruhge [92], although the authors used larger turbine blades.

The results obtained in the repeatability study showed that the non-repeatability of the excitation process did not affect the consistency of positive results in repeated inspections. Furthermore, the controlled variations in the experimental setup did not influence the consistency of results either. This however does not negate the view of several researchers which is that the thermosonic technique is non-repeatable [55, 75]. Their assertion primarily relates to the variability of the measured temperature rise and not the outcome of an inspection, which is the presence or absence of a defect. This variability of the measured temperature rise from test-to-test was also seen in this study. However, the adopted hit/miss analysis of the results, which is typically associated with thermosonics, obscures this variability. Therefore, if thermosonics is to be used as a screening technique for the presence or absence of defects, the important question is understanding how the non-repeatability of the excitation affects the outcome of an inspection, which in this study, had no effect.

The high degree of repeatability and high POD achieved in this work suggests the vibration levels excited in the blades were consistently above the threshold required to detect the known cracks. This consistent level of vibration may be attributed to the horn static force used in the inspections; although, other factors such as the vibration isolation material (i.e. cork) and the coupling material (i.e. electrical tape) may have also contributed. The use of vibration isolation material has been shown to improve the energy coupled into the specimen, which consequently increases the heat generated by a crack [94]. Similarly, the choice of coupling material was shown in this study to have a significant effect on the amount of heat generated by a crack. Han et al. [31] has also shown the effect the choice of coupling material can have on crack detectability. However, the horn static force has been shown to be a major, if not the most important experimental variable that influences crack heating [50, 90, 94]. This suggests that repeatable results may be achieved if the horn static force is consistent in repeated inspections on a component or between similar components. However, the required horn static force for reliable crack detection for a component must be obtained empirically, as it will depend on the component geometry, defect location and experimental setup.

The high POD from inspection of the 60 turbine blades was encouraging, considering the reliability concerns associated with the thermosonic technique. If this was a real inspection scenario where thermosonics was used as a screening technique and the defective status of the blades were unknown, the 52 blades with cracks detected in all

three inspections would have been rejected. The remaining 8 blades with cracks not detected in all three inspections would go through the mandatory FPI cleaning and inspection process where the cracks would have been later detected. The value of using thermosonics in this scenario is the cost savings that would have been realised by not putting 87% of the 60 blades through the cleaning and FPI process. Importantly, in the overall NDE associated with these blades, all the defective blades would have been detected but at a lower cost. . The total cost savings in this scenario would have been approximately £1,092 (£21 inspection cost per blade). It must be noted that the inspections carried out in this study were purely experimental and thus the two minute inspection time per blade exceeded the target one minute inspection time required for the business case to be valid. The experimental setup and inspection process can certainly be optimised to significantly reduce the inspection time per blade; however, this is best done after the technique has been shown to be reliable and fit-for-purpose.

Image processing plays an important role in detection of cracks in thermosonics [61, 75, 78], and its importance to this study cannot be over emphasized. This was particularly due to the IR camera used in the study. Uncooled cameras generally have a much higher baseline noise level compared with cooled cameras, and this noise level sometimes lie in the range of the temperature rise generated by a crack. This consequently prevents easy discrimination between the background and heat signal in the raw thermal images, thus the need for further image processing. Polimeno et al. [78] also used an uncooled camera

in their study and found it necessary to use further imaging processing techniques to discriminate a crack heat signal. Conversely, no image processing or at most only background subtraction is generally required for raw images obtained from cooled cameras [29, 30, 34, 65, 77, 81]. However, some researchers who have employed cooled cameras also found additional image processing to be useful in further reducing noise in the raw thermal images [47, 75]. This demonstrates the importance of image processing in thermosonics inspection, even when using advanced and expensive IR cameras.

Overall, thermosonics was shown to be reliable for detecting majority of the cracks in the set of 60 blades. However, in the inspection process there was no reliable method to determine whether or not the vibration excited in a blade was sufficient to detect the known cracks. In a situation where there is no prior knowledge of the presence of a crack on the component, having confidence in the vibration level excited in the component is important to ensure the inspection is considered reliable [75, 86, 105]. The next Chapter of this Thesis will explore the application of the Heating Index as tool for monitoring the vibration excited in a component during a thermosonic inspection.

3.5 Review of chapter

This Chapter investigated the reliability of thermosonics as a screening technique for finding cracks on a set of 60 turbine blades. Prior to inspection of all 60 blades, the excitation parameters were optimised and the repeatability of the thermosonic technique

was investigated. The optimised parameter settings determined in this study were: horn static force (107 N), vibration amplitude (100%), excitation time (1 second) and coupling material (electrical tape). After establishing an optimised testing technique, a repeatability study was carried out. A total of 300 tests were completed on four representative blades using a hit/miss approach. The known cracks in all four blades were detected in the 300 tests, making the testing technique 100% repeatable. Furthermore, variations in the excitation, which is inherent in the testing technique and also variations intentionally included to the testing process did not affect repeatability. Finally, the 60 blades set out for the empirical study were inspected. Each inspection comprised of three tests lasting no longer than 2 minutes. The known cracks in 52 out of the 60 blades inspected generated a detectable heat signal. These results demonstrated the robustness and crack detection capability of the thermosonic technique developed in this study.

Chapter 4

Validation of the Heating Index for a reliable thermosonic inspection

4.1 Introduction

4.1.1 Background

There has been growing industrial interest in thermosonics over the last decade because of its capability to rapidly detect defects in large or complex-shaped components [28, 77, 81]. In addition, thermosonics is known to detect defects missed by conventional methods such as FPI [95]. However, lack of repeatability of the technique has meant thermosonics has largely remained a laboratory method, rather than a reliable industrial NDT method [55, 75, 114]. The poor repeatability is related to the chaotic nature of the excitation mechanism, particularly when using an ultrasonic horn as the exciter [25, 68, 75]. The inconsistency of the excitation can lead to cracks being missed if sufficient vibrational energy is not excited at the crack location. If the reliability of the excitation process is fully addressed, this would be a major step in thermosonics becoming an industrial NDT technique for a number of applications.

Morbidini et al. [75] have proposed a calibration methodology to address the repeatability issue concerning thermosonics. Their methodology determines whether or not the applied excitation is sufficient to detect a defect of interest [75]. The method

involves computing a reference parameter from the vibration waveform of the test-piece. This reference parameter is called the Heating Index (HI), and it represents the potential of the excited vibration field to generate heat at any position in the component [75]. The HI is useful because it correlates linearly with the measured temperature rise from a defect [68, 75]. This linear relationship enables prediction of a threshold HI required to generate the minimum detectable temperature rise from a defect. The threshold HI is then used in subsequent tests as a reference parameter to ensure a test has been carried out satisfactorily. Results from Morbidini et al.'s studies showed the linear relationship between the HI and temperature rise to be excellent for cracks in simple beams [75], but poorer for cracks in complex geometries such as turbine blades [6].

This Chapter evaluates the linear relationship between the computed HI and the measured temperature rise from a crack on a turbine blade. This evaluation is important as it forms the basis of determining a threshold vibration level for a reliable inspection. Furthermore, this Chapter compares three different vibration measuring devices that may be used to compute the HI. These devices include a laser vibrometer, microphone and a strain gauge. Fundamentally, the temperature rise generated by a crack is directly related to the characteristics of the measured vibration (i.e. frequency and amplitude), where the frequency determines the heating rate, and the amplitude determines the amount of energy available for dissipation as heat [25, 75, 114]. Therefore, the method used to capture the vibration required for computing the HI is of paramount importance.

In this Chapter, the basis and theory of the HI is first presented, after which the methodology used for computing the HI is described. Next, results showing the linear relationship between the HI and measured temperature rise from a crack are presented. Finally, the strength of the linear relationship seen in the results and also the performance of the three vibration measurement devices are evaluated.

4.1.2 Heating Index

The fundamental basis of the Heating Index (HI) is the increased heating at a defect location due to the extra damping introduced by the defect itself [75]. Damping is an important material property of any structure subjected to cyclic stress, and this type of damping is generally referred to as structural or hysteretic damping [24, 115, 116]. Structural damping is caused by internal friction within the material and at joints within the structure. When a structure is subjected to a vibratory load, the ability of the structure to convert the vibrational energy to heat per cycle of vibration is referred to as its specific damping capacity (SDC), ψ [24].

$$\psi = \frac{\Delta U}{U} \tag{4.1}$$

where ΔU is the strain energy dissipated per vibration cycle and U is the maximum strain energy stored in the structure per cycle. The presence of a defect in a structure increases its specific damping capacity, and this increase may be caused by friction of

adjacent surfaces of the defect during each vibration cycle [24, 117]. The vibrational energy dissipated as heat causes a temperature rise within the structure; however, this heat is greatest at defect locations, due to its larger specific damping capacity.

The increased heating at defect locations was used by Pye et al. as a novel NDT method for detecting defects in composites [24]. Their method is similar to thermosonics, except their excitation method relied on the resonant frequencies (tens of Hz) of the component. Furthermore, Pye et al. investigated the possibility of predicting the vibration-induced temperature rise from a defect using damping measurements [24]. The basis of their prediction algorithm was the proportional relationship between defect temperature rise, ΔT and the power dissipated at the defect, P (see Equation 4.2) [24]. Furthermore, the power dissipated at the defect, P is proportional to product of the square of the cyclic stress or vibration amplitude (σ^2), excitation frequency (f) and specific damping capacity (ψ), assuming all other material related properties remain constant (see Equation 4.3) [24].

$$\Delta T \ \alpha \ P \qquad \textbf{(4.2)}$$

$$P \ \alpha \ \sigma^2 f \psi \qquad \textbf{(4.3)}$$

Equations 4.2 and 4.3 shows that the vibration-induced temperature rise at a defect can be predicted from knowledge of the damping introduced by the defect and characteristics of the input vibration (i.e. excitation frequency and vibration amplitude). The predicted and measured temperature rise in Pye et al.'s work compared favourably, although the predicted results were generally higher with varying degrees of error for different crack sizes [24].

Similar to Pye et al. [24], Morbidini et al. [70] investigated the prediction of temperature rise from a crack based on the extra-damping introduced by the crack. However, Morbidini et al.'s work involved metals as opposed to composites used by Pye et al. Furthermore, the excitation method used by Morbidini et al. was that typically used in thermosonics (i.e. forced vibrations) as opposed to resonant vibration used by Pye et al. In Morbidini et al.'s work, the extra-damping introduced by the crack was measured as the difference between the damping of a cracked beam and that of an uncracked beam [70]. Results from Morbidini et al.'s work showed moderate correlation between the predicted and measured temperature rise for several cracks, although with disagreements in a few cases [70].

Morbidini et al.'s prediction algorithm is desirable; however, crack damping measurement can be complicated and time-consuming [97]. In this respect, Morbidini et al. [75] proposed a new parameter that is proportional to the power dissipated by a crack,

but does not require any knowledge of crack damping. The authors observed that, for a small crack size, damping was almost independent of strain amplitude and frequency. Consequently, the authors assumed that for a crack of fixed size, the power dissipated was mainly dependent on the square of the vibration amplitude and excitation frequency (see Equation 4.2) [75]. Using this assumption, Morbidini et al. [75] introduced the Energy Index (EI), which represents the instantaneous power dissipated by a crack, as described by Equation 4.4 [75].

$$EI(t) = \sum_{n} \frac{f_n}{f_o} \varepsilon_n^2 \qquad \textbf{(4.4)}$$

where ε is strain and f is frequency. $\frac{f_n}{f_o}$ represents weighting of the strain frequency components(i.e. f_n) relative to the fundamental frequency of the exciter (i.e. f_o) [75].

The Energy Index (EI) is proportional to the power released by the crack, but cannot be correlated directly to the temperature rise measured by the IR camera [75]. This is because the measured temperature rise at the surface depends on the crack characteristics, such as crack depth, and on the thermal properties of the material (e.g. thermal diffusivity). If the heat is generated very close to the surface, the instantaneous heat measured by the IR camera is directly proportional to the EI. However, if the heat is

generated deep into the crack, the measured temperature rise is a function of the heat generated earlier in time. In this case, the EI is not a suitable parameter to describe the heating behaviour of the vibrating crack. Instead, Morbidini et al. introduced the parameter called the Heating Index (HI) which accounts for the crack depth and material behaviour [75]:

$$HI(t) = \int_0^t e^{k(t-\tau)} EI(\tau)\, d\tau \qquad \textbf{(4.5)}$$

In Equation 4.5, t is time, τ is the time integration variable, k is a time constant. The HI is simply a weighted integral of the instantaneous heat (i.e. Energy Index), where the weighting function is an exponential decay which accounts for the crack depth and material behaviour. The time constant k, describes how fast the vibration-induced heat decays after the excitation is turned off, and this gives an indication of the depth from which the heat was generated [75]. A large value of k, typically above 30, indicates that the heat was generated close to the surface, while a value of k below 5 indicates the heat was generated deep into the crack [75]. The next sub-section describes the methodology used to compute the HI in this study.

4.2 Methodology for computing the Heating Index

4.2.1 Experimental setup

A schematic of the experimental setup used in this study is shown in Figure 4-1. The ultrasonic excitation system is the same as that described in Chapter 3; however, the turbine blade used in this study was different (i.e. different engine model). A representative blade is shown in Figure 4-2, measuring 74 mm in height and 45 mm at the widest point. The blade was secured in a steel holder (70 × 30 × 30 mm), specifically designed to fit the geometry of the blade root, see Figure 4-2. In this study, excitation was delivered to the blade holder rather than the blade directly, as was the case in Chapter 3. The main advantage is the reduced likelihood of surface damage that may occur on the blade due to high amplitude vibrations, and therefore this approach is generally regarded as a more acceptable way of inspecting the blades. The horn tip was spring-loaded to the base of the blade holder via a piece of electrical insulating tape. The horn static force was varied in each test, between 42 N and 163 N (maximum) to ensure a wide range of vibration levels (i.e. HI levels) were excited in the blade. A wide spread of HI levels was important in the evaluation of the linear relationship between the HI and crack temperature rise.

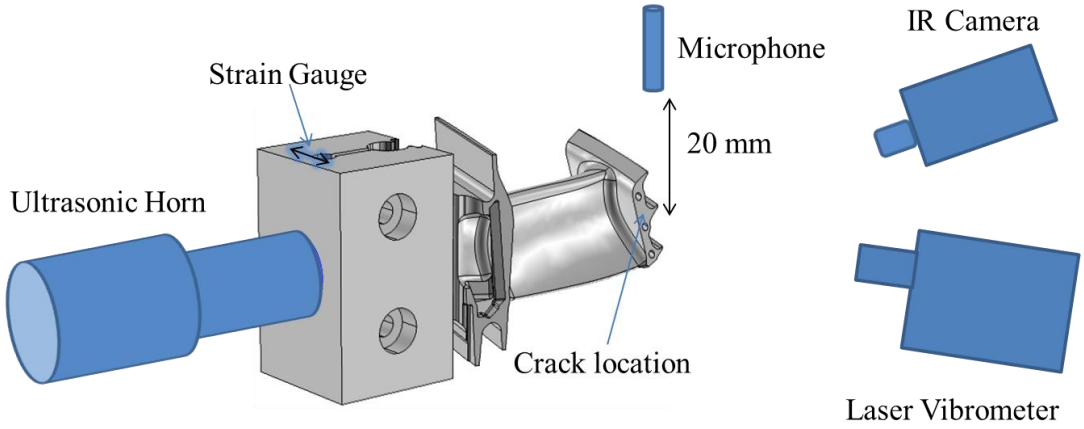

Figure 4-1 Schematic of experimental setup; comprising an ultrasonic horn, IR camera and vibration measuring devices (laser vibrometer microphone, strain gauge).

Figure 4-2 Image of turbine blade in blade holder.

The IR camera used in this study was a Cedip Silver 660M (cooled camera), with a detector array of 640 × 512 pixels, temperature sensitivity of 20 mK and a frame rate of up to 100 Hz. A cooled camera, as opposed to an uncooled camera, was required in this study for accurate measurement of crack temperature rise. In addition, images obtained

from the cooled IR camera required fewer post-processing steps compared to images obtained from the uncooled IR camera used in Chapter 3.

Figure 4-1 also shows the three different vibration measuring devices used in this study i.e. laser vibrometer, microphone and strain gauge. These measurement systems were chosen because of their capability of measuring the high frequencies typically excited in a thermosonic test. The strain gauge was a KYOWA KFG-120; 5 mm in length, 120.4 ohm resistance and a 2.09 gage factor. The strain gauge was permanently bonded to the blade holder as opposed to the crack location on the blade. This was due to the complexity of the geometry around the crack location. In addition, attaching and removing strain gauges from a large number of blades in a real inspection scenario would be time-consuming and costly. Morbidini et al. [6], in their HI study on turbine blades, also found it difficult to attach a strain gauge at the crack, and instead attached the strain gauge remote from the crack position. The strain gauge used in this study was connected to a calibrated FYLDE FE-537-SGA dynamic strain gauge amplifier with a 3dB frequency response of up to 100 kHz and gain of up to × 3000. One of the main advantages of a strain gauge is that it is significantly cheaper than a microphone or laser vibrometer.

The microphone employed in this study was a G.R.A.S 40DP pressure microphone, with a diameter of 3.2 mm and a frequency response of up to 140 kHz at ±3dB [118]. This

microphone was chosen because of its high bandwidth, which is amongst the highest for commercially available microphones. The microphone is classed as omni-directional; however, some form of directionality exists, as in most omni-directional microphones [119]. Figure 4-3 shows the directionality plot (i.e. polar plot) for the microphone [118]. This Figure shows that when sound is incident at 0 degrees the response level is the same at all frequency; however, as the angle of incidence increases, the microphone response level decreases, and this decrease is greater at higher frequencies. The characteristics of the polar plot shown in Figure 4-3 is typical of commercial microphones [119], which means responses from higher frequencies incident at an angle will be underestimated to varying degrees. This leads to a complicated sound field measured by the microphone. Nevertheless, even with this limitation, the microphone still presents a significant advantage, with its non-contact measurement capability and lower cost when compared to a laser vibrometer. In this study, the microphone was positioned at a distance of approximately 20 mm from the crack to ensure the vibration (or sound pressure) measurement closely represented the vibration excited at the crack location. The microphone distance from the crack (i.e. 20 mm) was specifically chosen to be in the far-field to ensure measurement errors due to near field effects were avoided [119]. The formula used to calculate the near-field distance is shown in Equation 4.6, where N is near field distance, D is diameter of source, f is frequency, c is sound velocity and λ is wavelength.

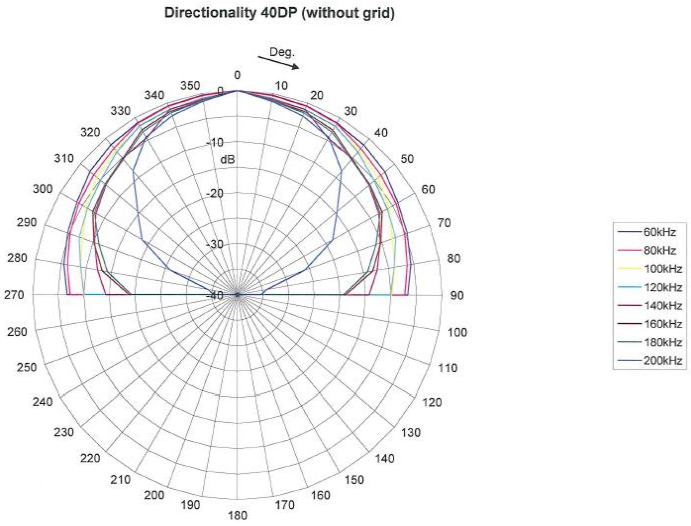

Figure 4-3 Directionality plot for GRAS Type 40DP pressure microphone (supplied by manufacturer, GRAS).

$$N = \frac{D^2 f}{4c} \tag{4.6}$$

The laser vibrometer system used in this study comprised a Polytec OFV-3001 controller (velocity decoder, 1MHz bandwidth) and OFV-3003 sensor head. A laser vibrometer was chosen because of its capability of measuring the surface vibration at the crack location. The laser beam is pointed at the surface and the amplitude and frequency of the vibration are extracted from the interference of the reflected laser and a reference laser beam [120]. The laser vibrometer was a single-point, out-of-plane vibrometer, meaning its capability was restricted to measurement of the out-of-plane velocity component of a point. This was considered a limitation because in-plane velocity components, which may contribute to crack heating, was not measured. All three

vibration measuring devices were connected to a 4-channel Lecroy WaveRunner oscilloscope, programmed to capture vibration for one second. The oscilloscope was controlled via National Instrument software (Labview) for simultaneous operation with the ultrasonic horn generator and IR camera.

4.2.2 Thermosonic inspection

Prior to the start of a test at least 20 background images of the blade were captured and then averaged to leave a single image representing the background. Next, the excitation was turned on for 0.5 seconds while the IR camera and oscilloscope simultaneously captured image and vibration data for one second respectively. One second was chosen to capture data during and post excitation. The captured images were processed in MATLAB using background subtraction. In this study, two different sets of tests, Set A and Set B, comprising 24 and 23 tests respectively were completed on the single cracked blade. The difference between the two sets of tests was the position of the microphone relative to the crack, although both at a distance of 20 mm from the crack. For Set A, the known crack was detected in all 24 tests, while for Set B, the crack was detected in 22 out of the 23 tests.

4.2.3 Computing the Heating Index

The first step in computing the HI is estimating the time constant *k* from the temperature decay profile of a crack [75]. Figure 4-4 (a) & (b) show, as an example, the temperature

profile of the crack for two different tests from Set B (test 8 & 23). Note in Figure 4-4 (a) 0.06 second delay between the start of IR camera measurements and excitation. In Figure 4-4 (a), the temperature gradually builds up and peaks at around 0.56 seconds, which is the time when the excitation was turned off, hence, the immediate temperature decay. However, Figure 4-4 (b) is different; in this case the temperature builds up but instead peaks earlier at around 0.34 seconds, decreases for a short period, before the final decay (around 0.56 seconds) due to the excitation being turned off.

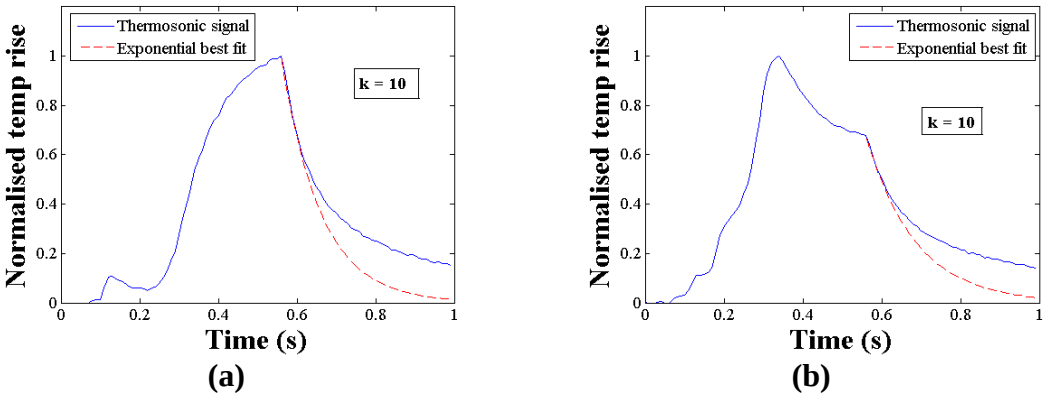

Figure 4-4 Temperature rise profile of two tests (solid line) from Set B and the exponential best-fit curve (dashed line) for the decay part of the temperature rise profile used to estimate the time constant *k*. (a) test 8, k = 10 (b) test 23, k = 10.

The *k* value was estimated from the shape of the temperature decay profile shown in Figure 4-4 (a) & (b). The decay profiles were approximated by an exponential decay function presented in Equation 4.7 [75]. In Equation 4.7, T_i is the initial temperature before decay and T is the final temperature of the exponential decay. Figure 4-4 shows the exponential best-fit curves (dashed red lines) that closely represents the temperature

decay profiles. In both cases the best-fit curves deviate towards the end of the decay. This is because the exponential function is a crude, but simple way of approximating the temperature decay [75]. However, more importantly for computing *k* is accurately representing the early part (i.e. initial decay) of temperature decay as this represents the short-time or immediate behaviour of the temperature decay [75]. In Figure 4-4 (a) and (b), the best-fit curves match the decay curves for 0.05 seconds (after 0.56 seconds), after which both curves begin to deviate. The computed *k* value for Figure 4-4 (a) and (b) was 10; however, more interestingly, the computed *k* value for the other 21 positive tests was also 10. This is however not always the case as seen in Morbidini et al.'s study where the computed *k* varied between tests on the same crack [75]. For a different blade/crack, the computed value will most likely be different, which is also seen in Morbidini et al.'s work where the *k* values ranged between 5 and 50 [75].

$$T = T_i e^{-kt} \tag{4.7}$$

The next step after estimating the time constant *k* is computing the Energy Index (EI). The EI of a vibration waveform is the sum of the product of the different frequency components and their respective amplitudes, as described by Equation 4.4. However, due to the transient nature of the vibration waveform typically seen in a thermosonic test, a Short-Time Fourier Transform (STFT) is first used to decompose the vibration waveform to its different frequency components (i.e. FFT) in short time segments. In

this study, the FFT of the vibration waveform was computed in 2 ms segments to reflect the transient nature of the vibration waveform.

Figure 4-5 and Figure 4-6 show the different stages in computing the HI for test 8 and test 23 from Set B respectively. Both figures show the respective vibration waveform (from laser vibrometer), STFT, EI profile and HI profile. As expected, the vibration waveforms for test 8 and 23 in Figure 4-5 (a) and Figure 4-6 (a) respectively were different; the former shows one sharp peak at around 0.1 seconds, while three different peaks can be seen in the latter between 0.1 and 0.3 seconds. The reason for the different vibration waveforms is due to the inherent chaotic nature of the excitation. This is further illustrated by their respective STFT in Figure 4-5 (b) and Figure 4-6 (b), which show the time-varying frequency content of the vibration waveforms, consisting of harmonics and multiples of the horn resonance. Figure 4-5 (b) and Figure 4-6 (b) clearly shows some frequency components appearing from the start of excitation, while some others appearing later in time, and this is different for the two tests. This gives a good visualisation of the complex nature of the excitation typically seen in thermosonics. The most dominant frequency component in both Figure 4-5 (b) and Figure 4-6 (b) is 80 kHz (2^{nd} harmonic of exciter resonance), and this evident by its strong presence throughout the duration of the excitation. Although other frequency components (i.e. harmonics and sub-harmonics due to non-linearities) can be seen, there

is no strong indication of exciter resonance at 40 kHz in Figure 4-5 (b) and Figure 4-6 (b). The STFT is important as it forms the basis for computing the EI profile.

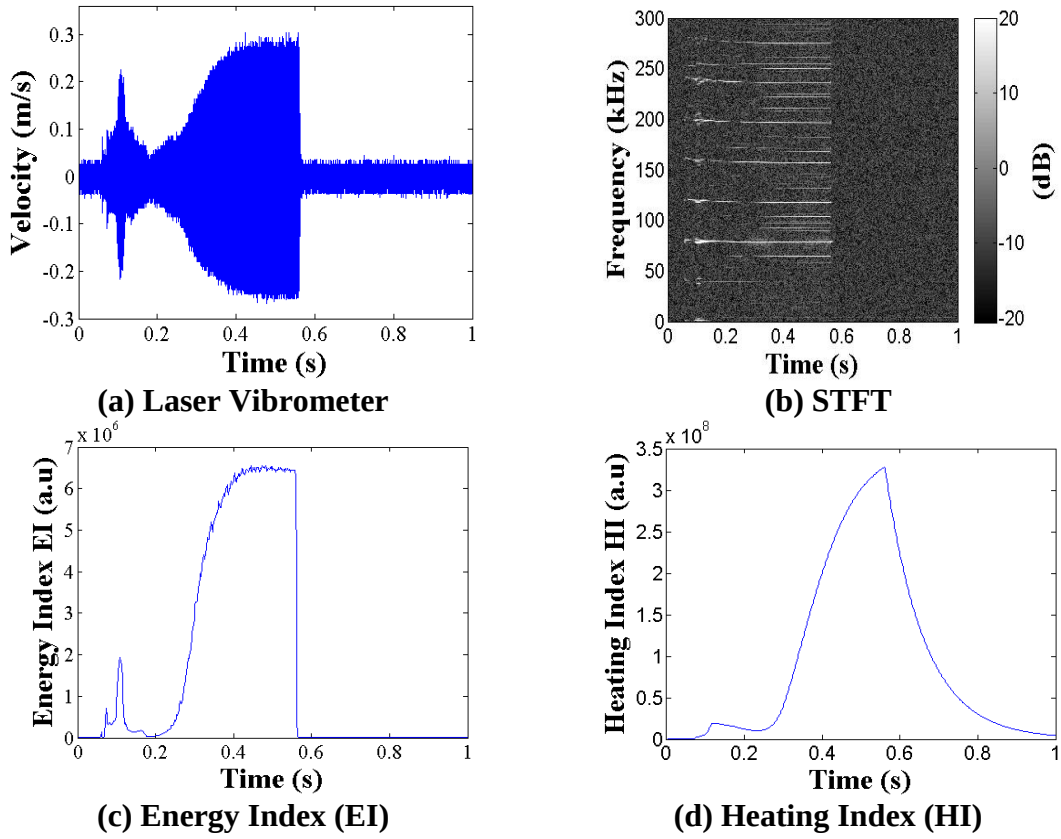

Figure 4-5 Vibration waveform, STFT, EI, and HI for test 8.

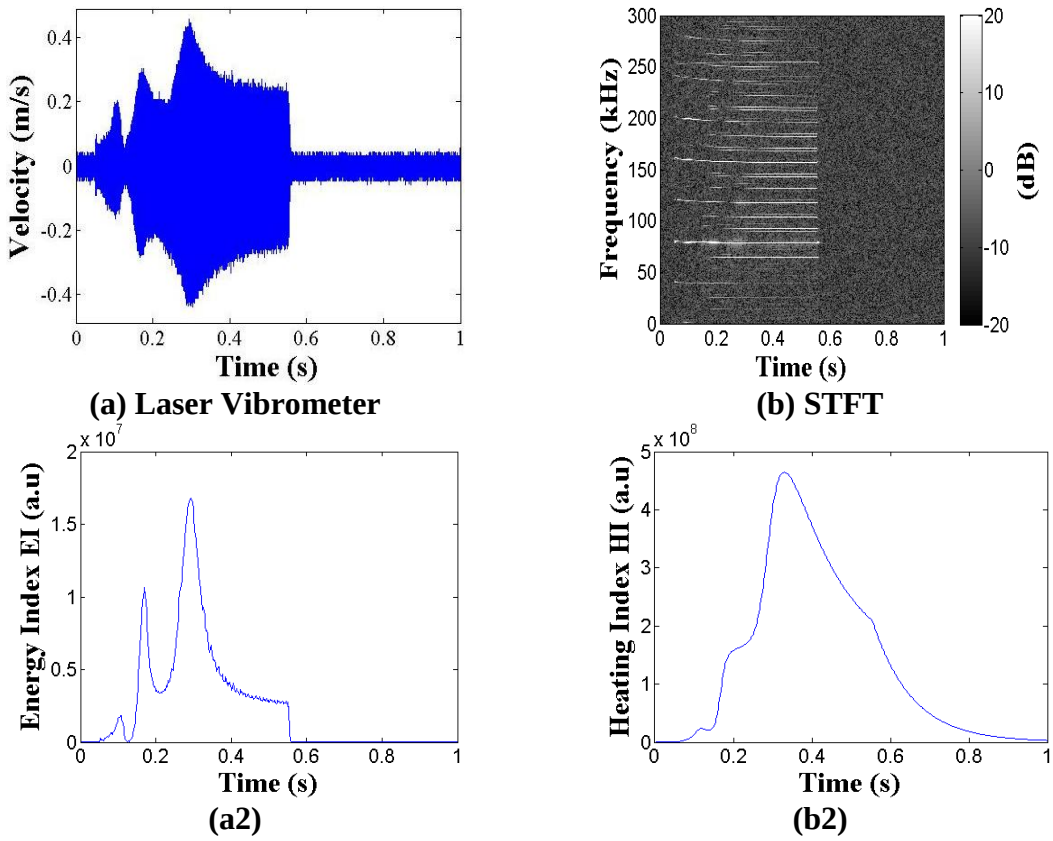

Figure 4-6 Vibration waveform, STFT, EI, and HI for test 23.

The computed EI profiles for test 8 and 23 are shown in Figure 4-5 (c) and Figure 4-6 (c) respectively. Both profiles are different, with the former having a small sharp peak around 0.1 second, while the latter three different sized peaks. These peaks can also be seen in their respective vibration waveforms in Figure 4-5 (a) and Figure 4-6 (a). The maximum EI represents the point during the vibration where the power released at the crack was greatest, which in Figure 4-5 (c) occurs just before the excitation was switched off (i.e. at 0.56 seconds), while in Figure 4-6 (c) the maximum EI occurred much earlier in time at around 0.29 seconds. As mentioned in Section 4.1.2, the EI

cannot be correlated directly to the measured temperature rise because the measured temperature rise also depends on the thermal response of the material and on the depth from which the heat was generated [75]. Instead, the HI is used to correlate to the measured temperature rise. Figure 4-5 (d) and Figure 4-6 (d) show the computed HI profiles for test 8 and 23 respectively. The HI profiles are different from their respective EI profiles because of the exponential weighting function (see Equation 4.5).

A comparison of the HI profile and the measured temperature rise for test 8 and 23 is better illustrated in Figure 4-7 (a) and (b) respectively. Both tests show very good agreement between the shape of the HI profile and the measured temperature rise, with all the peaks seen in the measured temperature rise also present in the HI profiles. However, more importantly is that the maximum temperature rise and maximum HI occurred at exactly the same time. This is important because the maximum HI represents the time during the vibration when the crack is most likely to be detected [68]. This agreement highlights the importance of using a function, in this case an exponential function [75], to account for the thermal response and crack depth.

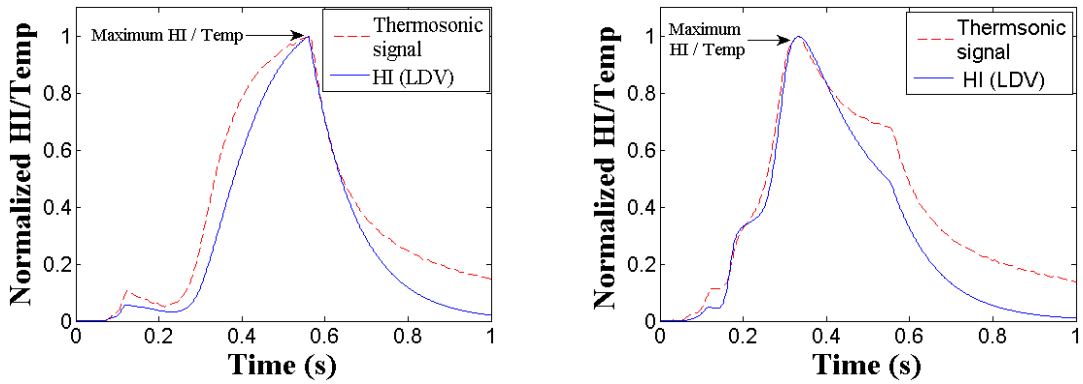

(a) Test 8 (b) Test 23

Figure 4-7 Comparison of normalised HI with normalised temperature rise for (a) test 8 (b) test 23.

4.3 Results

4.3.1 Examples of the HI computed from different vibration measurement devices

Figure 4-8 presents examples (from Set B) of comparisons between the shape of the normalised HI and the normalised temperature rise for six different tests. In general, the patterns observed in the 6 tests reflect the results for the other 17 tests not shown. Figure 4-8 also includes the HI computed from the vibration captured by the microphone and strain gauge. Figure 4-8 shows good agreement between the shape of the HI and temperature rise for the laser vibrometer, while the result for the microphone and strain gauge are mixed (i.e. good and poor results). For the laser vibrometer, the shape of the HI closely follows the shape of the temperature rise in all the tests except for test 4 (Figure 4-8 (b)) where there is a slight disagreement. In test 4, after approximately 0.3 seconds, the HI increases at a much faster rate than the temperature rise, leading to the maximum HI peaking at a different time (0.56 seconds) compared to the maximum

temperature rise (0.18 seconds). In this case, the maximum HI suggests that the crack would most likely be detected at 0.56 seconds rather than at 0.18 seconds when the crack generated the most heat.

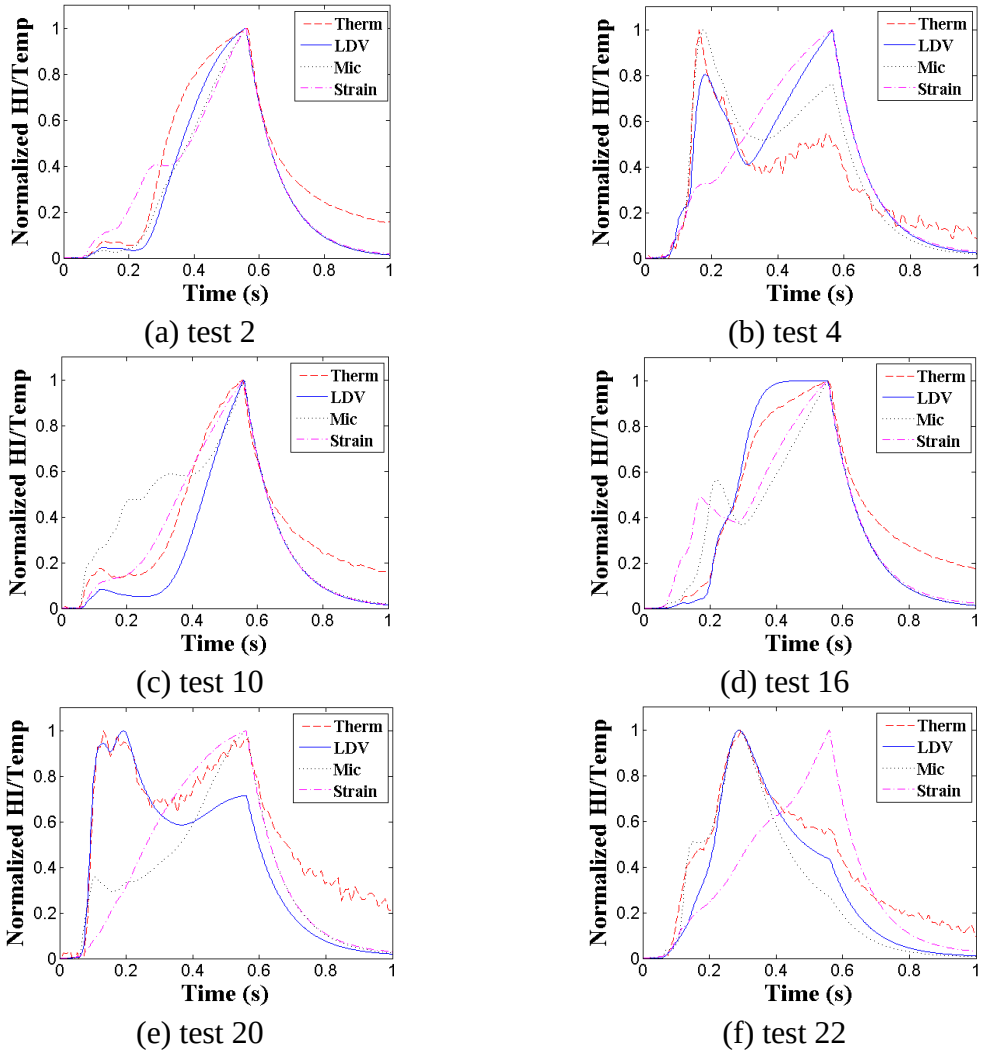

Figure 4-8 Comparison of the normalised HI vs. temperature rise for the three vibration measurement devices for several tests in Set B (a) test 2 (b) test 4 (c) test 10 (d) test 16 (e) test 20 (f) test 22.

For the microphone results, there is good agreement in test 2, 4 and 22; however, for test 10, 16 and 20, the agreement is only fair, and this because of the mismatch between certain sections of the profiles. For example in test 20, shown in Figure 4-8 (e), there is a significant difference between the trajectory of the HI and temperature rise. Again, this mismatch gives a false indication as to when the crack generated the most heat. For the strain gauge, the results in test 2 and 10 can be described as good, test 16 as fair, but test 4, 20 and 22 as poor. Tests 2 and 10 are described as good as most sections of the HI profile follow the temperature rise profile, whereas for test 16, which is described as fair, the HI profile follows the temperature rise profile except for the peak around 0.1 seconds. For test 4, 20 and 22, the shape of the HI profile does not match that of the temperature rise in any way. The results in this section shows that the vibration data captured in a test may be used to predict the heating profile of vibrating crack. However, in order to validate the HI parameter, a linear relationship must be established between the HI and the measured temperature rise [75].

4.3.2 Relationship between the HI and crack temperature rise

For the HI to be considered a valid parameter, a good degree of linear correlation must exist between the HI and measured temperature rise [75]. Morbidini et al. [75] demonstrated the linear relationship using the maximum temperature rise and the maximum HI as these two parameters represents the time during the excitation when the crack is most likely to be detected. Figure 4-9 shows the plot of maximum temperature

rise against maximum HI for the two sets of tests (i.e. Set A and Set B). The result for the 24 tests in Set A is shown in the first column of Figure 4-9, while the result for the 23 tests in Set B is shown in the second column. Furthermore, Figure 4-9 (a), (b) and (c) show the results for the laser vibrometer, microphone and strain gauge respectively. The HI for the laser vibrometer in Figure 4-9 (a) was computed using frequency components up to the highest frequency of interest (i.e. 300 kHz); however, for the microphone and strain gauge, the HI was computed using the maximum measurable frequency of the respective device, which are 140 kHz and 100 kHz respectively.

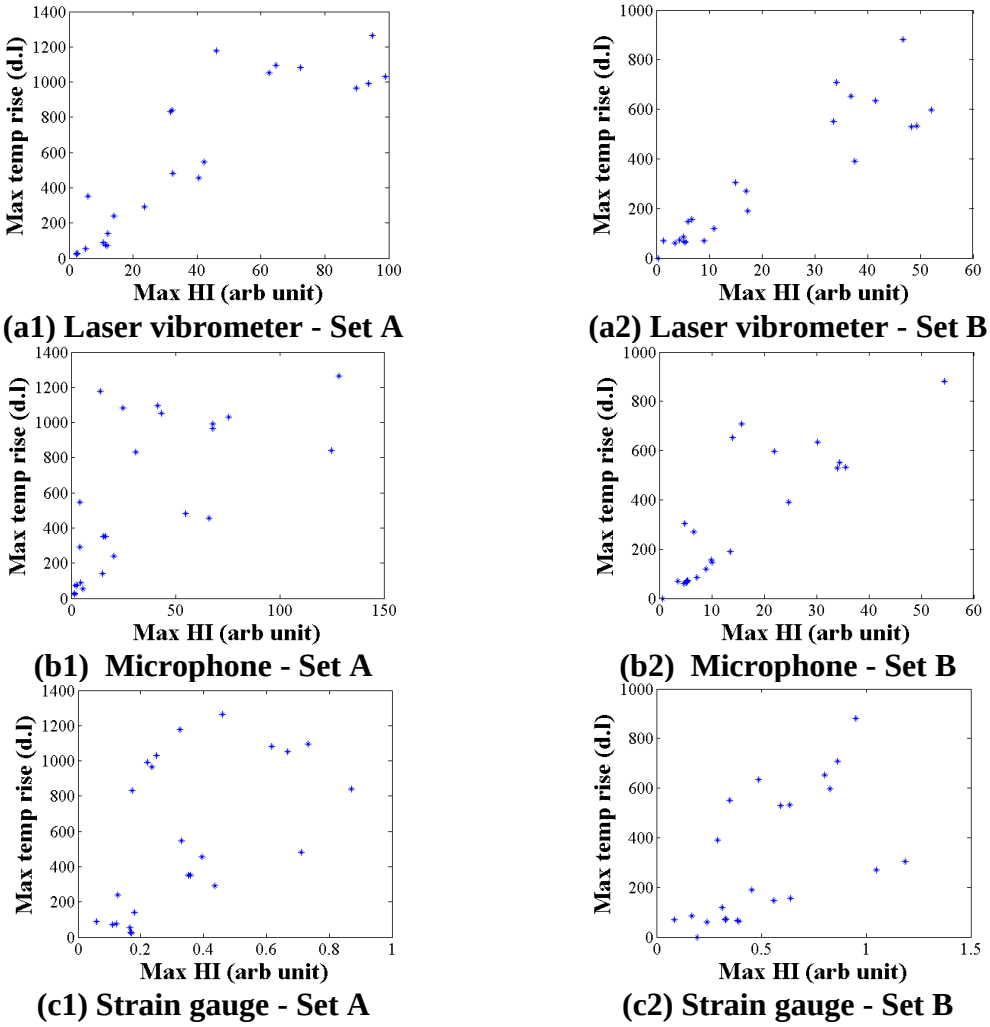

Figure 4-9 Maximum temp rise vs. maximum HI for Set A and Set B (a) Laser vibrometer (b) Microphone (c) Strain gauge.

The laser vibrometer results in Figure 4-9 (a1 & a2) show a linear trend with little scatter in the data, whereas for the strain gauge results (c1 & c2), significant scatter can be seen with no recognisable linear trend. The result for the microphone is mixed, where no clear linear relationship can be observed for Set A in Figure 4-9 (b1), whilst for Set B in Figure 4-9 (b2), there is evidence of a linear trend. In this study, the strength of linear

correlation was quantified using the square of the normalised correlation coefficient, r^2, described by Equation 4.8 [121]. The square of the correlation coefficient, also referred to as the coefficient of determination, is a useful statistical quantity that measures the proportion of variance of the dependent variable (i.e. temperature rise) that can be predicted from the independent variable (i.e. HI) [122]. The correlation coefficient always lies between +1 and -1; however, a coefficient between 0 and +1 was only valid in this study as crack temperature rise only increases with increasing HI [75]. For example, a coefficient of 0.7 means only 70% of the variation of the temperature rise can be predicted from the variation of the HI, while the remaining 30% of the variation cannot be explained by the linear relationship and is due to other unknown factors.

The strength of linear correlation in this thesis was classed into the following categories: strong, moderate, weak and no correlation. A strong correlation is one with a correlation coefficient > 0.7, moderate correlation between 0.4 and less than 0.7, weak correlation between 0.2 and less than 0.4 and no correlation between 0 and less than 0.2. This is an established classification seen in several fields where correlation coefficients are commonly used [122-124] and was therefore adopted in this study.

$$r_{xy} = \frac{\sum_1^N \left[x(n) - \bar{x}\right]\left[y(n) - \bar{y}\right]}{\left[\sum_1^N \left[x(n) - \bar{x}\right]^2 \sum_1^N \left[y(n) - \bar{y}\right]^2\right]^{1/2}} \qquad \textbf{(4.8)}$$

Table 4-1 shows the calculated correlation coefficient for Set A and Set B for the three vibration measurement devices. Table 4-1 shows the laser vibrometer with the largest coefficients for both Set A and Set B, followed by the microphone. The linear trend observed for the laser vibrometer in Figure 4-9 (a) is reflected in the computed coefficients of 0.77 and 0.85, and these values suggest a strong linear correlation between HI and temperature rise. Similarly, the absence of a linear trend for the strain gauge in Figure 4-9 (c) is also reflected in the correlation coefficients of 0.30 and 0.36, which can be described as weak. This is because a significant proportion of the variation of temperature rise cannot be associated with variation of the vibration levels (i.e. HI). The mixed coefficient for the microphone at 0.43 and 0.70 is also reflected in the plots in Figure 4-9 (b). The likely reasons for the different strengths of linear correlation for the vibration measuring devices are discussed in Section 4.4.

Table 4-1 Normalised correlation coefficient for Set A and Set B when using the maximum measurable frequency components of the respective vibration measuring devices.

Correlation coefficient r_{xy}^2	**Laser vibrometer**	**Microphone**	**Strain gauge**
Set A (24 tests)	0.77	0.43	0.30
Set B (23 tests)	0.85	0.70	0.36

The computation of the HI for the different vibration measurement devices involved the use different frequency components; up to 300 kHz for the laser vibrometer, up to 140 kHz for the microphone and up to 100 kHz for the strain gauge. Holland [65], Zhang [64] and Han [125] in their respective studies have shown the dependence of crack

heating on the excitation frequency. Therefore, it was reasonable to determine the effect of using different frequency components to compute the HI for the different devices. Figure 4-10 shows the revised results of Set A and Set B for the three devices when using only frequency components up to 100 kHz. Comparing the results in Figure 4-10 with Figure 4-9, there appears to be no obvious difference, and this is further confirmed with the new normalised correlation coefficients shown in Table 4-2. Table 4-2 shows only a marginal change, suggesting that frequency components above 100 kHz did not contribute significantly to the computed HI or the heat generated by the crack. Nevertheless, this conclusion can only be attributed to the blade/crack used in this study, as higher frequency components may contribute to the heat generated by other cracks. In such a case, a higher bandwidth device such as a laser vibrometer will have an advantage over the microphone and strain gauge.

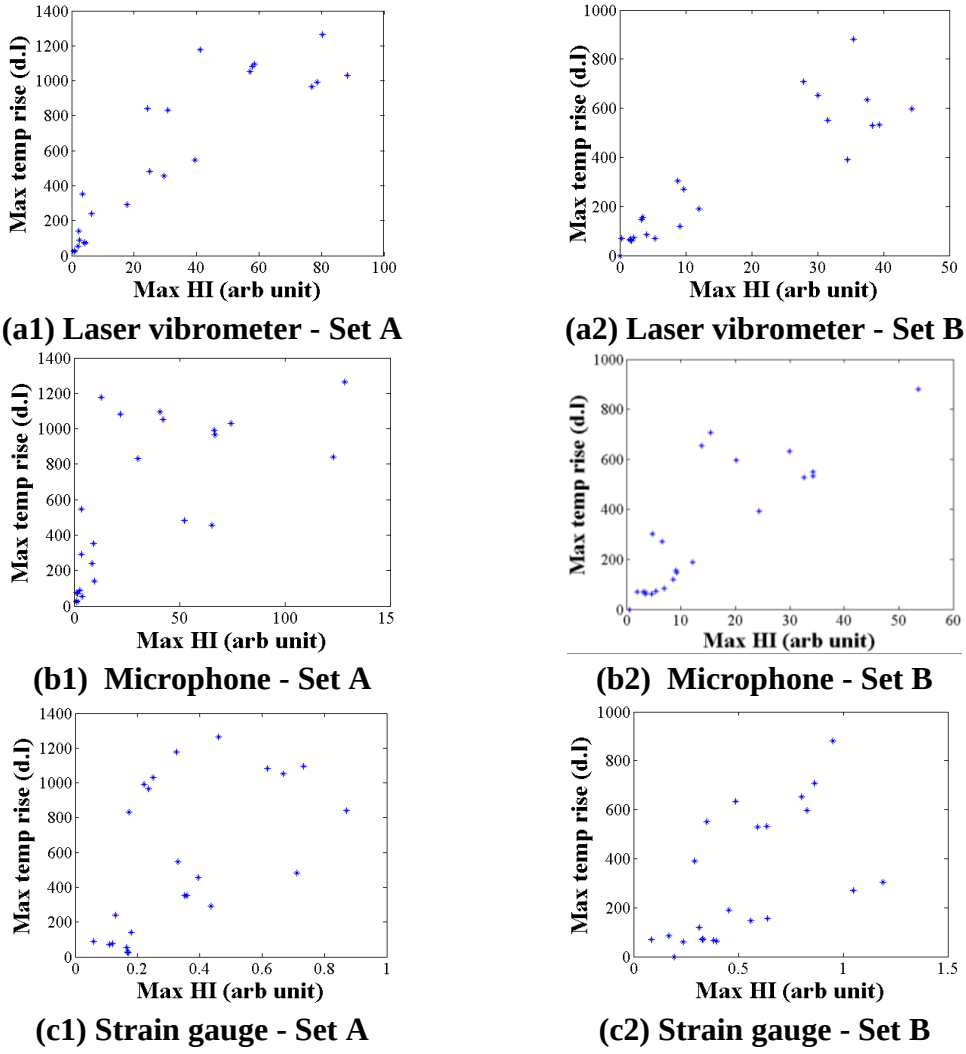

Figure 4-10 Maximum temp rise vs. maximum HI for Set A and Set B, using only frequency components up to only 100 kHz (a) Laser vibrometer (b) Microphone (c) Strain gauge.

Table 4-2 Normalised correlation coefficient for Set A and Set B when using frequency components up to only 100 kHz to compute the HI.

Correlation coefficient r_{xy}^2 (up to 100 kHz only)	**Laser vibrometer**	**Microphone**	**Strain gauge**
Set A (24 tests)	0.80	0.45	0.30
Set B (23 tests)	0.83	0.71	0.36

4.4 Discussion

Prior work by Morbidini et al. [6, 75] show the Heating Index (HI) to be a potentially useful parameter for assessing whether the excitation applied in an inspection is sufficient to detect a defect of interest. This is because of the linear relationship found between the HI and the measured temperature rise from a vibrating crack. However, this linear relationship was shown in Morbidini et al.'s work to be weak for turbine blades [6] compared to a simple beam [75]. The aim of this study was not only to build on Morbidini et al.'s work by further validating the HI on a turbine blade, but also to compare the strength of the linear relationship when using different vibration measurement devices to compute the HI. This comparison will highlight the advantages and limitations of different vibration measurement devices for computing the HI.

In this study, the HI was computed from the vibration captured by a strain gauge, microphone and laser vibrometer. Overall, the strength of linear correlation between the HI and temperature rise for the laser vibrometer was higher than that of the microphone and strain gauge. This was expected because the laser vibrometer measured the local vibration at the defect, which was not the case with the microphone and strain gauge. Several authors have demonstrated, in their respective studies, that the heat generated by a crack is directly related to the vibration at the crack location, and in those studies, a laser vibrometer or a strain gauge attached at the crack location were used [60, 75, 126].

The strength of the linear correlation for the strain gauge can be described as weak, and this was primarily due to the position of the strain gauge on the blade. Morbidini et al.'s [75] study has shown the strain gauge to be most effective when positioned at the crack location. In this study however, it was not possible to attach the strain gauge at the crack location, and as a result, not capture the vibration at the crack. This limitation presented an opportunity to attach the strain gauge in a more practical location i.e. blade holder, which would be the most likely and accepted attachment location in a real inspection scenario. The outcome however, was a weak correlation, which rules out the use of a strain gauge as a practical device for computing the HI on a turbine blade.

The strength of the linear correlation for the microphone was stronger than that of the strain gauge, although it can only be described as moderate. The reason for this may be due to the complicated nature of the vibration measured by the microphone, which is dictated by the microphone's relative position to the vibrating test-piece and other objects around the experimental station [120]. During a thermosonic test, the sound picked up by a microphone is sound pressure emanating not only from the crack location but also from the other parts of the test-piece and components attached to the test-piece (i.e. experimental setup) [10]. In addition, the microphone picks up reflected sound from surrounding objects. Consequently, the measured vibration will not be a true representation of the local vibration at the crack. This means that the characteristics of the vibration (i.e. frequency and amplitude) that do not directly contribute to crack

heating are used in the computation of the HI. This may be one of the reasons for the mixed and at best, modest linear correlation achieved by the microphone in this study. Morbidini et al.'s HI study on similar-sized turbine blades using a microphone provides the best comparison with the microphone results in this study, although their study did not compute the correlation coefficient between the HI and temperature rise. Nevertheless, the results (i.e. degree of linear correlation) in Morbidini et al.'s study compared favourably with the results seen in this study.

The ideal result in this study would be a correlation coefficient between 0.9 and 1. This level of correlation gives a high degree of confidence in predicting the threshold HI for a reliable inspection. This level of correlation would have been expected for the laser vibrometer, considering the vibration was captured at the crack location. Three possible reasons why this level of correlation was not achieved are: first, the assumption made in the formulation of the HI; second, dependency of crack heating on excitation frequency, and; third, the limitation of the laser vibrometer in measuring only out-of-plane vibration. Firstly, the assumption made in formulation of the HI is that the damping of a crack of fixed size is constant at all frequencies and amplitude. However, this is not strictly the case, as highlighted by several researchers [24, 127, 128] and also by Morbidini et al. [70] . These different studies show damping can vary with vibration amplitude and frequency, particularly with the former. The purpose however, of Morbidini et al.'s assumption, was to simplify the computation of the energy released by

a vibrating crack, which otherwise would require knowledge of the damping at the crack. However, by way of good experimental results in several studies [6, 75], including this one, this assumption is reasonable. Therefore, it is also reasonable not to expect an ideal level of linear correlation due to the assumptions made in the formulation of the HI.

Secondly, the frequency dependence of crack heating must be considered as a factor for less than ideal correlation. Frequency dependence here simply means cracks responding differently to different frequencies, through which each frequency will contribute individually to the overall heat generated by the crack. In a typical test, the number of excited modes (i.e. harmonics and multiples of horn resonance) is very high, and the HI cannot distinguish between the frequencies that contributes most to crack heating from those that don't contribute to crack heating [6, 65]. Finally, the limitation of only out-of-plane vibration measurements by a laser vibrometer means that any other vibration modes (e.g. in-plane or torsional) that contribute to the crack heating would not be taken into account in the computation of the HI. This again may have contributed to the less than ideal correlation coefficient achieved by the laser vibrometer in this study.

The findings in this work extend those of Morbidini et al. by confirming the linear relationship between the computed HI and the measured temperature rise from a crack. Additionally, this study has highlighted the importance of using the vibration measured

at the crack, if a strong linear correlation is to be achieved. However, what dictates the vibration measurement device used in a real inspection scenario is its practicality and the inspection environment. In a real inspection scenario, as opposed to a research environment, the crack location is unknown. This automatically raises questions about where on the blade a laser vibrometer is pointed to measure the vibration. The characteristics of the vibration at a location is not representative of the vibration in other parts of the blade. Therefore, the HI computed for laser vibrometer measurements cannot be used to assess the vibration across all parts of the blade. This is also the case with the strain gauge. The microphone is the only device that does not measure the vibration of a single point; rather, the vibration measured is a gross representation of the vibration of the whole component. However, as shown in this study and also in Morbidini et al.'s study, the strength of linear correlation for the microphone is only moderate. Nevertheless, it remains the most practical option due to the need to capture the vibration of the whole component as the crack location will be unknown in a real inspection scenario. In addition, the microphone has other advantages such as its non-contact capability and lower cost compared to a laser vibrometer.

Another important finding from this study, and from other similar HI studies, is related to the requirement of k in computing the HI. k plays a key role in the computation of the HI as it accounts for the thermal response of the crack. However, k is dependent on the crack characteristics and therefore unique for each crack. For example, in Morbidini et

al.'s study on beams [75], the *k* value for 18 different cracks varied between 5 and 50, and in most cases the *k* value also varied in between repeated tests on a crack. This highlights the significant dependence of *k* on the crack morphology and input vibration. This dependency poses a problem as the *k* values used in calibration to determine threshold HI for an inspection may not be appropriate for any potential cracks within an inspection batch. In addition, in a real inspection scenario, most blades would be crack free, raising questions as to whether a vibration monitoring parameter, such as the HI, should require prior knowledge of crack behaviour (i.e. *k*).

The next Chapter of this Thesis focuses on exploring a more robust parameter that would remove the requirement of the *k* factor, but at the same time correlates linearly with the measured temperature rise. In addition, this new parameter will be developed based on vibration measurements from a microphone only.

4.5 Review of chapter

A study to validate the Heating Index (HI) on an aero engine turbine blade was presented in this Chapter. In addition, this Chapter compared three different vibration measuring devices that may be used to compute the HI. The devices included a laser vibrometer, a microphone and a strain gauge. The validation involved measuring the strength of linear correlation between the HI and the temperature rise from a crack. The strength of linear correlation was quantified using the square of the correlation

coefficient, and was found to be highest for the laser vibrometer followed by the microphone. The linear correlation for the strain gauge was weak due to the position of the strain gauge on the blade holder rather than on the blade itself. The complicated nature of the vibration measured by the microphone limited the strength of the linear correlation compared to the laser vibrometer which measured the vibration at the crack location. The microphone was however found to be the most practical device for computing the HI in an industrial setting. This is because in a real inspection scenario, the number of cracks and their locations will be unknown, therefore requiring a device that capture a vibration waveform that represents the vibration of the whole blade, rather than a single point. Finally, this Chapter highlighted a limitation to the use of the HI, which is the required knowledge of k (i.e. crack behaviour) prior to inspection. This is not ideal as every crack is unique, but more importantly, a crack may not exist in test-piece to be inspected.

Chapter 5

An alternative vibration monitoring parameter for a reliable thermosonic inspection

5.1 Introduction

Monitoring the vibration in a thermosonic test ensures sufficient vibrational energy is applied to the component to detect a defect [75]. Morbidini et al. [75] have developed a vibration monitoring parameter called the Heating Index (HI) that correlates linearly with the heat generated by a crack [75], and thus may be used to determine whether a test has been carried out satisfactorily. However, one disadvantage of the HI is choosing an appropriate time-constant, *k*, for computing the HI in post-calibration inspections. The methodology for computing the HI is described in Chapter 4. The time–constant, *k*, is a unique characteristic of each individual crack that can only be measured from the heat signal generated from the crack during vibration. However, in a real inspection, it is unknown whether a crack exists on the blade or its position on the blade. At present, the majority (over 90%) of blades inspected in Rolls-Royce at overhaul are crack-free. Therefore, using a vibration monitoring parameter that requires prior knowledge of crack behaviour (i.e. HI) is not appropriate. This Chapter proposes an alternative vibration monitoring parameter which does not require prior knowledge of crack behaviour (i.e. *k*), but simply indicates whether sufficient energy has been applied to the component.

This alternative vibration monitoring parameter is referred to in this Thesis as the A^2 parameter, and it is related to the total energy content of the time-domain vibration waveform. The energy content of a time-domain vibration waveform is proportional to the square of the vibration amplitudes. In a thermosonic context, the A^2 parameter relates to the total energy available for dissipation in the component, not the temperature rise measured at the top of the crack, as with the HI. Nevertheless, there is a relationship between the total amount of energy available for dissipation and the eventual energy dissipated as heat by the crack. If the total energy available for dissipation increases, the potential of a crack generating a higher temperature rise also increases, as more energy becomes available to be damped by the vibrating crack. The main difference between A^2 and HI parameter, apart from the requirement of prior knowledge of the crack behaviour for the HI technique, is that the former accounts for the total energy of all frequencies present in the excitation, while the latter only represents the energy of a short section of the vibration where the HI content is largest (i.e. maximum HI) [75]. For the HI, this means only the frequencies present in a short section of vibration is used in the computation. This is not valid in all cases; for example if the component under test has a high modal density, the maximum HI may not take into account the energy of frequencies that contributed greatest to crack heating. Several researchers have demonstrated the frequency dependence of crack heating [6, 64, 65], with cases shown where the dominant frequency excited in the component did not contribute to crack heating [65]. Furthermore, using a parameter that takes into account all frequencies is

advantageous for components with multiple cracks, as different cracks respond differently to different frequencies.

This Chapter evaluates the A^2 parameter as a practical vibration monitoring parameter for turbine blade inspection. First, a validation exercise was carried out to measure the degree of linear correlation between the A^2 parameter and the maximum temperature rise from a crack. This validation involved the use of a set of blades with single and multiple cracks, and a high-frequency microphone to capture vibration. Furthermore, a comparison between the degree of linear correlation for the A^2 and HI is presented. Finally, a threshold vibration level was determined for the set of blades, and then applied retrospectively to the set of blades.

5.2 Methodology

5.2.1 Specimens and experimental setup

A total of 17 turbine blades with single and multiple shroud cracks were used in this study. The blades were all from the same engine type and a representative blade is shown in Figure 5-1. This blade is made of high-strength nickel alloy and is approximately 112 mm in height and 34 mm at the widest point. There were single cracks on 7 blades and at least three cracks on each of the other 10 blades. The single cracks were located at the shroud interlock, while the multiple cracks were located across the shroud, as indicated in Figure 5-1. In total, there were 43 cracks on the 17

blades, and the length of each crack was measured using a calibrated optical microscope/CCD camera (Leica MZ8/ JENOPTIK ProgRes® C12).

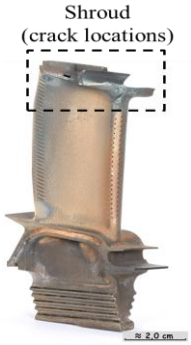

Figure 5-1 Image of turbine blade used in this study.

The experimental setup used in this study was similar to the setup described in Chapter 4 (see 4.2.1), except the microphone was the sole vibration measurement device and the IR camera was different. The microphone was chosen as the sole vibration measuring device after the evaluation carried out in Chapter 4 showed it to be the most practical device for an industrial setting. The microphone in this study was placed in the far-field at a distance of 1.2 m away from the blades and was therefore different from the setup described in Chapter 4. In Chapter 4, the microphone was placed closer to the crack at a distance of 0.02 m to ensure the vibration at the crack location was dominant in the microphone response. However, due to the use of blades with multiple cracks, a far-field position was considered more appropriate as it ensures the vibration measurement was insensitive to any particular location on the blade [6]. The IR camera used in this study

was a Cedip Jade medium-wavelength cooled IR camera, with a detector array of 320 x 240 pixels, temperature sensitivity of 30 mK and a frame rate of up to 140 Hz. This camera was used to ensure accurate and repeatable measurements of the temperature rise generated by a crack.

5.2.2 Thermosonic inspection

At least 20 tests were carried out on each blade (except two blades, 15 tests), with the horn force varied in each test and the coupling material changed after every five tests. The vibration data was processed in MATLAB to compute the HI and the A^2 parameters. The methodology used in computing the HI is described in Chapter 4, while the method of computing A^2 is described in the next subsection, 5.2.3. However, computing the HI for blades with multiple cracks differed from the process described in Chapter 4, where the blade had a single crack. The presence of multiple cracks on a blade resulted in multiple *k* values, and consequently, different HI profiles.

Figure 5-2 shows an example of the crack temperature rise profiles and *k* values obtained for four different cracks on a single blade. The difference in the magnitude of the temperature rise between the cracks is illustrated in Figure 5-2 (a) and (b), where the former shows the absolute temperature and the latter, the normalised temperature plot. Figure 5-2 (b) shows the difference in the slope of temperature decays and hence the different *k* values expected. Figure 5-2 (c) – (f) show the individual crack temperature

rise profiles and the exponential fit (dashed red line) from which the *k* values were estimated. For this example, the *k* for Crack 1 – 4 were 18, 30, 3 and 10 respectively.

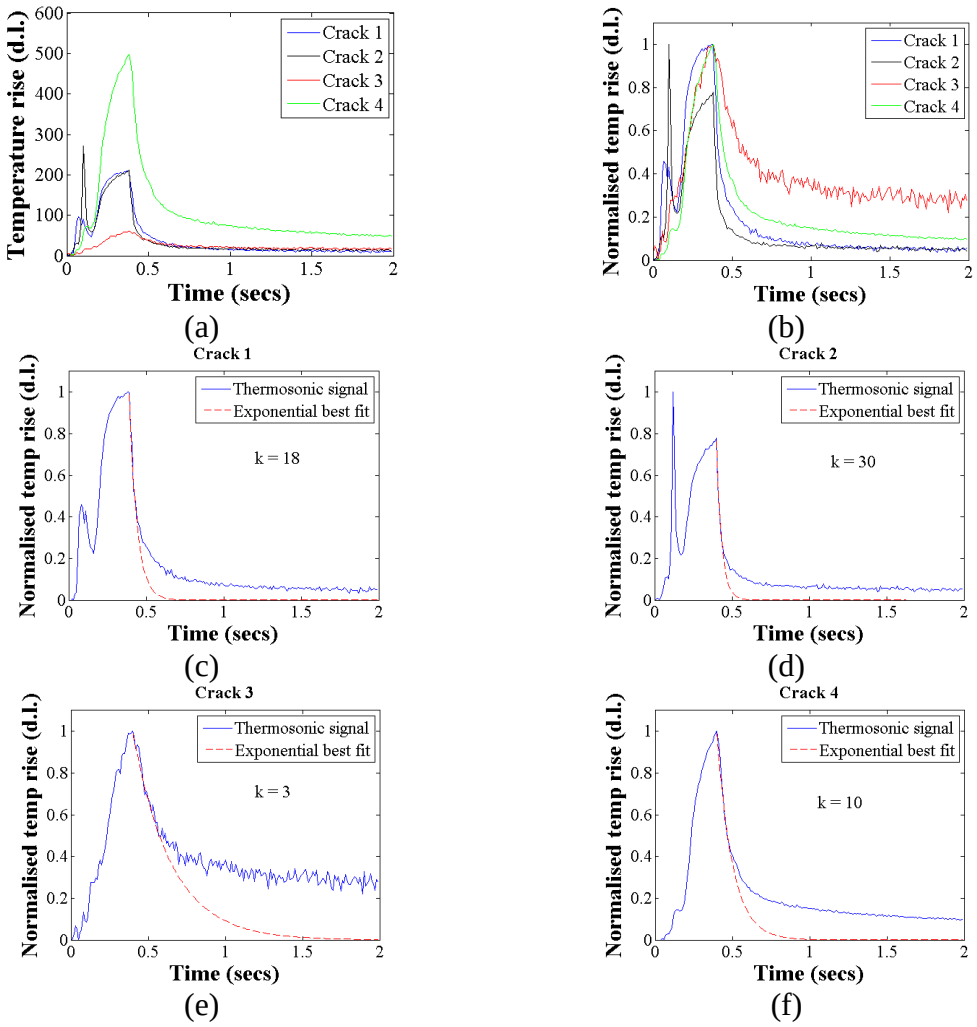

Figure 5-2 Crack temp rise profile of four different cracks on blade D06 (a) all four temp rise profiles (b) normalised temp rise profiles of four cracks (c) temp rise profile for Crack 1 (d) temp rise profile for Crack 2 (e) temp rise profile for Crack 3 (f) temp rise profile for Crack 4.

Table 5-1 shows a summary of the crack lengths, number of inspections per blade, number of positive detections, average *k* for each crack and variability of *k*. In Table 5-1, the blades with single cracks have labels beginning with 'Z', while those with multiple cracks, beginning with 'D'. A total of 341 inspections were conducted on the 17 blades, with a positive detection achieved in 327 inspections. The remaining 14 inspections where the cracks were not detected was spread over five blades (Z42, Z76, D06, D07 and D18), and non-detection was due to the low horn force used in those inspections. Table 5-1 also shows the average *k* values computed for the different cracks and its variability as a percentage of its mean. This Table shows a wide range of *k* values for the different cracks and also variation of *k* between tests on the same crack. This variability of *k* was also seen in Morbidini et al.'s HI study [75]. According to Morbidini et al. [75], the highest value of *k* obtained during calibration tests should be used for computing the HI in post-calibration inspections. This is because *k* tends to be larger for small cracks, which are more difficult to detect compared to large cracks. Therefore, the highest computed *k* (i.e. 65) shown in Table 5-1 was used later in computing the HI for all the cracks.

Table 5-1 Number of thermosonic tests carried out on each blade and the number of positive detection tests. Also shown is the average k value and variability of the k computed for each crack.

Blade	Crack length (mm)	Number of inspections	Number of detections	Average 'k' ($\bar{k}$)	Variability $\sigma_k / \bar{k}$ (%)
Z42	5.5	25	20	18	29
Z44	2	20	20	53	40
Z47	2.9	20	20	65	27
Z48	4.4	25	25	20	0
Z55	6.7	21	21	50	0
Z67	3.6	15	15	50	0
Z76	0.8	20	14	60	20
D06	Crack 1: 2.5	20	19	18	50
	Crack 2: 0.5		19	30	0
	Crack 3: 9.2		19	3	77
	Crack 4: 1.1		19	10	0
D07	Crack 1: 2.2	20	19	30	0
	Crack 2: 0.5		19	30	0
	Crack 3: 4.6		19	6	60
	Crack 4: 1.7		19	23	38
D10	Crack 1: 2.1	20	20	18	16
	Crack 2: 1.0		20	25	23
	Crack 3: 9.0		20	6	40
D17	Crack 1: 1.8	20	20	20	0
	Crack 2: 0.2		20	30	0
	Crack 3: 8.5		20	5	12
D18	Crack 1: 2.2	20	19	20	35
	Crack 2: 0.8		19	23	25
	Crack 3: 8.5		19	11	56
	Crack 4: 2.7		20	15	0
D22	Crack 1: 1.4	15	15	13	40
	Crack 2: 1.1		15	23	43
	Crack 3: 8.6		15	11	22
D23	Crack 1: 2.4	20	20	13	40
	Crack 2: 1.4		20	10	71
	Crack 3: 8.3		20	15	67
	Crack 4: 0.5		20	12	15
D26	Crack 1: 1.1	20	20	15	0
	Crack 2: 1.0		20	30	0
	Crack 3: 9.1		20	6	59
D32	Crack 1: 2.5	20	20	10	0
	Crack 2: 1.2		20	18	29
	Crack 3: 8.9		20	1	0
	Crack 4: 2.8		20	16	47
D34	Crack 1: 0.5	20	20	30	0
	Crack 2: 2.7		20	28	18
	Crack 3: 3.7		20	28	18
	Crack 4: 2.4		20	24	53

5.2.3 Computing and validating the A^2 parameter

The A^2 parameter relates to the total energy content in a vibration. The A^2 parameter is defined as the square root of the average of the squared vibration amplitudes over a period of time, as shown in Equation 5.1 [129].

$$A_{rms}^2 = \sqrt{\int v(t)^2 \, dt} \qquad (\mathbf{5.1})$$

where $v(t)$ represents the vibration waveform. For the A^2 parameter to be considered valid, a good degree of linear correlation must exist between A^2 and the maximum temperature rise from the crack. In addition, the linear correlation for the A^2 must compare favourably with that of maximum HI, which has been validated by several researchers [10, 75]. Figure 5-3 (a) shows an example of a plot of maximum temperature rise vs. A^2, while Figure 5-3 (b) shows the equivalent result for the maximum HI. For both figures a positive linear correlation can be seen, although in this case, the computed correlation coefficient (r^2) for A^2 (0.71) was higher than that of maximum HI (0.52). It must be noted that the scales of A^2 and maximum HI are arbitrary units since they are a function of the amplification and position of the microphone. Therefore, the absolute values of the A^2 and maximum HI in this study cannot be compared to results with a different thermosonic setup. This also implies that, when using a microphone as the vibration measurement device, the experimental setup and microphone position must be the same for both calibration and post-calibration tests.

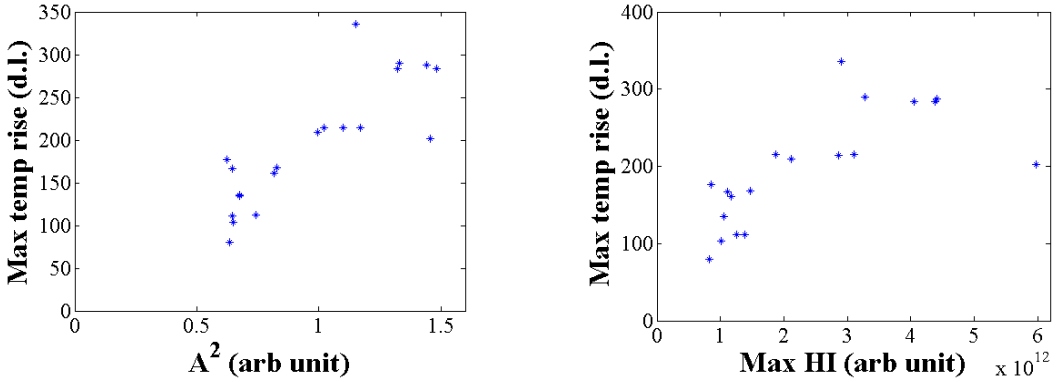

Figure 5-3 Plot of maximum temp rise vs. (a) A^2 (b) maximum HI.

5.2.4 Computing the threshold vibration required for a reliable inspection

In order to assess whether the vibration level in an inspection is sufficient for crack detection, the vibration must be compared to a threshold determined prior to inspection (i.e. calibration test). If the measured vibration level is above the threshold, the inspection is considered satisfactory; otherwise, the inspection is repeated until the threshold is surpassed. Linear regression analysis was used in this study to determine the threshold vibrational level for the set of cracked blades tested. Linear regression is a widely used statistical tool for examining the relationship between two measured variables. It is closely related to correlation analysis, except the regression analysis yields a formula for predicting the value of one variable when the value of the second variable is known [122]. The predicted variable is called the response variable (or dependent variable) and the known variable is called the predictor variable (or

independent variable). In this study, the response variable is crack temperature rise and the predictor variable is the vibrational level (i.e. HI or A^2).

A linear relationship between the dependent and independent variable is assumed in regression analysis [122]. Therefore, the formula obtained from regression analysis represents the equation of a straight line that best fits the data. The regression equation used to predict the dependent variable is shown in Equation 5.2, where $\hat{Y}$ is the predicted value of the dependent variable Y, X is the value of the independent variable, b is the regression coefficient or the slope and a is the intercept, which is the point where the regression line intersects the y-axis. In this study, the intercept a, was set equal to zero, thereby forcing the regression line through the origin. The reason for this approach is that, theoretically, there cannot be a temperature rise at zero energy input; therefore the line must go through the origin. The effect of this however is that the regression line through the data is not necessarily the line of best fit, particularly for data plots with a significant y-intercept value. This approach was also used by Morbidini et al. [6] and Weekes [10] in their respective thermosonics studies.

$$\hat{Y} = bX + a \qquad \textbf{(5.2)}$$

An estimate of the slope b of a regression line passing through the origin can be computed using the following equation [130]:

$$b = \frac{\sum X_i Y_i}{\sum X_i^{\,2}} \qquad \textbf{(5.3)}$$

where X_i is the independent variable and Y_i, the dependent variable. Once the slope of the regression line is known, a predicted value of the response variable Y can be obtained for any value of X. Figure 5-4 shows an example of a scatter plot with a regression line fitted through the data. The scatter plot shows a positive correlation with a regression line (solid black line) going through the origin. The dashed green lines next to the regression line in Figure 5-4 are the limits of the 95% confidence intervals. The confidence interval represents the interval where the predicted response is likely to lie. The confidence intervals in Figure 5-4 was computed using Equation 5.4, where CI_{95} is the 95% confidence interval, b is the slope, t is the critical t-distribution value and $s(b)$ is the standard error of the slope b. The upper and lower confidence lines give the maximum and minimum obtainable response for a given vibration level.

$$CI_{95} = b \pm t_{(95,df)} s(b) \qquad \textbf{(5.4)}$$

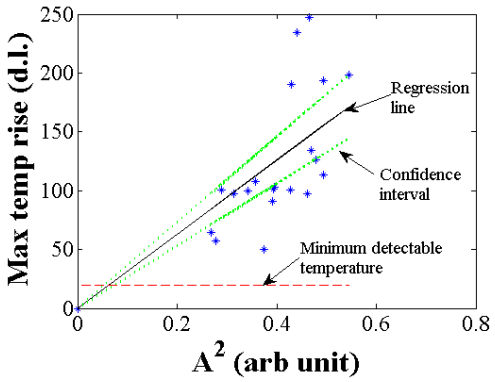

Figure 5-4 Plot of maximum temp rise vs. A^2 for blade D34 Crack 3. Solid black line is regression line through the origin and dashed green lines are the limits of the upper and lower 95% confidence intervals. Dashed red line is the minimum detectable temperature (20 d.l.) by the IR camera.

The dashed red line in Figure 5-4 represents the minimum detectable temperature (i.e. 20 d.l.) by the IR camera used in this study. Knowledge of the minimum detectable temperature enables the threshold vibration level for detecting the respective crack to be determined. The threshold chosen in this study for each crack is the point where the dashed red line intersects the lower confidence line. For the crack in Figure 5-4, the threshold vibration required to ensure the crack is detected with a 95% probability is 0.07. It must be noted that the threshold vibration level will differ for the various cracks. The higher the threshold for a crack, the higher vibration level required to generate a specific temperature rise. Furthermore, in this study, the threshold was only determined for cracks with a linear correlation above +0.2, which in total were 21 cracks. This was to ensure only cracks that demonstrated the expected positive linear correlation between the excited vibration and the resulting temperature rise from a crack were used.

5.3 Results

5.3.1 Comparison of the A^2 and HI parameters

A few examples of the maximum temperature rise vs. A^2 and maximum temperature rise vs. maximum HI plots are shown in Figure 5-5 and Figure 5-6. Figure 5-5 shows the plots for four different blades, each with single cracks, while Figure 5-6, the plots of four different cracks on a single blade. In both Figures, the first column (i.e. (a1) – (d1)) shows the plot for max temperature rise vs. A^2, while the second column (i.e. (a2) – (d2)) shows the plot for maximum temperature rise vs. maximum HI.

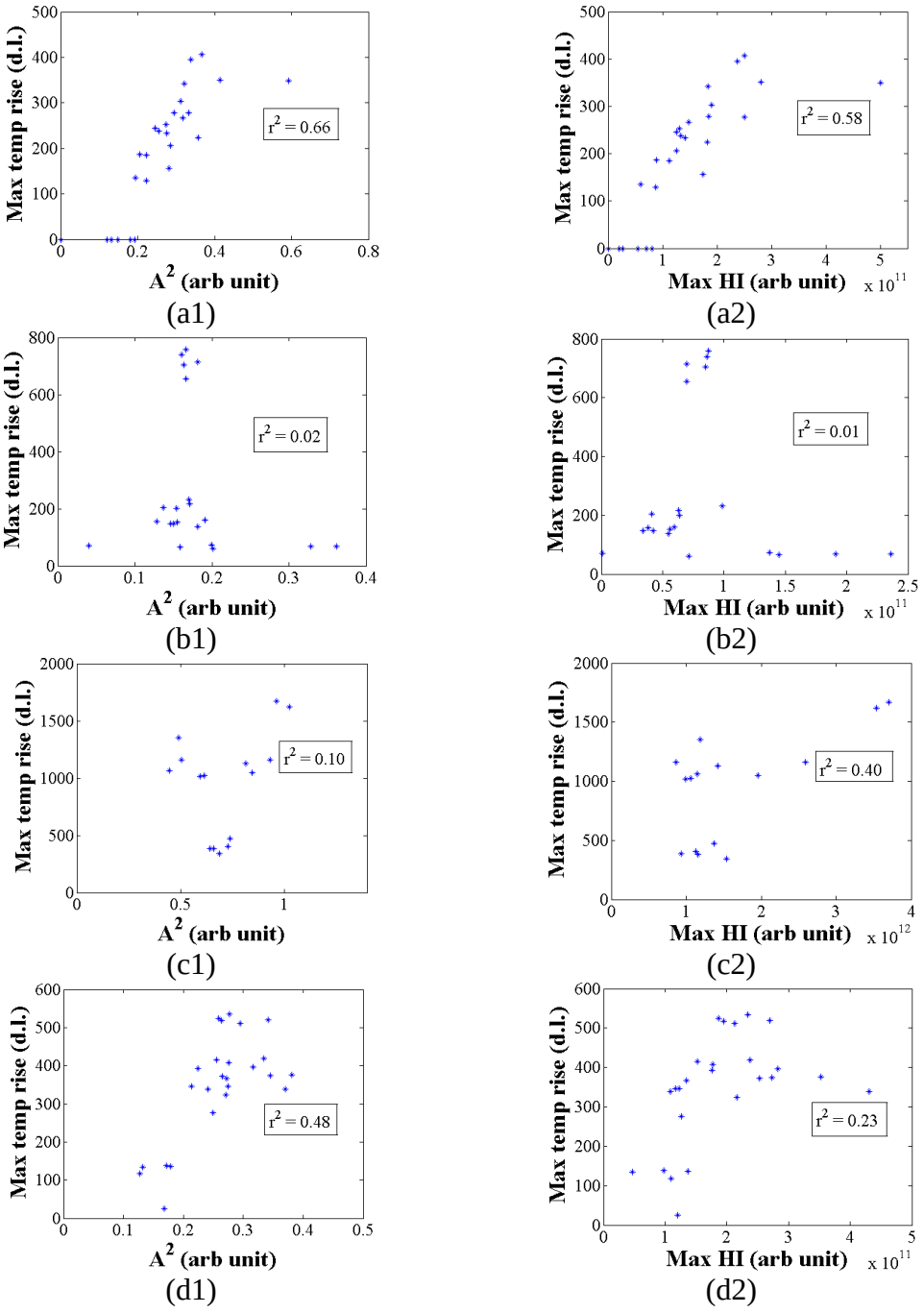

Figure 5-5 Maximum temperature rise vs. A^2 (column 1) and maximum temperature rise vs. maximum HI (column 2) (a) Blade Z42 (b) Blade Z55 (c) Blade Z67 (d) Blade Z48.

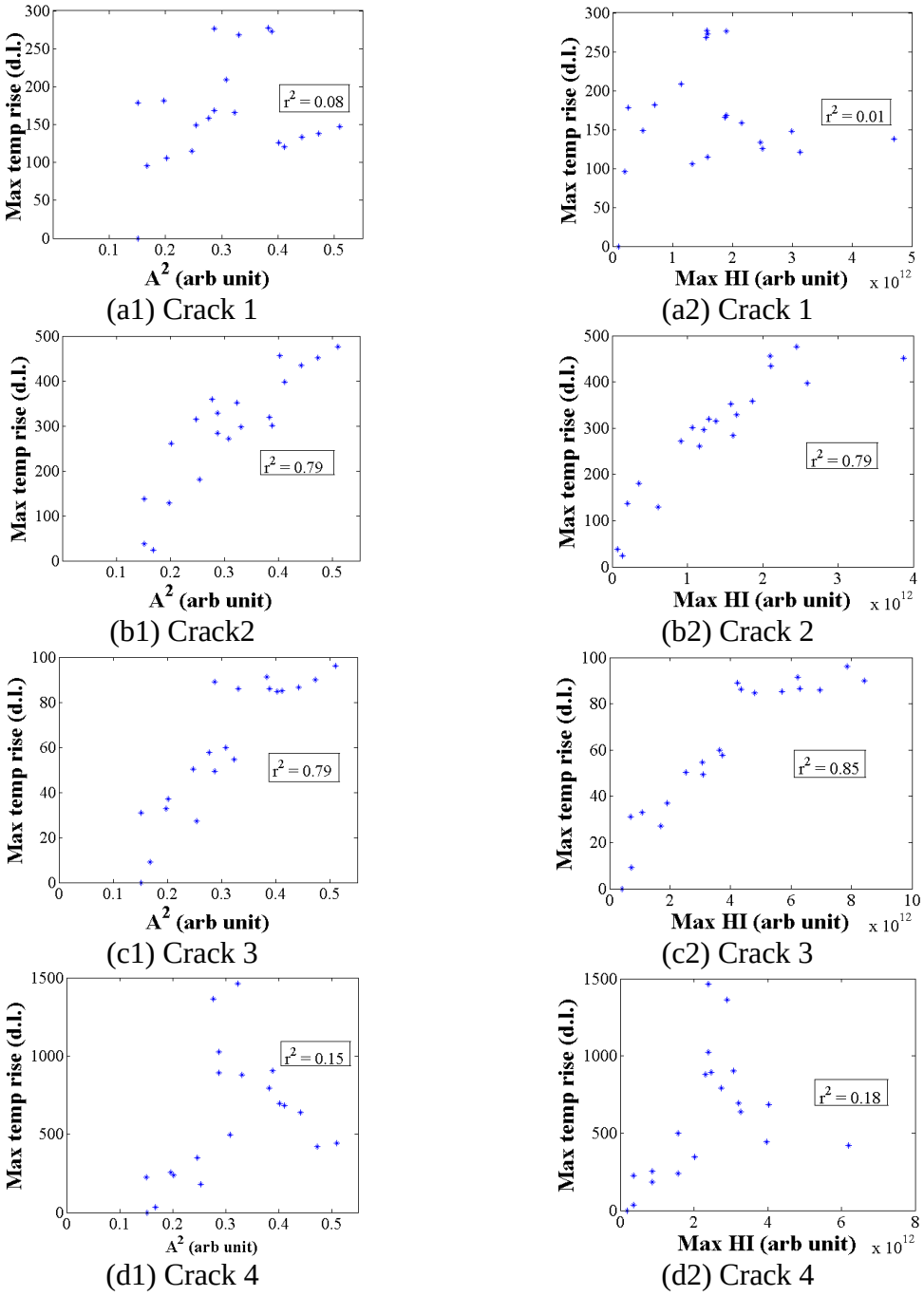

Figure 5-6 Maximum temperature rise vs. A^2 (column 1) and maximum temperature rise vs. maximum HI (column 2) for four different cracks on Blade D06 (a) Crack 1 (b) Crack 2 (c) Crack 3 (d) Crack 4.

In Figure 5-5, (a) and (b) illustrates examples where the degree of linear correlation for A^2 and maximum HI were similar, (c) illustrates a case where maximum HI had a better correlation, and (d), a case where A^2 had the better correlation. In Figure 5-5 (a), a positive and strong linear correlation can be seen for both the A^2 and maximum HI, with little scatter. The computed correlation coefficient was 0.66 and 0.58 for A^2 and maximum HI respectively. In Figure 5-5 (b), the degree of linear correlation for the A^2 and maximum HI is also similar, but instead with significant scatter and correlation coefficients for both are effectively zero, meaning no correlation. In Figure 5-5 (c) and (d), some scatter can be seen but observation alone does not clearly differentiate which parameter has the higher correlation coefficient. For the crack in Figure 5-5 (c), the correlation coefficient for A^2 and maximum HI is 0.10 and 0.40 for respectively, and in Figure 5-5 (d), 0.48 and 0.23 respectively.

Figure 5-6 (a) – (d) shows the plot of maximum temperature rise vs. A^2 and maximum temperature rise vs. maximum HI for a single blade with four different cracks. The degree of linear correlation for Crack 1 and 4, shown in (a) and (d) are weak, while that of Crack 2 and Crack 3 in (b) and (c) respectively show a strong linear correlation. However, more importantly, the correlation coefficient for A^2 compared favourably with the corresponding correlation coefficient for maximum HI for all four cracks. For Crack 1, the correlation coefficient of A^2 and maximum HI were 0.08 and 0.01 respectively, for Crack 2, 0.79 for both, for Crack 3, 0.79 and 0.85, and for Crack 4, 0.15 and 0.18. A

summary of the computed correlation coefficients of all the blades/cracks used in this study is shown in Figure 5-7.

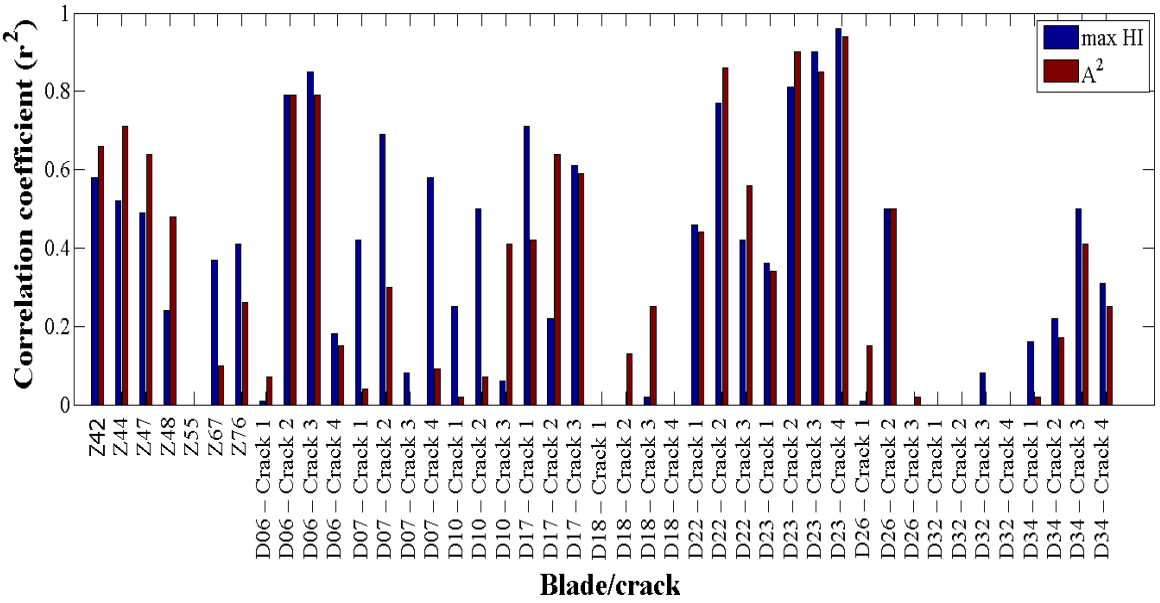

Figure 5-7 Correlation coefficient (r^2) of all blades/cracks. The first bar for each crack represents the correlation coefficient for the max HI and the second bar for the A^2 parameter.

Figure 5-7 shows the normalised correlation coefficients for the 43 cracks used in this study. In this Figure, the first bar for each blade/crack represents the correlation coefficient for maximum HI and the second bar for A^2. Furthermore, cracks with a negative correlation coefficient, such as Z55, D18 (Crack 1 & 4) and D32 (Crack 1, 2 & 4), were assigned a value of zero, since a negative coefficient is contrary to the initial hypothesis which suggests a positive correlation between the maximum temperature rise and vibration. Figure 5-7 shows mixed results, with 50% of cracks having similar correlation coefficients for both A^2 and maximum HI, while the correlation coefficient

was higher for A^2 in 25% of the cracks and maximum HI higher for the remaining 25% of the cracks.

Figure 5-8 further illustrates the difference in the strength of linear correlation between maximum HI and A^2. For each category, the upper bar represents maximum HI and the lower bar, A^2. Figure 5-8 shows a slightly higher number of cracks with a strong correlation when using the A^2, although the maximum HI had a higher number of cracks with a moderate and weak correlation. The percentage of cracks with a classification of no correlation was relatively high, approximately 37% and 47% for the maximum HI and A^2 respectively. Nevertheless, the overall degree of linear correlation for A^2 parameter compared favourably with that seen for the maximum HI parameter.

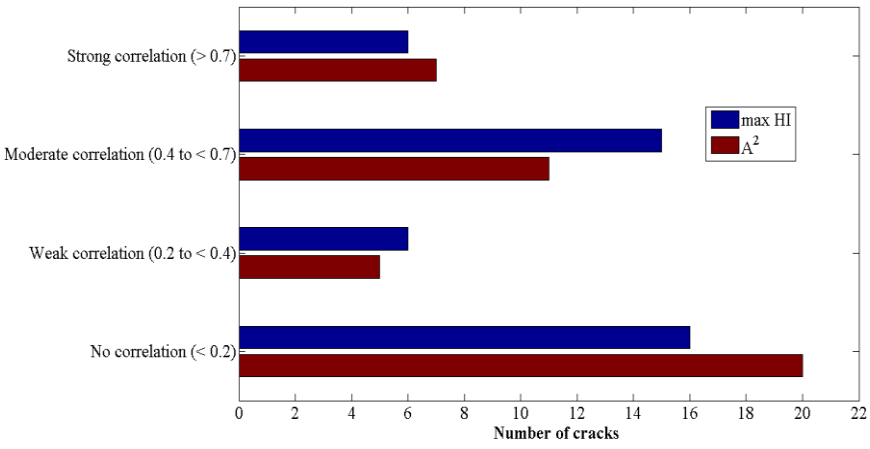

Figure 5-8 Number of cracks with coefficients classed as strong (> 0.7), moderate (0.4 to < 0.7), weak (0.2 to < 0.4) and no correlation (0 to < 0.2).

5.3.2 Threshold vibration level

Figure 5-9 shows as examples, six different plots used to determine the threshold vibrational energy (A^2) for six different cracks. Figure 5-9 (a) - (f) shows the plots for D06 Crack 2, D06 Crack 3, Z44, Z42, D17 Crack 3 and D26 Crack 2 respectively. Note that only A^2 plots are shown in Figure 5-9; however, the same methodology can be applied to the maximum HI plots. Figure 5-9 illustrates the different vibration levels (i.e. threshold) required by different cracks to generate the minimum detectable temperature rise of 20 d.l. The thresholds for the six cracks in Figure 5-9 (a) – (f) are 0.02, 0.11, 0.11, 0.03, 0.05, 0.02 respectively. Table 5-2 presents the threshold computed for the 21 different cracks nominated for determining the threshold vibration level for the set of blades used in this study.

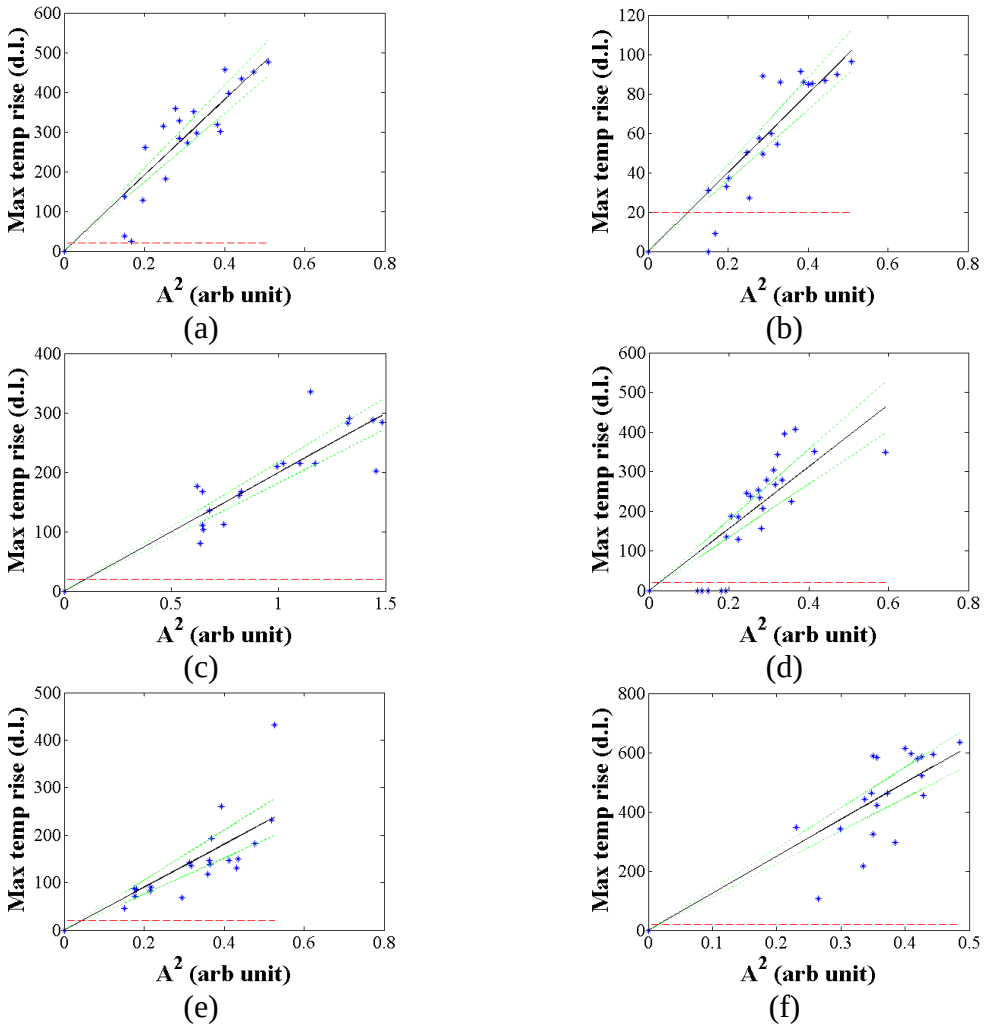

Figure 5-9 Maximum temperature rise vs. A^2 (a) D06 Crack 2 (b) D06 Crack 3 (c) Z44 (d) Z42 (e) D17 Crack 3 (f) D26 Crack 2. The dashed red line in plots represent the minimum detectable temperature at 20 d.l.

Table 5-2 Computed threshold energy for cracks with correlation greater than 0.2.

Blade/Crack	Vibration threshold A^2 (with 95% confidence)
Z42	0.03
Z44	0.11
Z47	0.06
Z48	0.02
D06 – Crack 2	0.02
D06 – Crack 3	0.11
D07 – Crack 2	0.01
D10 – Crack 3	0.10
D17 – Crack 1	0.04
D17 – Crack 2	0.03
D17 – Crack 3	0.05
D18 – Crack 3	0.05
D22 – Crack 1	0.32
D22 – Crack 2	0.03
D22 – Crack 3	0.13
D23 – Crack 1	0.09
D23 – Crack 3	0.01
D23 – Crack 4	0.02
D26 – Crack 2	0.02
D34 – Crack 3	0.08
D34 – Crack 4	0.03

In Table 5-2, 14 out of the 17 blades set out for this study are represented. This shows that most of the blades involved in this study were used in the determination of the final vibration threshold for the full set of blades. Table 5-2 shows a wide range of threshold values for the different cracks, further confirming one of the differences between thermosonics and other common NDE techniques, which is that detectability is a strong function of crack morphology, and not necessarily crack length. Figure 5-10 shows a plot of thermosonic efficiency vs. crack length for the 21 cracks. Thermosonic efficiency

describes the ability of a crack to generate heat from a given vibrational input (see Equation 5.5). The higher the thermosonic efficiency, the less energy required to generate a given temperature rise. Figure 5-10 shows no correlation between thermosonic efficiency and crack length. Similar results have also been obtained by Morbidini et al. [6] and Weekes [10].

$$Thermosonic\ Efficiency = \frac{Avg.\ T_{\max}}{Avg.\ A^2} \qquad \textbf{(5.5)}$$

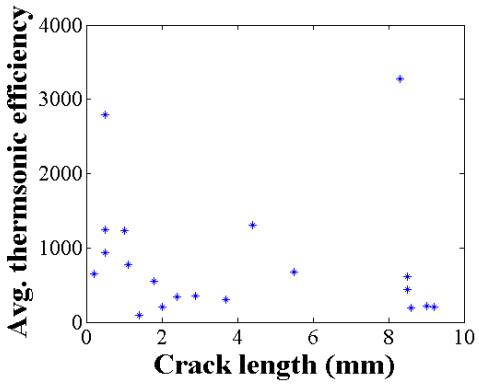

Figure 5-10 Thermosonic efficiency vs. crack length (only the 21 cracks used in the threshold study).

According to Morbidini et al. [6], the largest threshold obtained in the calibration tests should be nominated as the representative threshold for the blade type for post-calibration inspections. Therefore, a threshold of 0.32, obtained for D22 Crack 1, is the nominated threshold for the set of blades used in this study. The next step in this study

was to apply the nominated threshold retrospectively to the 341 inspections carried out in this study, and the results are shown in Figure 5-11.

Figure 5-11 shows the range of vibration levels (i.e. A^2) excited in the 341 inspections conducted on the 17 turbine blades used in this study. Figure 5-11 (a) shows the vibration levels for the 327 positive inspections, while Figure 5-11 (b) shows the vibration levels for the 14 inspections were the crack was not detected. The dashed horizontal line in both Figures represents the nominated threshold at 0.32. For the positive inspection case, 178 inspections were above the threshold; however, more interesting was the 8 out of 14 inspections in the non-detection cases were above the threshold. These 8 inspections are effectively false indications as they suggest the excitation was satisfactory even though the crack did not generate a detectable heat signal. It must be noted that 6 out of the 8 false indications occurred in consecutive inspections on just one blade, Z76, and the vibration levels of these 6 inspections were in the same range as the other 14 inspections on the blade where the crack was detected. There is no obvious reason why these 6 inspections did not generate a detectable heat signal, other than the characteristics (i.e. modes) of the vibration excited at the crack differed from that of the other 14 inspections where the crack was detected. The number of false indications compared to the number of positive inspections was insignificant, especially if the 6 inspections on blade Z76 are excluded. Also encouraging is the high number of inspections over the threshold for each blade, as shown in Table 5-3. This

table shows an average of 10 inspections per blade had a vibration level above the nominated threshold.

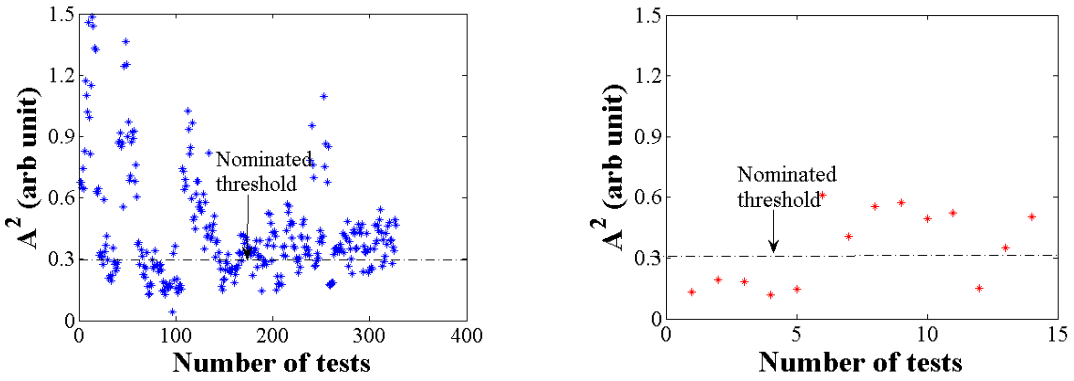

Figure 5-11 Vibration levels excited in the 341 inspections carried out in the 17 blades (a) 327 positive inspections (b) 14 inspections where crack was not detected.

Table 5-3 Number of positive tests for each blade that exceed the threshold of 0.32.

Blade	Total number of tests above threshold
Z42	4
Z44	20
Z47	20
Z48	2
Z55	1
Z67	15
Z76	15
D06	7
D07	5
D10	5
D17	11
D18	15
D22	7
D23	12
D26	13
D32	11
D34	15

5.4 Discussion

The aim of the work carried out in this Chapter was to demonstrate the potential of the A^2 parameter as an alternative and practical vibration monitoring parameter to the HI. Although the HI has been shown to be valid, determining an appropriate *k* for computation of the HI in post-calibration inspections is challenging. The potential of the A^2 parameter was investigated using 43 cracks on 17 turbine blades (same type) and a microphone positioned in the far-field. Furthermore, the A^2 parameter was validated by evaluating its strength of linear correlation with the temperature rise from a crack, and then compared to the corresponding results for the HI parameter. The results showed the A^2 to compare favourably with HI, and in some cases showed a stronger linear correlation. After validating the A^2 parameter, the threshold vibration level was computed for each crack and subsequently, a single threshold was nominated for the set of 43 cracks. Overall, the results obtained in this work showed the A^2 as a viable alternative to the HI parameter.

The results relating to *k* presented in this study were consistent with results obtained by Morbidini et al. [75], although their work involved the use of simple beams with artificially generated fatigue cracks and a smaller number of cracks in total. The authors found a similar level of variability of *k* between tests on a crack and also no correlation between crack length and *k*. The reason for the inconsistency in the estimated *k* value is fundamentally related to the uniqueness of each crack morphology and local vibration at

the crack [6, 54, 55]. In a real inspection, both crack morphology and the local vibration at a potential crack site cannot be predicted. Therefore, an alternative parameter that has no requirement of *k* is desirable.

The A^2 parameter was shown to perform comparably to the HI parameter. However, strength of linear correlation seen in this study for both the A^2 and the HI parameters were mixed, and this was consistent with the HI results seen in similar studies carried out Morbidini et al. [6] and Weekes [10]. Morbidini et al. [6] used similar-sized turbine blades and a microphone for capturing the vibration. However, the degree of linear correlation between maximum temperature rise and maximum HI in Morbidini et al.'s study was not quantified. Therefore, only a qualitative comparison was made using the plot of maximum temperature rise vs. maximum HI. The HI study carried out by Weekes [10] was different, in terms of type of specimens used (beams) and the vibration measurement device (strain gauge) employed. However, the degree of linear correlation in Weekes's study was quantified, although using the correlation coefficient (r), which is related but different to the square of the correlation coefficient (i.e. r^2) used in this Thesis. Therefore, a careful comparison must be made between the correlation coefficients obtained in this Thesis and in Weekes's study.

The correlation coefficients (i.e. r^2) obtained in this study for the A^2 parameters were mixed, with approximately half of the cracks classed as a having no correlation or a

weak correlation. The possible reasons of the weak or no correlation are due to several factors, but most importantly: frequency dependence of crack heating and characteristics of the microphone vibration measurement. The implication of not having a moderate or strong correlation coefficient is that it limits the accuracy of the A^2 parameter in predicting crack temperature rise. This was the reason why 21 out of the 43 cracks were used in the process of setting a threshold for the set of blades. The only way to achieve ideal correlation is through knowledge of crack damping and vibration at the crack [70]; however, this is not practical, hence the reason for simple parameters such as the HI and A^2. Their purpose is simply to give an indication of whether the vibration in the component is equal to or greater than that seen in the calibration tests.

The next step after validating the A^2 parameter was determining the vibration level (i.e. threshold) required to generate the minimum detectable temperature rise (20 d.l.) for each crack. Linear regression analysis was used because of its established statistical methodology of predicting the response of a variable from knowledge of another, assuming both variables have a causal linear relationship. In addition, confidence intervals were used to increase the certainty of the computed threshold. The methodology used in this study was similar in principle, but with some computational differences, to the methodology employed by Morbidini et al. [6]. In Morbidini et al.'s work, the threshold for each crack was determined from the plot of maximum temperature rise vs. maximum HI using the intercept of the slope. However, the slope in

this work was computed as the average thermosonic efficiency (with the slope constrained to the origin). In addition, the confidence interval used in Morbidini et al.'s work was a 68% confidence, compared to a 95% used in this study. The latter was used in this study as it provides a more conservative estimate of the vibration threshold. In addition, Morbidini et al. multiplied the determined threshold by a safety factor, which depends on the number of specimens, range of locations of potential defects and on the scatter observed in the calibration inspections [6].

The threshold vibration level determined using the 21 cracks was applied in a retrospective manner to the 341 inspections carried out for the full set of 17 blades. The purpose for this was to evaluate the number of inspections that were above and below the threshold. Although only 67% of all positive inspections were above the threshold, the threshold was exceeded in every blade, demonstrating that the threshold could be achieved consistently in a large number of this blade type. The reason for some positive inspections not exceeding the nominated threshold in this study was simply because the vibration levels were intentionally varied by varying the horn force at the inspection stage. In a real inspection scenario, a predetermined horn force capable of achieving the threshold will be used initially, and only increased if the threshold is not surpassed. Also encouraging was that the vibration levels in six out of the eight inspections were the crack was not detected (excluding Z76) were below the threshold. This result adds credibility to the A^2 parameter as a viable vibration monitoring parameter.

The number of blades, cracks, and crack locations can be considered more than adequate for this study and also as a guide when choosing a calibration set. For the blade type used in this study, most of the known potential crack locations were represented. Furthermore, there was a good distribution of crack lengths, although crack length is not a critical function of detectability. Nevertheless, detecting a wide range of crack lengths, including sub-millimeter cracks, increases confidence in crack detection capability of thermosonics. The use of blades with multiple cracks was very important in this study, not only because such samples have never been used in a similar study, but it also demonstrated the capability of detecting multiple cracks in several locations of a complex geometry using a single excitation. This further confirms the advantage of using chaotic excitation over single frequency or resonance excitation.

This Chapter demonstrated the A^2 parameter as a viable alternative to the HI. However, the practical implementation of using this vibration monitoring parameter in a real inspection scenario must be further investigated. Issues relating to the calibration test-pieces and thermosonic equipment must be considered [6, 75]. Each blade type to be inspected by thermosonics must have its own set of calibration test-pieces. This is because the vibration excited in a component is a function of geometry. In addition, the calibration test-pieces for each blade type must have representative cracks for the batch of blades to be inspected post-calibration. Typically, most blade types fail in the same locations; however, it is likely that the crack morphology will differ for every crack.

Therefore, true crack representation cannot be achieved in the calibration test-pieces. Nevertheless, it is fair to assume that cracks generated by the same failure modes and in the same location will have some similar characteristics. This simplifies the crack representation aspect for choosing the calibration test-pieces. Finally, the experimental setup and the location for the calibration tests and post-calibration inspections have to remain the same. This is because the vibration threshold determined in calibration will be a strong function of the equipment and location, particular when using a microphone. In order to gain more insight into the practicality of applying a vibration monitoring parameter, more trials on different blade types is required. These trials must be carried out in an industrial environment and must include blind trials to confirm the validity of the determined vibration threshold.

5.5 Review of chapter

This Chapter evaluated the A^2 parameter as an alternative vibration monitoring parameter to the Heating Index (HI). The A^2 parameter was first validated by measuring its strength of linear correlation with crack temperature rise, after which a comparison was made with the equivalent HI results. The strength of linear correlation for the A^2 parameter was shown to compare favourably with that of the HI for the same set of 17 blades/43 cracks used in this study. After the A^2 parameter was validated, a threshold vibration level was determined for the set of blades/cracks using linear regression analysis.

Chapter 6

Simulation of the full-field vibrational response of a turbine blade under thermosonic excitation

6.1 Introduction

The vibration field generated in a turbine blade during a thermosonic test is non-uniform and complex. This is because of the non-uniform displacement fields associated with the numerous vibration modes excited in the component [25, 131]. Consequently, the excited vibrational energy will vary across the component, potentially leading to non-detection of defects in areas with insufficient vibrational energy. Vibration monitoring is a useful tool in a thermosonic inspection; however, current monitoring techniques do not capture the full-field vibrational energy of the component.

Full-field vibration measurement of a component under thermosonic excitation is a relatively new area of research. The only related published literature to date are those of Rothenfusser et al. [86] and Renshaw [25]. Rothenfusser et al. [86] proposed a calibration method that uses the thermal response of several pieces of material attached to the component. When the component is under thermosonic excitation, the thermal responsive materials generate a certain amount of heat that indicates the level of vibrational energy excited in that part of the component [86]. This method is useful; however, achieving

consistent attachment of the thermal-responsive material on the component is challenging, and thus may lead to inaccurate assessment of the vibrational energy excited at the several selected locations of the component. Renshaw's [25] methodology involves using an array of viscous material-filled synthetic defects that generate heat when under thermosonic excitation. Renshaw's methodology is useful for demonstrating vibration coverage; however, manufacturing synthetic defects in real components affects the geometry of the component and thus its true vibration characteristics.

This Chapter presents a new methodology for determining the full-field vibrational response of a component under thermosonic excitation. The proposed methodology involves a combination of vibration measurements and finite element analysis (FEA) to simulate the vibrational energy within a turbine blade under a typical thermosonic inspection. First, a laser vibrometer was used to measure the pseudo steady-state vibrational response of several points on a blade. Next, an input load was applied to an FE model of a blade to simulate the measured vibrational responses at the corresponding points. The input load was adjusted until a best-fit match between simulated and measured responses was achieved, thus validating the FEA approach. This validation allowed estimation of the full-field vibrational response of the blade using the input load. Finally, the predicted blade displacement field was used to determine the vibrational energy at every point on the blade, highlighting the energy distribution across a blade for a given thermosonic excitation. This proposed methodology would be most

useful prior to the introduction of a new blade or component to a thermosonic process. The methodology will potentially highlight the inspection dead zones where insufficient vibrational energy will be excited in the component. Thus, a judgement as to whether or not to proceed with the inspection of the component or change the inspection setup can be made at an early stage.

6.2 Methodology

6.2.1 Background

The methodology used to simulate the full-field vibrational response of a turbine blade under thermosonic excitation was based on determining the input excitation forces through experimentation and FEA, and then applying these excitation forces to an FE model of the turbine blade. Figure 6-1 illustrates the excitation process of a typical thermosonic test. An unknown excitation (input) is applied to the blade using a high power ultrasonic device and the vibration response (output) is measured using as a strain gauge, microphone or laser vibrometer. The input excitation forces in a thermosonic test are typically not measured, and this is partly due to the limitation of commercially available force transducers in measuring dynamic forces at high frequencies (> 20 kHz) [85]. This study proposes an indirect method of obtaining these input excitation forces for a given thermosonic test. The proposed method aims to use knowledge of the measured output of selected points on the blade to estimate the unknown input excitation

forces. Once the input excitation forces are known, these forces can be applied to an FE model of the turbine blade to simulate the full-field vibrational response of a blade. Figure 6-2 presents a flow chart that represents the proposed methodology. Each step in the flow chart is described in more detail in next few sub-sections.

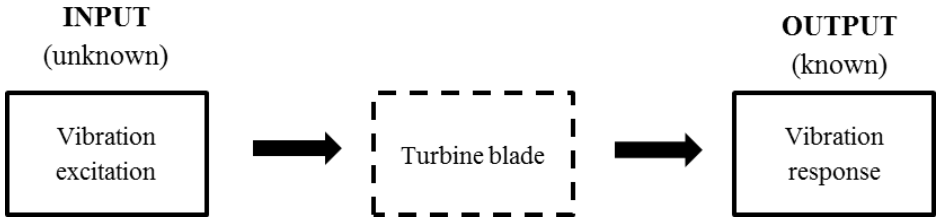

Figure 6-1 Excitation process of turbine blade. An unknown input excitation is applied to the blade and its vibration response is measured.

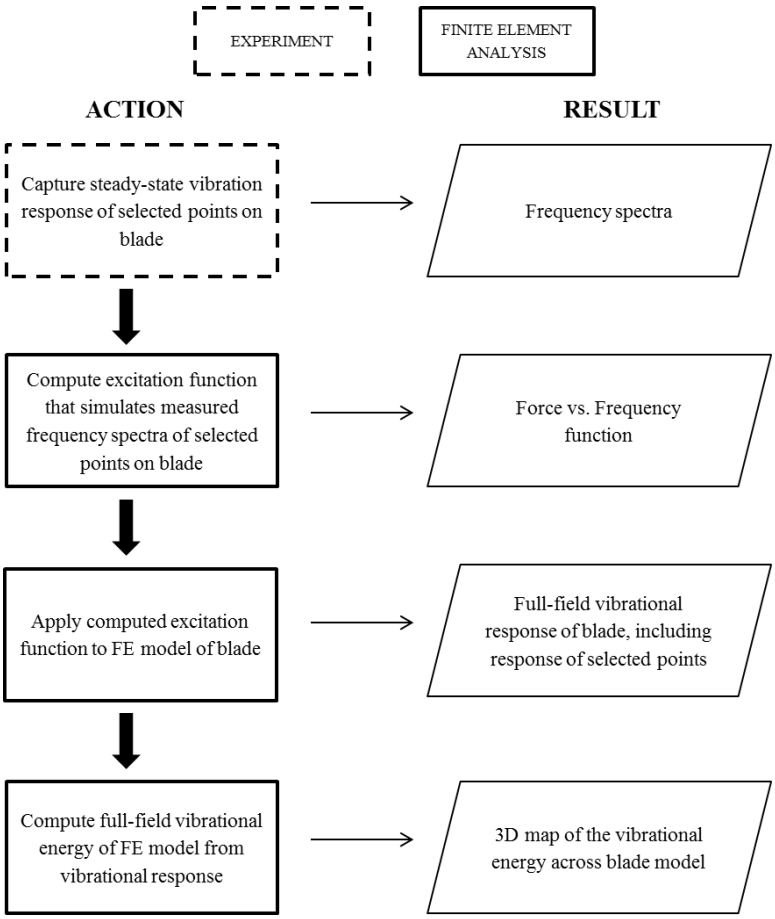

Figure 6-2 Proposed methodology for simulating the full-field vibrational response of a turbine blade under thermosonic excitation.

6.2.2 Pseudo steady-state vibrational response of selected points on a turbine blade

6.2.2.1 Pseudo steady-state vibrational response of turbine blade

Figure 6-3 shows a schematic of the experimental setup used for capturing the vibrational response of a blade in this study. This setup shows the turbine blade, the ultrasonic exciter and a laser vibrometer used to capture vibration. Throughout this

study, only frequencies up to 140 kHz were measured, although, the laser vibrometer was capable of measuring much higher frequencies. This limit was set to reduce the number of excitation frequency components used in the FEA and is consistent with the reported work by Morbidini et al. [6].

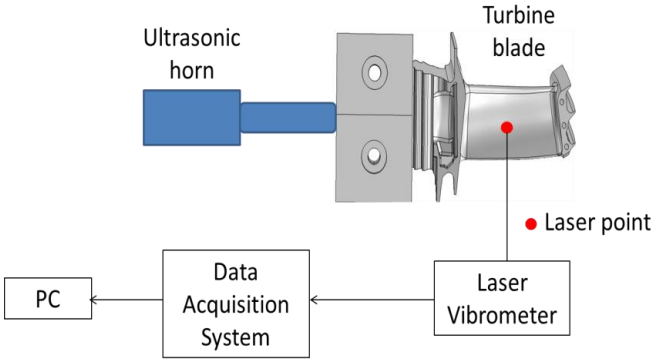

Figure 6-3 Schematic of thermosonic setup for measuring vibration of turbine blade.

The vibration waveform of a typical thermosonic test is highly transient [70, 75]. This was the case for the vibration waveforms seen in this study, although, pseudo steady-state conditions were typically observed about 0.4 seconds after the onset of vibration. Figure 6-4 shows an example of the vibration waveform captured in a test in this study. Figure 6-4 (a) shows the full vibration waveform, indicating two different sections, A & B. Section A is the transient portion, while Section B is the pseudo steady-state portion. Figure 6-4 (b) shows the STFT of the full vibrational waveform, which reveals the transient nature (i.e. amplitude) of the different frequency components. Figure 6-4 (c) and (d) shows the pseudo steady-state portion of the waveform (i.e. Section B) and its respective STFT. The STFT of Section B confirms pseudo steady-state behaviour, with

constant amplitude of the frequency components over time. Therefore, this stead-state portion was used to represent the vibration for each test performed in this study.

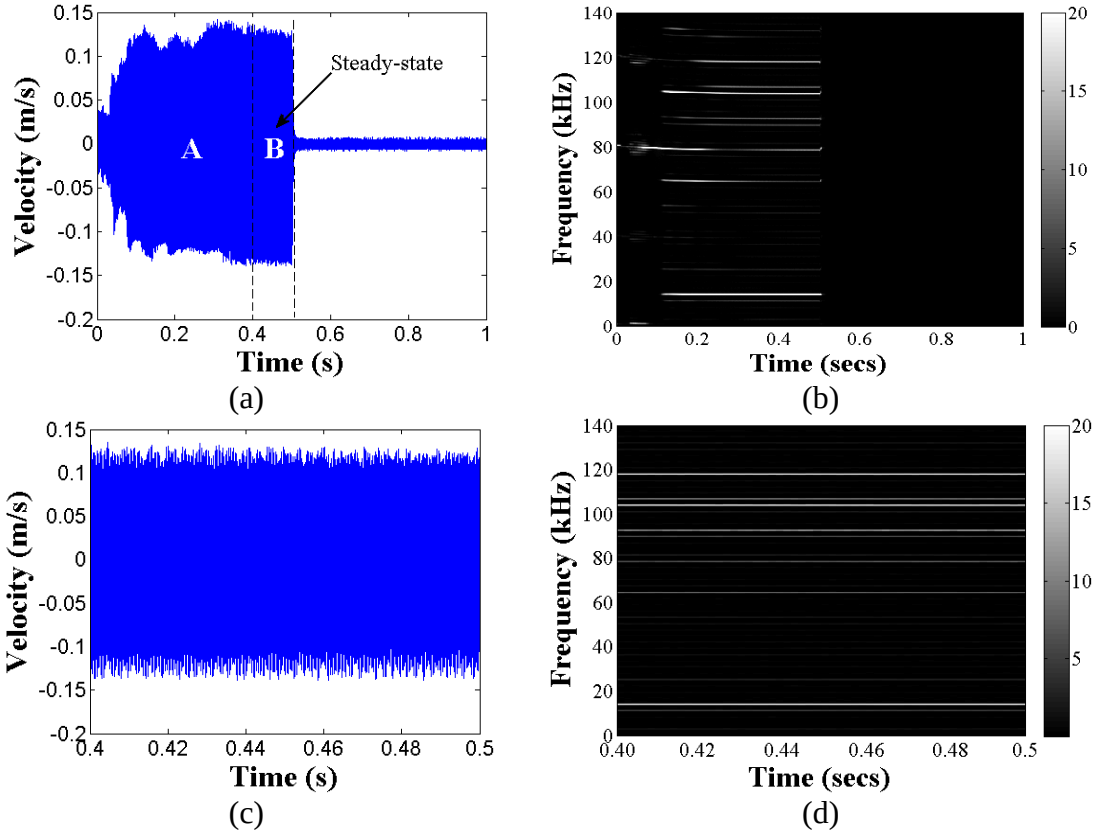

Figure 6-4 (a) Vibration waveform of a typical test (b) Short Time Fourier Transform (STFT) of the full vibration waveform (c) steady-state portion of the full vibration waveform (i.e. Section B) (d) STFT of the steady-state portion.

6.2.2.2 Vibration measurement of selected points on turbine blade

Five vibration measurement points were chosen on the turbine blade to validate the proposed methodology. The locations of these five points represented potential defect

sites on the blades. These locations are indicated by the red dots in Figure 6-5, which include locations on the shroud, trailing edge, leading edge, middle of aerofoil and under platform. Vibration measurements were taken from both the convex and concave side of the blades. In total, 10 separate thermosonic tests were completed on seven blades, with measurements of the five different points captured in each test. Table 6-1 details the ten different tests completed in this study.

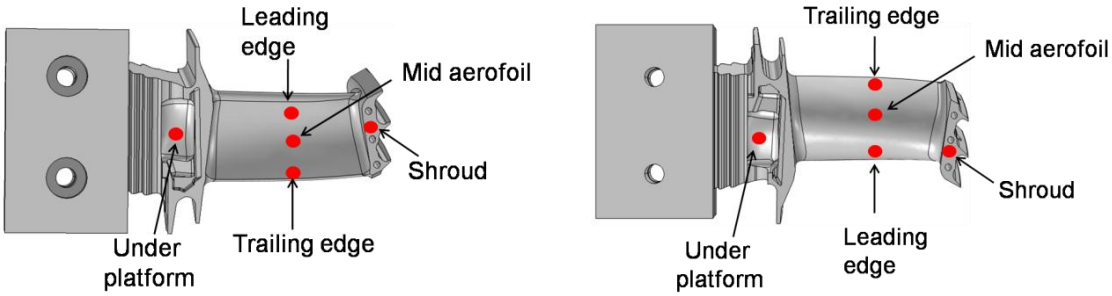

(a) Concave side (b) Convex side

Figure 6-5 Selected points on blade for vibration measurement.

Table 6-1 Ten different tests carried out seven different turbine blades.

Blade	Blade side measured	Horn force (N)
B29	Concave	175
B26_1	Concave	175
B18_1	Concave	175
B50_1	Concave	175
B10	Convex	175
B48	Convex	175
B26_2	Convex	175
B01	Concave	107
B18_2	Concave	107
B50_2	Concave	107

Simultaneously capturing the vibrational response of five points on a blade in a single test was not possible, given the short excitation time (0.5 seconds) and the transient nature of the excitation. Therefore, a different approach which involved measuring the vibrational response for each point in five different tests was used. However, this approach is only valid if the excitation in all five tests is repeatable. Repeatability was demonstrated by capturing the vibration of a single point in 15 consecutive tests and then comparing the vibrational response (i.e. frequency response) of all 15 tests. All 15 tests were carried out with excitation parameters kept constant (including coupling material). This repeatability demonstration was performed on four different points on the same blade to increase confidence in the approach. These points included all but one (mid aerofoil) of the points shown in Figure 6-5. The coupling material was changed for each of the four points due to degradation after 15 tests.

Figure 6-6 (a) - (d) presents a summary of the frequency response obtained in the 15 repeated tests of the four specified locations. Figure 6-6 only shows the top 12 excited vibration modes which together account for over 90% of the total energy content in the respective vibrations. The energy content of the measured vibration was computed as the sum of the square of the vibration amplitudes. Each bar in Figure 6-6 represents the average amplitude of a mode (for the 15 tests), while the error bar represents ±1 standard deviation. Note that the y-axis on all four plots in Figure 6-6 are normalised, allowing the differences in the frequency response of the four locations to be clearly seen.

However, more interesting is the variability in amplitude seen in the frequency response of the 15 tests for each of the four locations.

Qualitatively, the variability of the frequency response for the 15 repeated tests can be considered small. The level of variability was further assessed quantitatively by computing the coefficient of variation (CV), which is a normalised measure of variation as a percentage of the mean (i.e. Standard Deviation/Mean). Figure 6-7 shows a histogram of the CV computed for all 48 modes (i.e. 12 modes per location). Figure 6-7 shows 42 of the 48 modes with a variability of less than 20% and only 2 modes with a variability of approximately 40%. Furthermore, the average CV for all 48 modes was approximately 14%. This level of repeatability was considered acceptable, given the high number of repeated tests (i.e. 15) using the same coupling material, but more importantly, considering that the repeatability of the excitation in thermosonics is generally reported to be poor. It must be noted that this degree of repeatability was only achieved with all excitation parameters, including the coupling material, kept constant. Based on the results obtained in this repeatability study, the excitation was assumed to be determinable (with a 14% error), and therefore, the vibration response of five different points on a blade could be obtained for a given excitation, although in five separate tests.

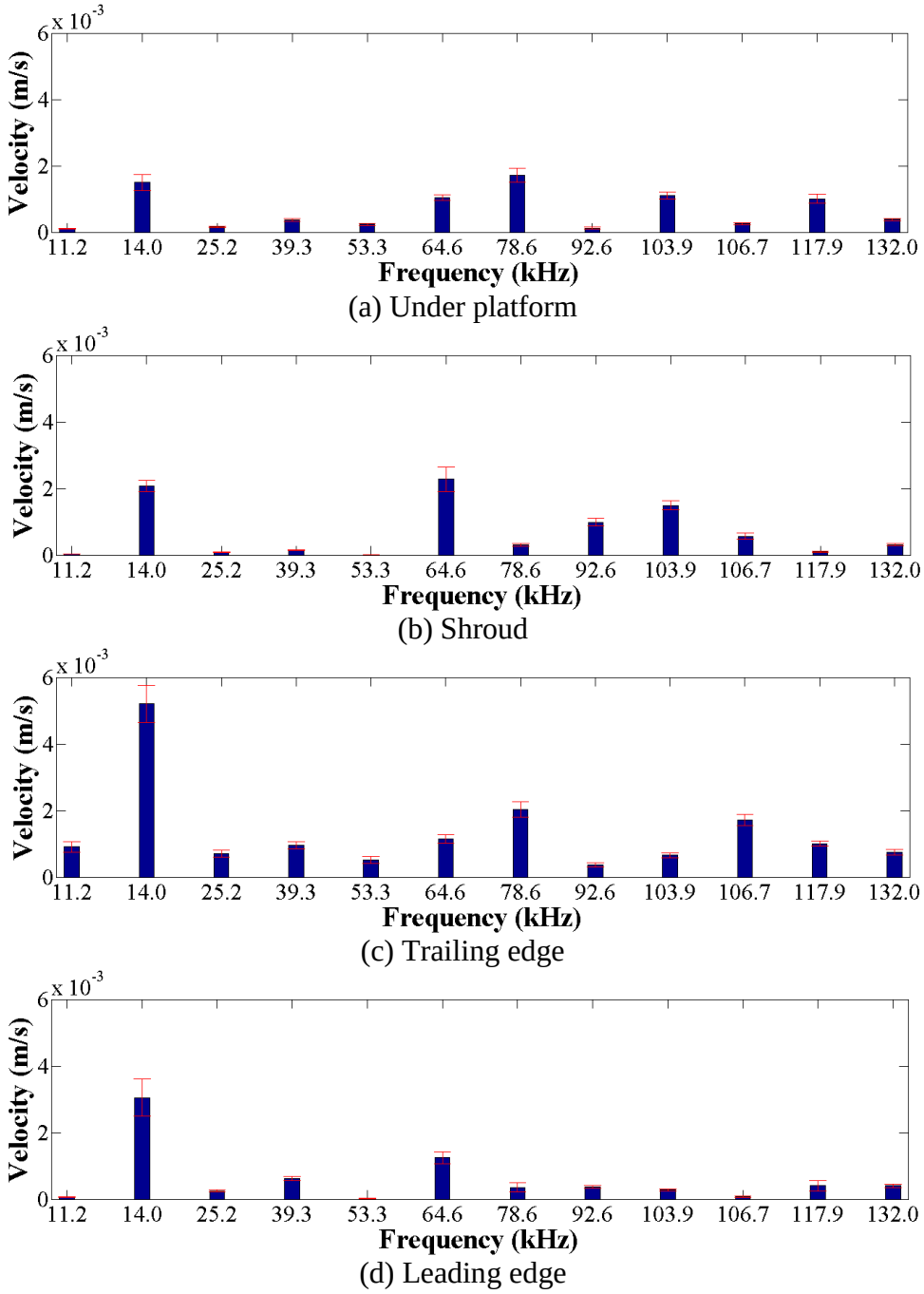

Figure 6-6 Frequency response of four different points on blade. Each bar represents the average of the respective mode over 15 repeated tests. The error bar is ±1 standard deviation (a) mid aerofoil (b) shroud (c) trailing edge (d) leading edge.

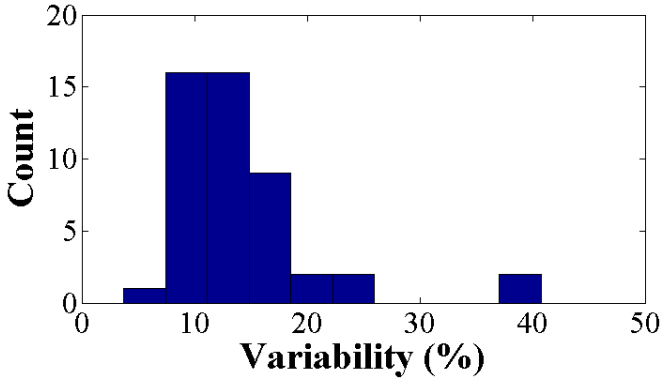

Figure 6-7 Histogram of the computed variability of the 48 modes measured in repeatability study.

6.2.3 Determination of input excitation

Section 6.2.2 presented the first step in the process of simulating the full-field vibrational response of a turbine blade under thermosonic excitation. This step involved simultaneously capturing the vibrational response (frequency spectra) of five different points on the blade. The second step described in this sub-section involves determining the unknown input excitation (i.e. load) that generated the measured vibrational responses. This process involved the use of the measured vibrational response data (i.e. frequency spectra) and finite element analysis (FEA) of the blade. The idea was to iteratively apply an input excitation to an FE model of the blade until the vibrational responses seen in experiment was matched in the FEA programme. However, prior to determining the unknown input excitation, the measured frequency spectra (i.e. vibrational responses) were adjusted to only account for the prominent vibration modes.

6.2.3.1 Selecting vibration modes for Finite Element Analysis (FEA)

In order to simulate the measured frequency spectra, the input excitation should include all the vibration modes seen in the frequency spectra. This is because the FEA software used in this study is completely linear, meaning that a load applied to a structure at a discrete frequency results in a response at the same frequency, with no non-linearities (e.g. harmonics) excited. For example, Figure 6-8 (a) and (b) respectively show the measured vibration responses of a point on the shroud and trailing edge of the same blade for a given excitation. Both figures show a large number of distinct vibration modes which all have to be included in the input excitation function for the FEA. Applying each distinct frequency in the FEA programme was however impractical, as it required significant computer resources (i.e. memory) and a long computation time to execute. Therefore, it was decided to select a single set of modes for the 50 different measured vibration responses to be used in the FEA. Note, the 50 measured vibration responses refers to the 5 vibration measurements completed in 10 separate tests (see Section 6.2.2.2). The criterion for selecting this single set of modes was that for each measured vibration response, the single set of modes combined to give at least 80% of the total energy of the measured vibration. This approach ensured a reduced number of vibration modes were included in the input excitation function.

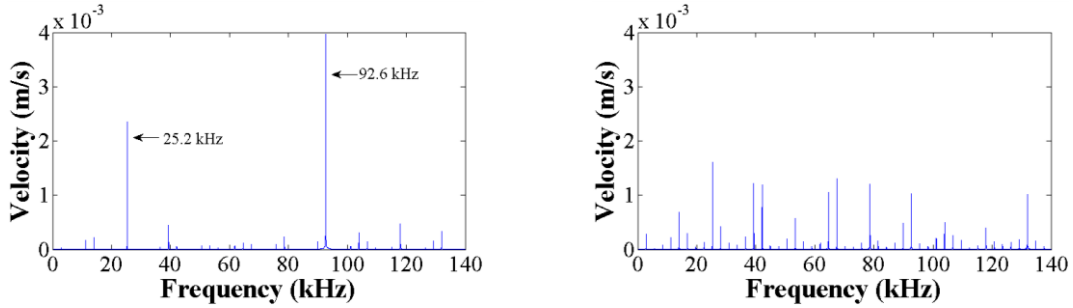

(a) Shroud (b) Trailing edge

Figure 6-8 Frequency response of two points on a blade. (a) one mode (92.6 kHz) containing over 80% of the total energy content (b) several modes of equal dominance with at least 12 modes combining to give 80% of the total energy content.

As expected, a different set of modes combined to achieve the 80% target for the 50 different vibration responses. For some, only 1 mode was required, while for others, over 10 modes were required, as illustrated in Figure 6-8 (a) and (b). Figure 6-8 (a) (i.e. shroud) clearly has two dominant modes at 25.2 kHz and 92.6 kHz, while in Figure 6-8 (b) (i.e. trailing edge), there are several modes of equal dominance. For the shroud, the 92.6 kHz mode contains approximately 82% of the total energy content of the vibration, whilst for the trailing edge, 12 different modes are required to achieve approximately 80% of the total energy content. In order to select a common set of modes that combined to give 80% of the total energy content for all 50 different measured vibrational responses, the following process was used:

- Firstly, the top five dominant modes for each of the 50 measured vibrational responses were selected.
- Secondly, a histogram was plotted to highlight the number of occurrences of the different modes selected

- Finally, a common set of modes that combine to give 80% of the total energy content was chosen from the most occurring modes shown in the histogram

The top five dominant modes were first selected as they had a combined energy content greater than the 80% for 45 out of the 50 vibrational responses. However, the set of five modes differed for each of the measured vibrational responses, although some modes occurred repeatedly. Figure 6-9 shows a histogram count of all the modes that were seen in the top five modes of the 50 measured vibrational responses. A total of 17 different modes are shown in Figure 6-9. The 39.2 kHz mode was the highest occurring mode, closely followed by the 78.6 kHz mode. However, more important was the set of modes which when combined for any of the 50 vibration responses, contained at least 80% of the total energy content. Figure 6-10 (a) and (b) respectively show the combined energy content when using the top 5 and 13 most occurring modes.

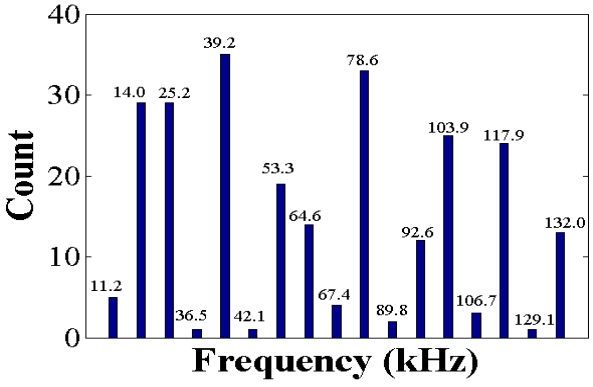

Figure 6-9 Number of occurrences of the dominant modes in all the 50 vibration measurements.

The x-axis of Figure 6-10 represents the set of 10 tests, while the y-axis represents the combined energy of the set of modes for the five different locations on the blade. Each of the five locations is represented by a different legend in Figure 6-10. The combined energy of the 5 most occurring modes, as shown in Figure 6-10 (a), were well below the 80% threshold for all five locations. However, using the 13 most occurring modes gives an enhanced result as shown in Figure 6-10 (b), where all but three measured responses were above the 80% threshold. Two of the three responses below the threshold were for points on the trailing edge (at 40% and 70%) and the third was for a point on the leading edge (at 74%). Increasing the number of modes did not have a significant improvement on the results. Using all 17 modes shown in Figure 6-9 only improved the number of responses over the 80% threshold by one. This marginal increase was deemed not significant enough to use an extra four modes in the FE analysis. Therefore, the 13 most occurring modes, as shown in Figure 6-9, were chosen as the set of modes for the FE analysis.

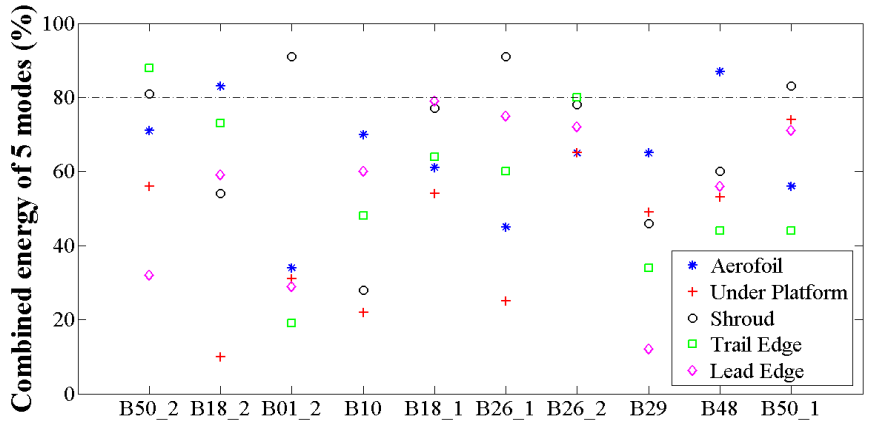

(a)

Top 5 modes (39.3 + 78.6 + 14.0 + 25.2 + 103.9 kHz)

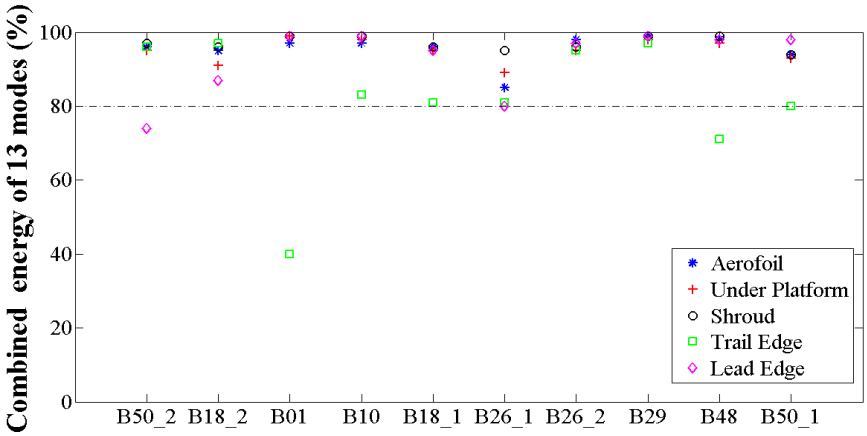

(b)

Top 13 modes (39.3 + 78.6 + 14.0 + 25.2 + 103.9 + 117.9 + 53.3 + 64.6 + 132.0 + 92.6 + 11.2 + 67.4 + 106.7 kHz)

Figure 6-10 Combined energy content of a set of modes (a) top 5 most occurring modes (b) top 13 most occurring modes.

6.2.3.2 Finite Element Analysis (FEA)

Finite Element Analysis (FEA) was used as part of this study to predict the full-field vibrational response of a turbine blade under thermosonic excitation. The FEA method is an established and reliable numerical method for analysing the behaviour of a

structure under a variety of conditions. The basic concept behind FEA is finding a numerical solution to a complex problem by breaking it down into a simpler one made up of discrete parts called elements, connected together by a finite number of points called nodes. The FEA software used in this study was the Comsol Multiphysics Structural Mechanics module [132]. This software package is used for predicting the behaviour of structures subjected to mechanical loads. For this study, the software was used to compute the displacement field of a turbine blade subjected to harmonic loads of varying frequencies, although, other quantities such as strain, stress etc. can be computed from the displacements. Furthermore, the analysis carried out in this study was completely linear, ignoring all material and geometric non-linearities.

Typically, structural mechanics in FEA is used to determine the distribution of stress within a structure. First, the structure is divided into discrete elements connected by nodes. The displacement field, u within the elements is then approximated by a set of functions generally known as a "shape functions" and denoted by N_i [133].

$$u = N_i u_i \tag{6.1}$$

where u_i is the unknown displacement vector at each nodal point. Next, equations relating the forces acting on the nodes and the resultant nodal displacements are derived for each element:

$$F = Ku \quad (\mathbf{6.2})$$

where F is a vector of nodal forces and K is the element stiffness matrix. The stiffness matrix is related to the geometry and properties of the structure. The equations of the individual elements are then assembled into global matrices, forming the overall system of equations that describe the behaviour of the structure [133]. After taking into account all boundary conditions, the system of equations is solved for the unknown nodal displacements. The computed displacements can then be used to obtain the element strains and stresses using the governing equations of solid mechanics [133]. In this study however, the displacement field was of primary interest.

6.2.3.3 FE Model

Figure 6-11 (a) and (b) respectively show the 3D FE blade model and photograph of the blade, both attached to a clamp. The FE model closely resembles the blade and clamp geometry except for the cooling holes at the trailing and leading edge, which could not be easily added to the model. The blade model shown in Figure 6-11 (a) was produced from an X-ray CT scan of a real blade, where both the external and internal structure of the blade was captured, as shown in Figure 6-12. The blade and clamp were modelled as a single geometry as opposed to separate components in contact. This was to avoid contact analysis which introduces non-linearities and a significant increase in computation time and resources [132].

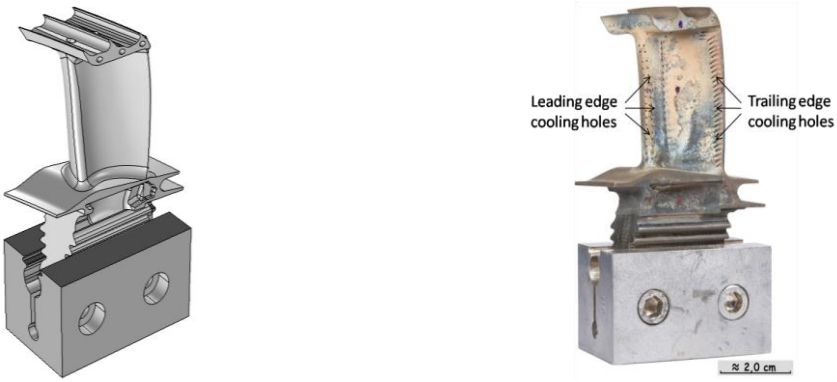

(a) (b)

Figure 6-11 Turbine blade representation (a) FE model (b) image of turbine blade.

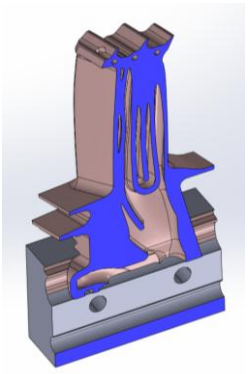

Figure 6-12 Internal and external structure of turbine blade model

Table 6-2 details the blade and clamp material properties required to perform the analysis on the model. The clamp is made of mild steel, while the blade is made of a single crystal nickel-based superalloy (CMSX-4) with cubic symmetry. For anisotropic materials such as CMSX-4, 21 independent variables (elastic constants) are generally used to describe the material in a FEA programme [134]. However, due to the combination of cubic symmetry of CMSX-4 and the equivalence of the shear conditions,

only three variables would be required [134, 135]. Equation 6.3 shows the elastic properties of a cubic material in matrix notation, while Table 6-3 shows the three elastic constants used for CMSX-4 in the FEA programme [134]. Furthermore, Figure 6-13 shows the coordinate system used to define the anisotropic material properties with respect to the blade geometry [85]. The (001) in Figure 6-13 refers to the orientation of the single crystal used in the manufacture of the turbine blade. The (001) direction, aligned along the blade longitudinal axis, is the direction of lowest elastic modulus and highest creep resistance, and therefore the preferred growth direction of the crystal [136]. However, it must be noted that in real systems, such as the blade used in this study, the orientation of the single crystal is not perfectly aligned with the blade longitudinal axis. For the blade used in this study, the alignment is generally accurate to within ±0.8° [134].

Table 6-2 Material properties of turbine blade and clamp.

Material property	CMSX-4 (Blade)	Mild steel (Clamp)
Young's Modulus, E	127 GPa	210 GPa
Shear Modulus, G	130.9 GPa	-
Poisson's ratio, ν	0.377	0.33
Density, ρ	8720 kg/m3	7850 kg/m3
Loss factor	0.0025	0.008

$$D(elasticity\ \ matrix) = \begin{bmatrix} c_{11} & c_{12} & c_{12} & 0 & 0 & 0 \\ c_{12} & c_{11} & c_{12} & 0 & 0 & 0 \\ c_{12} & c_{12} & c_{11} & 0 & 0 & 0 \\ 0 & 0 & 0 & c_{44} & 0 & 0 \\ 0 & 0 & 0 & 0 & c_{44} & 0 \\ 0 & 0 & 0 & 0 & 0 & c_{44} \end{bmatrix} \quad \textbf{(6.3)}$$

Table 6-3 Elastic constant for CMSX-4 [values supplied by Rolls-Royce].

Material property	Value at room temperature (298 K)
c_{11}	235 GPa
c_{12}	142 GPa
c_{44}	131 GPa

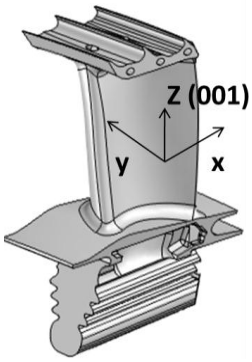

Figure 6-13 Coordinate system used for the blade material property in the FEA programme

The optimal finite element mesh for the FE model was obtained through convergence testing. This involved gradually increasing the mesh density (i.e. no of elements) and solving the model at each mesh setting. As the mesh density increased, the solution was monitored until convergence (i.e. stable condition), at which point the mesh density was considered optimal. The mesh of the FE model in this study was an unstructured mesh with 222,923 elements, comprising mostly of tetrahedral elements.

The boundary conditions applied in the FE model reflected the experimental setup, and can be split into constraint and load. Figure 6-14 illustrates the constraints and horn load applied on the blade/clamp in the experimental setup. The blade clamp was securely held at its sides by a vice, constraining the blade and clamp from any movement during vibration. This setup was modelled as a fixed constraint in the FEA programme, as shown in Figure 6-15 (a). This constraint set the displacement of the clamp sides in all directions (i.e. x, y, z) to zero. The circular area (17 mm diameter) highlighted in Figure 6-15 (b) is the location on the clamp where the horn excitation is applied.

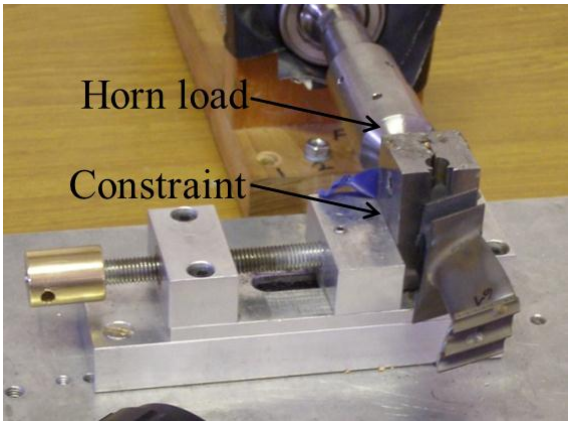

Figure 6-14 Constraints and horn load applied on the blade.

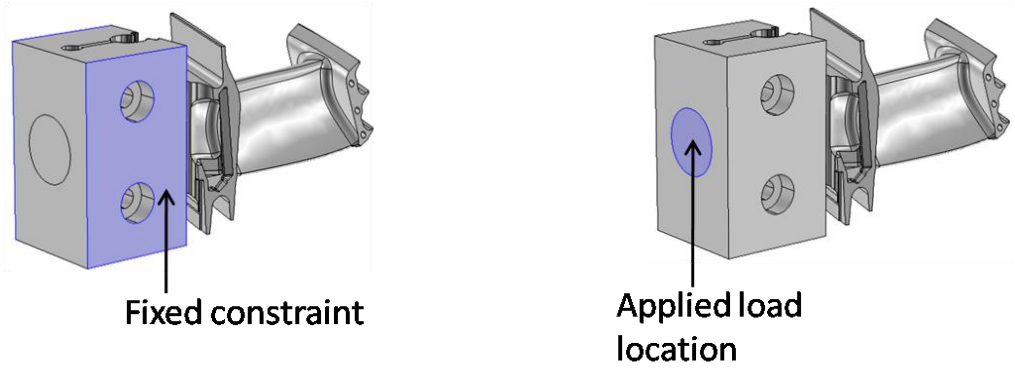

(a) (b)

Figure 6-15 (a) Fixed constraint on FE model (b) Location of applied load on FE model.

6.2.3.4 Input excitation

The input excitation for a given thermosonic test was determined using knowledge of the measured vibrational responses of several points on the blade and FEA. The determined input excitation was considered valid, if when applied to the FE model, the vibrational responses obtained in the FEA closely matched the experimental vibrational responses. The input excitation to be determined was a series of loads applied at discrete

frequencies i.e. frequencies observed in the experimental vibrational responses. For a given thermosonic test, the following process was used to determine the input excitation function:

- Firstly, the vibrational responses (frequency spectra) of five points on a blade were measured (see Section 6.2.2).
- Next, a common set of prominent frequencies were selected from the measured vibration responses of the five points (see Section 6.2.3.1)
- A 1 N base load at the selected frequencies was applied to the FE blade model. The weightings of the base load were then adjusted until the vibration responses of the FE model closely matched the vibration responses observed in experiment
- Once best-fit between FEA and experiment was achieved, the adjusted input load was considered optimal and applied to the FE model again, but this time to obtain the full-field vibrational response of the blade through summation of the individual frequency responses.

6.2.4 Full-field vibrational energy of turbine blade

The full-field vibrational energy of the blade was computed after the input excitation function was validated by comparison of the FEA and measured vibration responses. Two vibrational energy parameters were computed: the A^2 and the Energy Index (EI). The EI represents the heating potential of a system as it takes into account vibrational

energy and frequency, whereas, the A^2, simply represents the energy available for damping by the vibrating system. Methodology for computing the EI and A^2 are described in Chapter 4 and 5 respectively. For each of the 10 tests carried out in this study, the EI and A^2 were computed on each point (i.e. element) of the FE model to give the full-field vibrational energy of a blade.

6.3 Results

6.3.1 Comparison of the FEA and measured vibrational response

This Section presents a comparison of the vibrational response obtained in FEA and experiment for blade B29 and B50_1. The result for the other eight blades can be found in Appendix B. The results for B29 and B50_1 highlights all the important observations found in the other eight results. Firstly, the input excitation function obtained for B29 and B50_1 are shown in Figure 6-16 and Figure 6-17 respectively (Note: input excitation for other eight blades is presented in Appendix A). The input excitation function shown in both Figures were divided into two parts ((a1) & (a2)) due to the presence of a wide dynamic range (i.e. large and small) of forces. A log scale was not used in this case as the range of the forces was not large enough to give a reasonable representation of the variation in the data. Results in this study generally showed the first four modes with larger forces compared to the remaining nine modes, and therefore split accordingly. Hence, the y-axis scale shown in (a1) was made 10 times that of (a2) to

allow for easier comparison. Figure 6-16 and Figure 6-17 represents the input load applied to the blade in the FEA programme to simulate the vibrational responses seen in experiment. Figure 6-18 and Figure 6-19 shows a comparison of the vibrational responses obtained in FEA and experiment for B29 and B50_1 respectively.

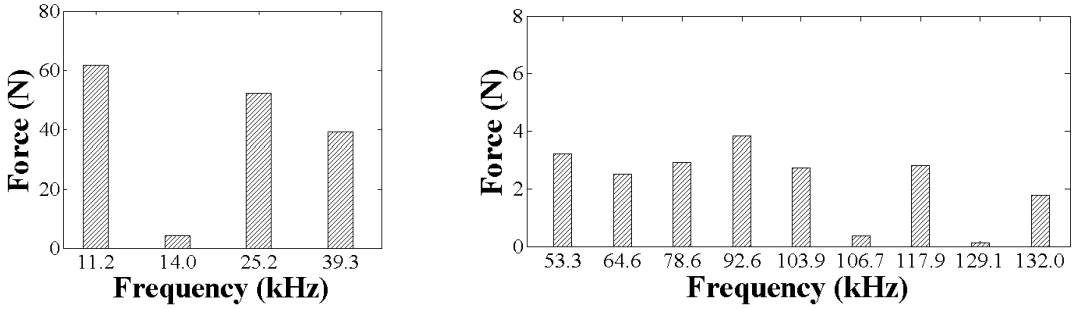

Figure 6-16 Input excitation function for blade B29. The input excitation was split into two parts due to the presence of a wide dynamic range of forces. (a1) shows the first four modes and (a2), the remaining nine modes. The y-axis of (a1) is 10 times that of (a2).

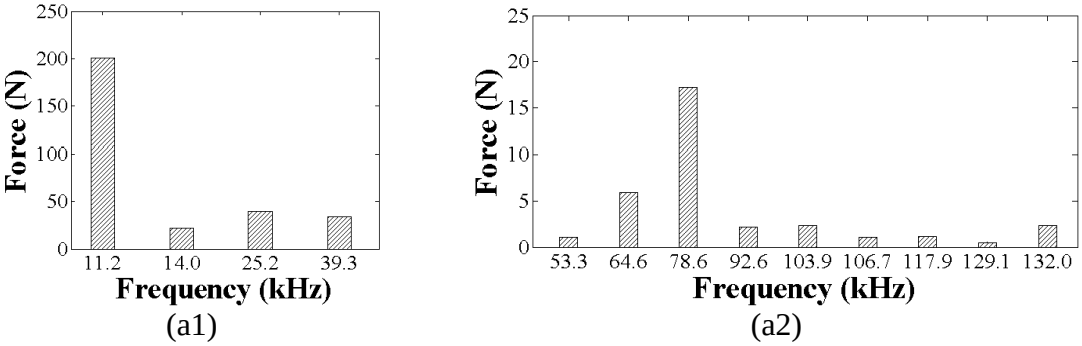

Figure 6-17 Input excitation function for blade B50_1. The input excitation was split into two parts due to the presence of a wide dynamic range of forces. (a1) shows the first four modes and (a2), the remaining nine modes. The y-axis of (a1) is 10 times that of (a2).

Figure 6-18 and Figure 6-19 each show five different frequency response plots, representing the five different points on the blade where vibration data was captured. Plot (a) – (e) respectively show the result for points on the (a) mid aerofoil, (b) under platform, (c) shroud, (d) trailing edge, (e) leading edge. The y-axis is the velocity amplitude, while the x-axis represents the 13 different modes that combine to give at least 80% of the total energy content of their respective vibration. The vibration amplitude measured by the laser vibrometer was the out-of-plane velocity component and this was mirrored in the FEA by using the y-component (out-of-plane) of the velocity amplitude. For each mode on the plots, the first bar represents the measured frequency response and the second bar, the FEA frequency response. The error bar on the measured frequency response is the average error of 14% computed in the repeatability demonstration described in 6.2.2.1.

The result for B29 in Figure 6-18 demonstrates a good qualitative agreement between the simulated and measured vibrational response for majority of the modes in the five different locations. This good agreement can be particularly seen in Figure 6-18 (c) and (d): shroud and trailing edge locations. In both locations, the FE response was within the limits of the measured response for several modes, such as in the 25.2 kHz, 39.3 kHz and 78.6 kHz modes for the shroud and 11.2 kHz, 39.3 kHz and 106.7 kHz modes for the trailing edge. For most of the other modes in these two locations, there is a small discrepancy between the FE and measured responses, except for the 92.6 kHz and 132

kHz modes for shroud, and the 53.3 kHz mode for the trailing edge where the discrepancy is much larger. For the shroud, the FE overestimated the measured response by approximately 25 times and 2 times for the 92.6 kHz and 132 kHz modes respectively, while for the trailing edge the 53.3 kHz mode was underestimated by FEA by approximately 2 times. The overestimation of the 92.6 kHz mode in the shroud by 25 times was considered extremely high and not typical of the results for the other eight blades shown in Appendix B.

The result of B50_1 shown in Figure 6-19 also demonstrates good qualitative agreement between the FEA and measured vibrational response for majority of the modes. The level of agreement is similar to that observed for B29 in Figure 6-18. For B50_1, the shroud and trailing edge location (Figure 6-19 (c) and (d)) had the best agreement. For the shroud, the FE response for the 11.2 kHz, 39.3 kHz and 78.6 kHz modes is within the limits of the measured responses, while the same is seen for the 11.2 kHz, 14.0 kHz, 25.2 kHz, 39.3 kHz, 78.6 kHz, 103.9 kHz and 106.7 kHz modes for the trailing edge. The mode with the worst agreement for B50_1 was the 39.3 kHz mode in the leading edge. For this mode, the FE response overestimated the measured response by approximately 10 times.

The error between the FEA and measured vibrational response for each mode was quantified by calculating the percentage error. The percentage error represents the

relative error between the predicted and measured response and was computed using Equation 6.4, where e is the percentage error, $u_{measured}$ is the measured velocity response and u_{FE} is the FE velocity response.

$$e = \left| \frac{u_{measured} - u_{FE}}{u_{measured}} \right| \times 100\% \qquad (\mathbf{6.4})$$

Figure 6-20 and Figure 6-21 show the percentage errors of the 13 modes for each of the five different locations for B29 and B50_1 respectively. The percentages error are presented in a box-plot format, showing the median and quartiles, while the box-plot whiskers indicate the extreme data points not considered outliers. The outliers shown as a plus sign were calculated as points greater than 1.5 times the top whisker. The box-plot illustrates the distribution of the percentage errors for the modes in the five different locations. Note that in Figure 6-20 for B29, four outliers at 2500%, 360%, 335% and 235% were excluded to give a better scale for the box plots. Similarly, two outliers at 1056% and 537% were excluded for B50_1 (Figure 6-21) For B29, percentage errors at the 75th quartile were approximately: 42%, 43%, 27%, 32% and 80% for the mid aerofoil, under platform, shroud, trailing edge and leading edge locations respectively. This demonstrates that the discrepancy between the predicted and measured response for majority of the modes in B29 were below 50%, except for some modes in the leading edge and the five modes considered as outliers. For B50_1, the percentage errors at the

75th quartile were generally higher than that of B29 at approximately: 125%, 49%, 50%, 23% and 53% for the mid aerofoil, under platform, shroud, trailing edge and leading edge locations respectively. Both B29 and B50_1 had the same number of outliers.

Figure 6-22 shows a summary of the percentage errors for all 10 blades including B29 and B50_1. This Figure shows the combined result for all five locations on each blade. Each blade has a total of 65 modes for the five locations. Note that five outliers at 3685% (B10), 2500% (B29), 1837% (B48), 1422% (B26_2) and 1225% (B26_2) were excluded in this Figure. Apart from the outliers, the range of percentage errors (i.e. box-plot) for each blade is fairly similar. The 75th quartile for the 10 blades ranged between 44% and 66%, meaning the vast majority of the error between the measured and predicted response was below 66%. In addition, approximately 16% of the 650 modes had no error i.e. predicted response was within the limits of the measured response. It can also be seen in Figure 6-22 that the number of outliers was equally distributed, with no single case having a disproportionate number of outliers.

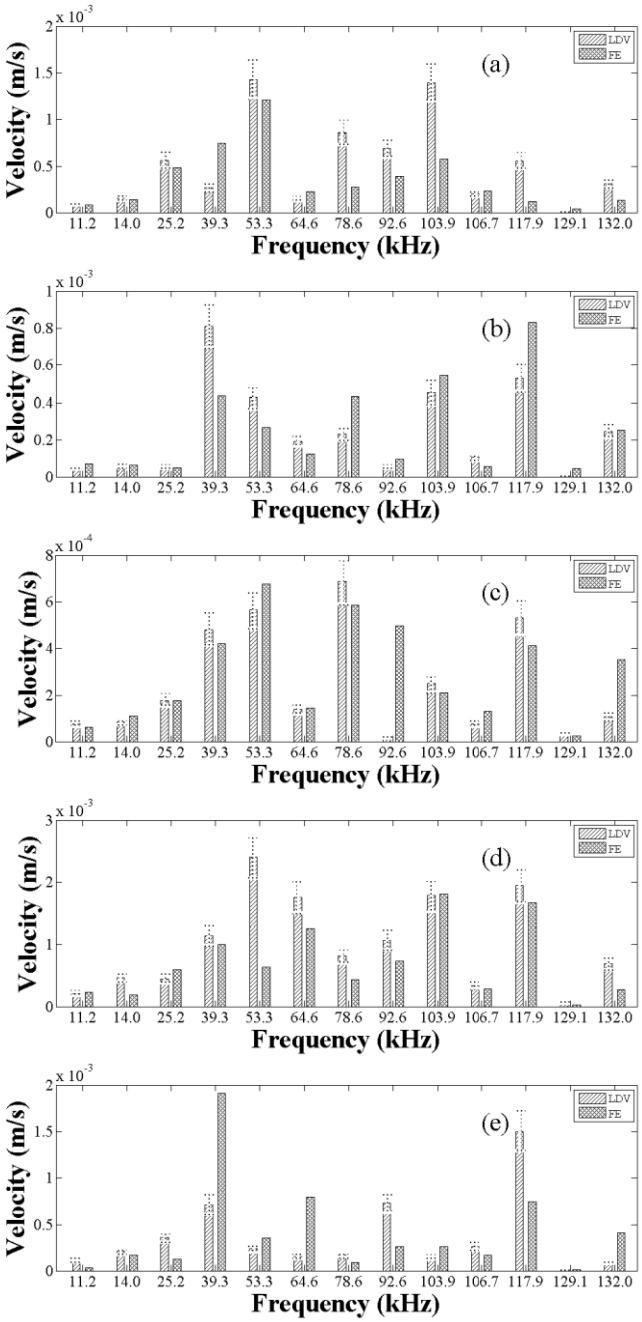

Figure 6-18 Comparison of measured frequency response and FE frequency response for B29 (a) Mid aerofoil (b) Under platform (c) Shroud (d) Trailing edge (e) Leading edge.

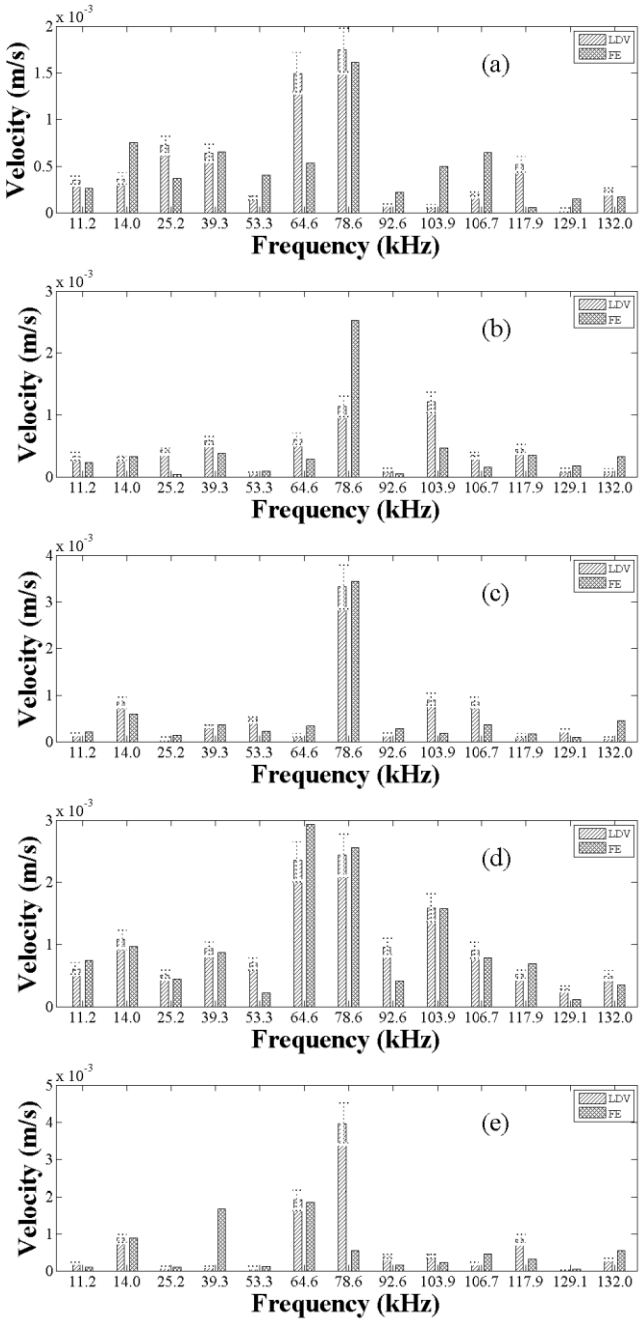

Figure 6-19 Comparison of measured frequency response and FE frequency response for B50_1 (a) Mid aerofoil (b) Under platform (c) Shroud (d) Trailing edge (e) Leading edge.

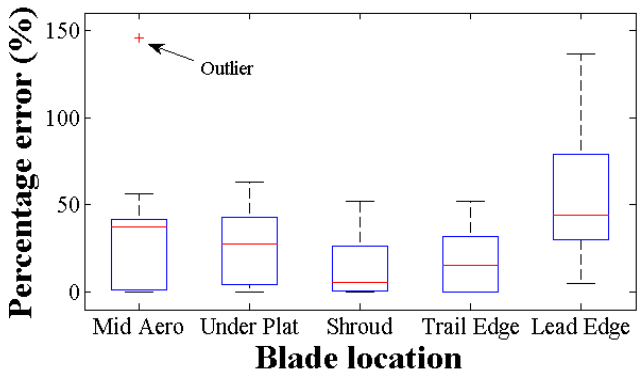

Figure 6-20 Percentage errors of the 13 modes for the five different locations on B29. The box-plots show the median and quartiles and the whiskers show extreme data points not considered outliers. Outliers are plotted with a plus sign. Note: four outliers at approximately 2500% (Lead Edge), 360% (Lead Edge), 335% (Lead Edge) and 235% (Under Plat) were excluded to improve scale.

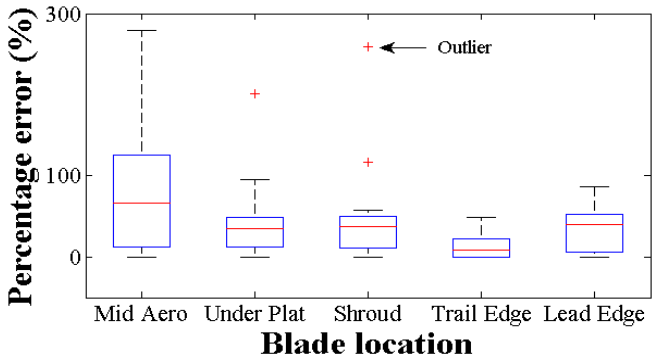

Figure 6-21 Percentage errors of the 13 modes for the five different locations on B50_1. The box-plots show the median and quartiles and the whiskers show extreme data points not considered outliers. Outliers are plotted with a plus sign. Note: two outliers at approximately 1056% (Lead Edge) and 537% (Mid Aero) were excluded to improve scale.

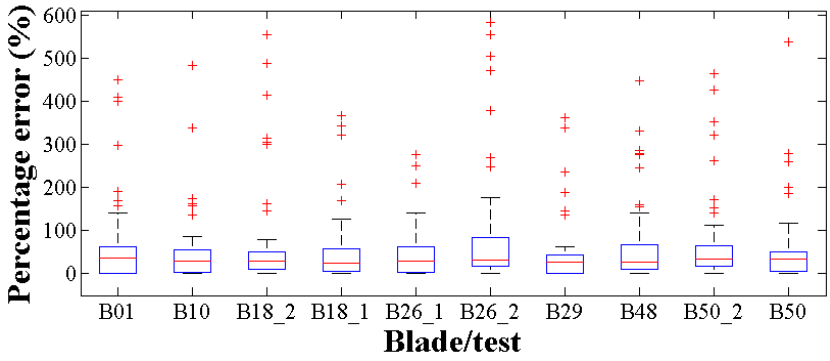

Figure 6-22 Percentage errors for the 10 blades/test. Each blade/test has a total of 65 modes for the five locations. The box-plots show the median and quartiles and the whiskers show the extreme data points not considered outliers. Outliers are plotted with a plus sign. Note: five outliers at 3685% (B10), 2500% (B29), 1837% (B48), 1422% (B26_2), 1225% (B26_2) and 1056% (B50) were excluded in this plot.

6.3.2 Full-field vibrational energy of turbine blade

Figure 6-23 and Figure 6-24 show the computed full-field vibrational energy for blade B29 and B50_1 respectively. The results of the remaining eight blades can be found in Appendix C. Figure 6-23 and Figure 6-24 illustrate the vibrational energy (i.e. A^2 and Energy Index (EI)) determined by combining the individual displacement simulations for each selected excitation frequency. The colour map is presented in a log-scale, with red and blue representing the highest and lowest vibrational energy respectively, while yellow and green, vibrational energy in-between. Note that the colour scales are not normalised, therefore vibrational energy cannot be compared between different blades. In addition, quantitative comparisons cannot be made between A^2 and EI. The aim of computing the full-field vibrational energy is to illustrate the vibrational energy distribution across a turbine blade, and hence, understand the extent of potential

coverage during the test on that blade. Figure 6-23 (a) highlights the five locations of interest in this study and also six other numbered points of interest (dashed circle).

The first observation in Figure 6-23 and Figure 6-24 is the non-uniform distribution of the vibrational energy across the blade and clamp. This is particularly evident when comparing the vibrational energy of the blade and clamp, with the former generally having the higher energy level. The absence of colour (i.e. transparent) on the sides of the clamp is due to the zero displacement constraint associated with that part of the clamp. It can also be noticed that the vibrational energy distribution across the blade for the A^2 and EI are similar. For B29 in Figure 6-23, the highest energy levels are not in any of the five locations of interest, but rather at the other points of interest highlighted by dashed circles, numbered 1 to 6. Points 1, 2 and 3 are the edges of the shroud seal fins, while point 4, 5 and 6 are edges of the blade platform. The trailing edge is the only location of interest that has similar energy levels to the numbered points. The vibrational energy distribution for B50_1 is slightly different from that of B29. For B50_1, points 2 and 3 and across the blade aerofoil and root, relatively higher energy levels can be seen, compared to B29. The vibrational energy distributions for all ten blades were different, although some general observations were noted, such as:

- The clamp had a lower vibrational energy than the blade
- Higher vibrational energy spread across the aerofoil, although mostly towards the thinner trailing edge region

- The highest vibrational energy levels were primarily found in points 1 – 6 highlighted in Figure 6-23. In addition, for some blades, high energy levels were observed in most parts of the seal fins
- For the blade, the lowest vibrational energy levels were mostly seen in some parts of the leading edge, platform, blade root and middle section of the shroud seal fins.
- Of the five locations of interest set out at the start of this study, the trailing edge had the highest vibrational energy level

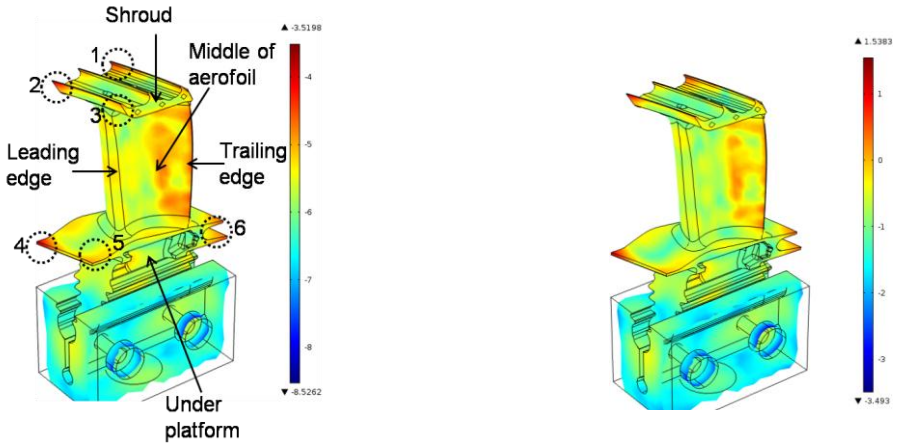

(a) A^2 (b) Energy Index (EI)

Figure 6-23 Full-field vibrational energy of blade B29. Colour map is presented in log-scale, with red and blue representing the highest and lowest vibrational energy respectively, and yellow and green, vibrational energy in-between.

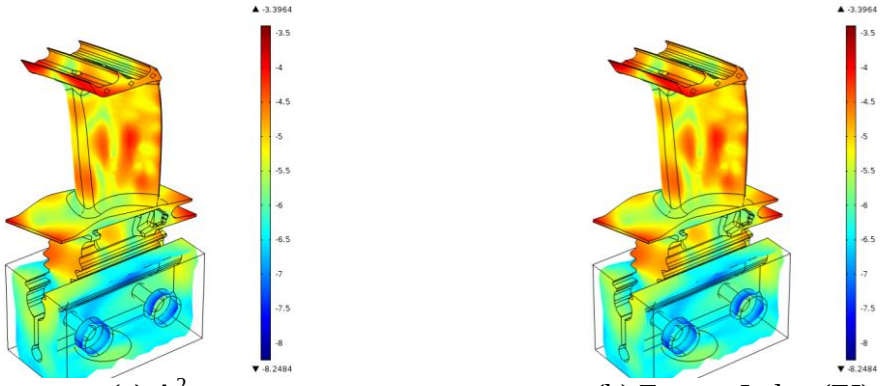

(a) A^2 (b) Energy Index (EI)

Figure 6-24 Full-field vibrational energy of blade B50_1. Colour map is presented in log-scale, with red and blue representing the highest and lowest vibrational energy respectively, and yellow and green, vibrational energy in-between.

6.4 Discussion

The aim of the work described in this Chapter was to simulate the full-field vibrational response of a turbine blade under thermosonic excitation. Knowledge of the vibration coverage of a blade can provide insight into the excited energy distribution across the blade for a typical thermosonic inspection. This would help in highlighting areas of the blade where higher or lower energy levels are generally excited. A methodology using vibration measurements and FEA was used to simulate vibration coverage of 10 tests using seven different blades. The methodology was validated by comparing the measured and simulated vibrational response of five different points on the blade, which generally, showed good qualitative agreement. This good agreement formed the basis for computing the full-field vibrational energy of the blade for a given thermosonic test.

The most critical aspect of the methodology was determination of the unknown input excitation (i.e. load). The aim was to obtain an input excitation function, which when applied to the FE blade model, generated a similar response to that measured in experiment. The simulated vibrational response was generally in good agreement with the measured response, although with an expected degree of error. The error was quantified using percentage error, which was on average approximately 35% for the 10 tests, excluding the extreme percentage errors (i.e. outliers). This means on average, the FE results overestimated or underestimated the measured response by 35%. The reason for the expected error between the measured and simulated results may be attributed to three main factors: simplicity of methodology, imperfections in FE blade model and material properties.

The methodology used in this study to simulate the full-field vibrational energy of a turbine blade was relatively simple in its approach. The reason for pursuing this simple approach was to get an initial insight into the methodology before considering whether a more rigorous approach is required. However, this may have contributed to the error between the simulated and measured results. The second potential reason for the error may be imperfections in the FE model. The FE model used in this study closely resembled the blade type, except for the trailing edge cooling holes which were absent in the FE model. The absence of such features will influence the dynamic behaviour of the model, particularly at that part of the blade. Vibration measurements were taken from

the trailing edge of the FE model, although it is uncertain exactly how the lack of cooling holes affected vibrational response results. In addition, all of the blades used in this study had some form of cracking or surface imperfections which were not represented in the FE model. These extra features on the blades will also affect the dynamic behaviour of the blades and hence the vibrational response may differ from the response seen in FEA. Han et al. [39] showed in a study how the presence of a crack can alter the effect of a vibration mode pattern in a component. The authors excited two identical aluminium specimens under the same boundary condition, but one specimen had a crack while the other was crack free. The authors found different acoustic mode patterns generated in each specimen. Therefore, it may be suggested that extra features, however small, not present in the FE model used in this study can affect the excited vibration field.

Material properties are generally one of the main sources of error in FEA [137]. This is because material properties are known to vary, and accurate properties can only be obtained from direct measurements on the component. The material properties used in FEA in this study were values generally quoted in text books and available within Rolls-Royce. However, it is more than likely that material properties for the blades used in this work vary from the text-book values (typically between 5 – 10%) and moreover, may also vary from blade to blade. This will contribute to errors in the FE predictions as one set of material properties was assumed for all ten 10 tests.

Another potential source of error relating to material properties is the blades crystallographic orientation relative to the geometry. This will affect the orientation of the elastic stiffness matrix (anisotropy) of the blade. In the FEA programme, the anisotropic material was positioned longitudinal to the blade, which is the ideal case for the single crystal turbine blade used in this study [136]. However, in reality, the orientation of the anisotropic material relative to the blade geometry will always vary from the ideal, and also vary from blade to blade. This means every blade would have a unique elastic stiffness matrix, which must be measured to obtain the true material characteristics of the blade [136]. However, measurement of the crystallographic orientation of the blades was not feasible for this study, and therefore, considered as a potential source of error in the FEA results. Considering all the potential sources of errors in the FE model and those from material properties, the match between the experimental and predicted vibrational responses was reasonable and thus, formed the basis computing the full-field vibrational energy of a blade under thermosonic excitation.

Knowledge of the full-field vibrational energy excited in a component can be valuable as it provides information of the dynamic behaviour of a turbine blade under thermosonic excitation. However, for a typical thermosonic inspection, the full-field vibrational energy cannot be measured during testing, hence, the need to investigate retrospectively. In this study, the vibrational energy was computed using the A^2 and Energy Index (EI)

parameters. Both parameters are useful, but present slightly different information. The former represents the energy of the vibrating system, while the EI is the heating potential. The EI can be further described as the amount of energy dissipated as heat in unit time. However, in this study both parameters can be considered similar because steady-state conditions were applied. Since time is constant (i.e. vibration not changing with time), the A^2 parameter is equivalent to the EI, thus the similar results shown in Section 6.3.2.

A non-uniform vibrational energy field was seen across the blades, and this non-uniformity differed for the 10 tests. However, there were common patterns seen in the 10 different tests. The highest energy levels were predominantly in certain areas of the blades, such as at the seal fins, trailing edge and parts of the platform. The similarity between these areas with higher energy levels is the relatively thinner geometry. Perez and Davis [94] have shown that for a given horn load, a crack generates a higher temperature rise in a thinner sample. It is reasonable to extrapolate their findings to defect free materials such as that used in the FEA in this study, as both cracks and defect free materials have the capacity to dissipate vibrational energy as heat. However, the former has a much higher capacity and therefore generates a higher temperature differential when viewed with an IR camera [24, 70]. Therefore, the areas of the blade with the highest energy levels may be because of their thinner sections compared to other parts of the blade. Thermosonic heating across a crack-free trailing edge (a

relatively thin section) of an aero engine turbine blade was also observed by Han et al. [33], although the authors were unsure of the origin of heating in that part of the blade. The effect of geometry on the thermosonic heating was observed in Mayton's [100] thermosonic study on military aircraft turbine blades. Mayton found increased heating per unit vibration amplitude in thinner sections (aerofoil) compared to thicker sections (shroud) of a turbine blade.

The vibrational energy map on the turbine blades highlights areas of the blade with relatively high and low energy levels. This however does not suggest that cracks in these areas will be detected or not detected. Using these energy maps to decide whether or not cracks will be detected in certain areas would require a reference or a threshold vibrational energy level to be first determined. However, this was not within the remit of this work, but will be useful and complementary to this study. Instead the energy maps presented in this study provides a useful image of how a turbine blade responds to a typical thermosonic excitation. These energy maps also reveal areas of the blade that may potentially heat up where no cracks are present in the sample, such as at the seal fins and trailing edge. Heating has been observed in these areas in several experiments, but with no visual evidence of a crack, even after an FPI inspection. This situation can be described as a false indication, and can potentially lead to scrapping a crack-free blade. Therefore, prior knowledge of vibrational energy distribution on a turbine blade is

important, considering that majority (> 90%) of the blades that would be inspected in a real inspection are generally found to be crack-free.

6.5 Review of chapter

This Chapter proposed a methodology for determining the full-field vibrational response of a component under thermosonic excitation. The aim of this work was to highlight the non-uniform and complex vibration field generated in a turbine blade. The proposed methodology was based on determining the input excitation forces through experimentation and FEA, and then applying these excitation forces to an FE model of a turbine blade. First, laser vibrometry measurements were used to capture the pseudo steady-state vibrational response of five locations on a blade. Next, the prominent modes in the vibration measurements were identified and used to generate an input excitation function for the FEA approach. The methodology was validated by comparing the measured and simulated vibrational response of five different points on the blade, which generally, showed good qualitative agreement. This good agreement formed the basis for computing the full-field vibrational energy of a blade for a given thermosonic test. The vibrational energy excited across a blade was found to be highly non-uniform, and this non-uniformity differed for the 10 tests completed in this study. However, common patterns were seen in the 10 tests, such as higher energy levels at the seal fins, trailing

edge and parts of the platform, compared with lower energy levels on the clamp and parts of the leading edge.

Chapter 7

Conclusions and further work

7.1 General overview

The aim of this Thesis was to assess the reliability of thermosonics as a rapid screening technique for detecting cracks in Rolls-Royce high-pressure turbine blades. The motivation for this thesis was discussed in the introduction in Chapter 1. This Chapter highlighted the extensive chemical cleaning process in-service turbine blades undergo prior to inspection with FPI during the overhaul process. Processing unserviceable turbine blades through the clean and inspect process is a non-value-added process, costing time and money. Therefore, a reliable and rapid NDT method that can filter these unserviceable blades due to cracking at the pre-cleaning stage is an attractive proposition. This will save cleaning and inspection costs, increase inspection capacity and also reduce the amount of hazardous chemicals used in the cleaning process.

After evaluating several NDT techniques, thermosonics was found to be the most viable technique to achieve the business benefit desired. Thermosonics has several advantages that make it an attractive NDT method for this project, such as: rapid inspection; inspection of complex geometries; minimal surface preparation of component; and detection of tight cracks. Furthermore, several successful studies have demonstrated the crack detection capabilities of thermosonics on simple and complex geometries.

Chapter 2 presented a review of published thermosonic literature to date. This chapter clearly highlighted two main reliability issues with the thermosonic technique: non-repeatability of the excitation process and non-uniform vibration field. Furthermore, it was shown that relatively few studies had been conducted on large sets of turbine blades to provide a well-informed assessment of the capability and reliability of thermosonics on Rolls-Royce turbine blades. Chapter 3 discussed an empirical study carried out to determine the optimal excitation parameters and assess the reliability of the newly developed thermosonic technique for a large set of turbine blades. The empirical study showed the developed technique to be rapid, robust and capable of detecting cracks in the turbines blades. However, the poor repeatability of the excitation was observed in this Chapter, even though the excitation for most tests exceeded the threshold required to detect the known cracks. This lack of repeatability would however be a problem in a case where the presence of a crack is unknown, as there is no way of confirming whether or not the excitation applied was sufficient to detect a crack, if one is indeed present.

Chapters 4 and 5 investigated two different parameters that may be used to determine whether or not the excitation in a thermosonic test is sufficient to detect a defect of interest. Chapter 4 evaluated a parameter called the Heating Index (HI), which was originally developed at the NDE research laboratory in Imperial College. The HI is useful because of its linear relationship with the temperature rise of a vibrating crack. This linear relationship enables a threshold vibration level to be determined in

calibration tests and then later used as a reference parameter in a real inspection. The study carried out in Chapter 4 aimed to build on the previous HI studies by evaluating its application to turbine blades. Results from this Thesis confirmed the linear relationship between the HI and crack temperature rise.

Furthermore, Chapter 4 highlighted the advantages and disadvantages of using different vibration measuring devices for capturing the vibration records required to compute the HI. The microphone was shown to be most practical and cost effective device after comparison with a laser vibrometer and strain gauge. The vibration measured by the microphone better represents the vibration of the whole component as opposed the single point vibration measured by a laser vibrometer or strain gauge. This is important because in a real inspection, the location of any potential crack is unknown. Finally, Chapter 4 highlighted a practical limitation of the HI, which is the required knowledge of k (i.e. crack behaviour) prior to inspection. This requirement of k is not ideal as every crack is unique and has a different value of k, but more importantly, a crack may not even exist in component under inspection.

Chapter 5 presented an evaluation of an alternative vibration monitoring parameter to the HI that does not require prior knowledge of crack behaviour. This alternative parameter, referred to as the A^2 parameter, relates to the total energy content of a vibration. The A^2 parameter was also found to have a linear relationship with crack

temperature rise, although, the strength of linear correlation varied for the different cracks used in the study. Nevertheless, the strength of linear correlation for the A^2 parameter compared favourably with that of the HI for the same set of cracks. After validating the A^2 parameter, a threshold vibration level was determined for the set of blades/cracks using linear regression analysis.

Finally, Chapter 6 proposed a new methodology to simulate the full-field vibrational response of a turbine blade under thermosonic excitation. The methodology involved a combination of vibration measurements and finite element analysis (FEA). A laser vibrometer was used to capture the pseudo steady-state vibrational response of several points on a blade. These measured vibrational responses were used to determine an input excitation function for the FEA approach. The input excitation function was validated by comparing the measured vibrational responses and the simulated vibrational responses. A reasonable agreement was observed for both the measured and simulated vibrational responses. The validated input excitation was then used to compute the full-field vibrational energy of a blade, which highlighted the vibrational energy distribution across a blade for a given thermosonic test.

7.2 Summary of key findings

7.2.1 Reliability of thermosonics on aero engine turbine blades

Optimisation of the excitation parameters

Several excitation parameters were evaluated to maximise the temperature rise generated by a crack. These parameters included: horn static force, coupling material, vibration amplitude and excitation time. All the excitation parameters showed a general increase in the crack temperature rise as the settings for the respective parameters were increased. However, the horn static force was seen to have the greatest effect on crack temperature rise. Various coupling materials, including commonly used materials, were evaluated; however, electrical insulating which has not been reportedly used before was shown to generate the highest crack temperature rise. In addition, this coupling material was seen to have the least degradation after several consecutive tests.

Repeatability of crack detection

A repeatability study, using a hit/miss approach, was conducted to assess the consistency of results in repeated tests and the robustness of the experimental process. At least 50 repeated inspections were carried out on each of four cracked blades. In addition, the blades were reclamped and the coupling material changed after a certain number of consecutive inspections. Despite the inherent non-repeatability of the excitation, the cracks were detected in all the inspections. The crack temperature rise varied between

inspections; however, was above the noise floor of the IR camera which ensured detection. The included variations to the experimental process did not affect crack detectability; thus demonstrating the robustness of the technique.

Reliability of thermosonic technique

The reliability of the thermosonic technique developed for this project was assessed on a set of 60 turbine blades with cracks of varying lengths. Three inspections were carried out per blade. The known cracks were detected in all three inspections for 52 blades, while the cracks in 5 blades generated a heat signal in only one inspection and no discernible heat signal was seen for the remaining 3 blades. Several stages of image processing were found to be crucial for crack detection, given the use of an uncooled IR camera for this study. In addition, optimisation of the excitation parameters at the initial stage of this study contributed to the high POD.

7.2.2 Vibration monitoring for a reliable thermosonic inspection

Chapters 4 and 5 evaluated two different parameters (HI and A^2) that may be used to monitor the vibration in a thermosonic test. Chapter 4 focused on the HI, which was shown to have a linear relationship with the temperature rise generated by a vibrating crack. However, the strength of the linear relationship varied depending on the device used to capture the vibration. In this study, the HI computed from the vibration captured

from a laser vibrometer was shown have the strongest linear relationship, followed by the microphone and then strain gauge. The linear relationship for the laser vibrometer was considered excellent, while that of the microphone and strain gauge, moderate and poor respectively. It must be noted that strain gauge was intentionally attached on the clamp rather than on the blade itself for practical reasons. This was a significant contribution to the poor linear relationship with crack temperature rise.

Chapter 4 highlighted the importance of using the vibration measured at the crack (as with the laser vibrometer), if a strong linear relationship is to be achieved. However, it was also shown that the use of a laser vibrometer for capturing the vibration in a real inspection scenario was not viable. This is because in a real inspection scenario, the location(s) of the cracks, if at all present, would be unknown, making the decision of where to point the laser prior to inspection difficult. Previous results in this study have already shown vibration measurement away from the crack (i.e. strain gauge) for computing the HI to be poor. The microphone which captures an aggregate of the vibration across the whole of a component, as opposed a single point, was recommended as the most viable device for capturing the vibration records required for computing the HI.

Another important finding in Chapter 4 was that the limitation of using the HI in a case the presence of a crack was unknown. This is because computation of the HI requires

prior knowledge of crack behaviour (i.e. *k*). The ideal vibration monitoring parameter must be one that can assess whether or not the vibration excited in a test is sufficient or not, irrespective of the presence of a crack. Chapter 5 evaluated an alternative vibration monitoring parameter called the A^2 parameter, which does not require knowledge of crack behaviour. The study in Chapter 5 demonstrated a linear relationship between the A^2 and crack temperature rise, thus validating this alternative parameter. In addition, the strength of the linear relationship compared favourably with that of the HI for a set of 43 cracks. For both the HI and A^2, the strength of linear correlation (i.e. square of correlation coefficient) with crack temperature rise was found to be mixed. The percentage of cracks with a classification of excellent linear correlation (i.e. > 0.7) was approximately 14% and 16% for the HI and A^2 respectively, while the percentage of cracks classified as having no linear correlation (i.e. < 0.2) were approximately 37% and 47% for the HI and A^2 respectively. The rest of the cracks were classified as having moderate correlation (i.e. between 0.2 and 0.7).

7.2.3 Simulation of full-field vibrational response of turbine blade under thermosonic excitation

Vibration measurements and FEA were used to simulate the full-field vibrational response of a turbine blade under a typical thermosonic excitation. The methodology used was validated by comparing the measured and simulated vibrational response of

five different points on the blade, which overall showed reasonable qualitative agreement. The simulated vibrational energy excited across a blade was found to be highly non-uniform, and this non-uniformity differed for the 10 different tests completed in this study. However, some general observations were noted:

- The clamp had a lower vibrational energy than the blade
- The highest vibrational energy levels were not located at predicted defect sites
- The lowest vibrational energy levels were mostly seen in some parts of the leading edge, platform, blade root and middle section of the shroud seal fins
- Of the five locations of interest, the trailing edge has the highest vibrational energy level.

7.3 Industrial impact

The motivation for this project was primarily driven from a business (Rolls-Royce) perspective to reduce overhaul costs, whilst maintaining a high quality inspection procedure. The ethos was to introduce an additional screening stage which must achieve 95% reliability in terms of NDE results and be completed in an inspection time of less than 1 minute per blade. Importantly, the work presented in this Thesis and during the project produced useful insight as to whether thermosonics can achieve the cost-savings desired by Rolls-Royce.

Firstly, this Thesis demonstrated thermosonics to be capable of detecting a wide range of crack sizes and morphologies in different blade geometries. In addition, detection of multiple cracks on a blade was demonstrated. POD over 90% was achieved in the empirical study described in Chapter 3 and also in several other experimental trials (on approximately 300 blades) not included in this Thesis, for brevity. This high POD was achieved with a microbolometer camera, which demonstrates the potential of using low cost cameras in thermosonic testing. However, to ensure or to improve on this level of POD, a high-end cooled camera would be recommended. This is because cooled cameras have better temperature sensitivities and readily reveal crack heat signals without the need for extensive image processing. The use of a high-end cooled camera is included in the business case so no additional cost will be required. The ultrasonic excitation system used in all the inspections presented in this Thesis is appropriate for use in an industrial setting.

Although the experimental trials carried out in this project demonstrated excellent crack detection capability, it must be noted that the blades inspected all had known cracks. This is important to note as inspections to be carried out in industry would be blind inspections i.e. the number of cracks and their locations would be unknown. The challenge in this scenario is to ensure that the excitation applied to a blade in a test is sufficient for crack detection. This is a challenge because the excitation is non-repeatable. The A^2 parameter was shown to be a reasonable tool for monitoring the

vibration; however, this parameter is crack location dependent. This means that the crack locations used to obtain the vibration threshold (i.e. A^2 threshold) in calibration must match the cracks being inspected for in the real inspection. This will not be a problem if the blade type under inspection only has cracks in certain known locations. Otherwise, the vibration threshold obtained in calibration may be invalid for a real inspection.

The microphone was shown to be the most practical and cost-effective as the vibration monitoring device; however, issues relating to the positioning of the microphone (relative to the test-piece) and reverberations from other surrounding object need to be investigated. This is particularly important in an industrial setting where noise is commonplace. One potential solution may be to carry out the inspections (calibration and real inspection) in a custom-built sound proof room, not only to avoid external noise but also to prevent noise from the thermosonic equipment irritating other working personnel. This solution however, will significantly increase costs (i.e. capital expenditure), and also require extra floor space outside the vicinity where the current inspection of turbine blade is carried out.

The second criterion for achieving the desired cost-savings is a one minute inspection time per blade. This time would include loading the blade onto the blade holder, excitation, imaging and interpretation of results. The measured time for a complete

inspection in this Thesis was between 1.5 and 2 minutes; although each blade inspection involved three separate tests, which may not be the case in a real inspection. Nevertheless, there is scope to further reduce the inspection time achieved in this Thesis. A significant proportion of the inspection time in this Thesis involved loading the blade and allowing the blade to cool down straight after a test. The latter can be avoided if only one inspection is performed, while the former will require a better designed blade holder than that used in this project. This new blade holder would be designed to allow for rapid loading and unloading of a blade. One inspection consideration that may increase the inspection time is the required number of areas of the blade to be inspected. In this Thesis, most of the blades inspected required only one field of view; however, several field of views may be required to cover all parts of a blade. This will increase the number of inspections performed and also the inspection time. An alternative to using just one camera with several tests is to employ multiple IR cameras in fixed positions; however, this will inevitably increase equipment costs, which in turn will reduce the projected cost savings.

The business case for this project assumes a large volume of blades would be inspected and a certain percentage scrapped prior to cleaning. During the course of this project, this assumption was found to be unrealistic as the turbine blades planned for this project are subject to different repair schemes. Currently, not all turbine blades with cracks are scrapped automatically – cracks found in certain parts of the blades, such as in the

shroud area, can be repaired depending on the length of the crack. Each blade type has its own repair scheme, meaning the criteria for scrapping blades varies from blade to blade. Typically, only blades with cracks found in the aerofoil are scrapped automatically, irrespective of crack length. According to the repair scheme, the decision to scrap a blade is made after the blade has gone through the cleaning process and inspected with FPI to identify and size any cracks present. The repair scheme directly affects the implementation of thermosonics as a screening method primarily because thermosonics cannot be used for crack sizing, rather can only be used to identify the presence or absence of a crack. Therefore, if the thermosonic process identifies a crack, the blade cannot be scrapped unless the crack length is known or the crack is within the aerofoil section. An alternative idea would be to only focus the inspections on the aerofoil section of the blades. However, this approach may not be viable as the number of blades with cracking in that part of the blade is relatively few compared to cracking in other parts of blades such as the shroud. In over 95% of the blades inspected during this project, the known cracks were located in the shroud area of the blade. This means that business case will be invalid if inspecting areas where crack sizing is not required as the blade volume will insufficient. This crack sizing limitation of thermosonics could therefore be the most significant hindrance in the implementation of thermosonics as a screening technique in the overhaul process in Rolls-Royce.

Going forward, the original business case for this project has to be reviewed to decide how best to implement thermosonics in the overhaul process to achieve meaningful savings. For this project the scope for the business case was to inspect for all cracks in a blade irrespective of location or length. However, as described previously, the criteria for scrapping a blade is much more complex than simply detecting the presence of a crack. What would be useful is a more detailed understanding of the inspection schemes of the several types of high-pressure turbine blades (i.e. different engines) to determine how best thermosonics can be implemented to filter defective blades that would be normally classed as scrap. The capability of the inspection technique proposed for this project (i.e. thermosonics) has already been demonstrated in this thesis; however, a well-defined and viable inspection scope is required in order fully define the specifications, and consequently costing, for this project. Once the project scope is redefined, the next step should be carrying out trials in a production environment (i.e. overhaul base) with 'real' blades (i.e. not scrap). These trial blades will later be inspected as normal to validate the thermosonics results. This trial work must however be restricted to a small number of sample blades as there are other studies that must be conducted to fully understand the safety of using thermosonics on critical components such as turbine blades. Some of these studies are suggested in the next section.

7.4 Suggestions for further work

7.4.1 Impact of thermosonics on the turbine blade inspection process

7.4.1.1 Effect of thermosonics on the structural integrity of a turbine blade

This Thesis has successfully demonstrated the crack detection capability of thermosonics on turbine blades. However, the effect of the high-power ultrasonic excitation on the structural integrity of a turbine blade is still uncertain. Several studies, including this Thesis, have shown that the high-power excitation does not necessarily cause measurable crack growth. Nevertheless, the exposure to such excitation may cause changes to the microstructure of a turbine blade, which can potentially affect its life or performance. Removing any doubt on its impact on the structural integrity of a component will add more credibility to the technique.

7.4.1.2 Effect of thermosonics on FPI

The proposed inspection process for this project (see Section 1.1) involves using thermosonics to filter cracked blades, while the rest of the blades still go through the mandatory FPI process. It is important therefore to understand the impact thermosonic excitation will have on the FPI inspections carried out on the cracked blades not identified at the thermosonics inspection stage. This work may be carried out by investigating the results from FPI inspections before and after thermosonics is applied on a crack. Preliminary results not published or presented in this Thesis suggest no

detrimental impact; however, this preliminary work was undertaken using only a limited sample size. A study with a larger set of samples with well-defined and varying crack sizes is required.

7.4.2 False indications

7.4.2.1 Effect of surface condition on thermosonic inspection

The turbine blades used throughout this Thesis were relatively clean. However, most of the turbine blades proposed to be inspected have been exposed to different environments and have not be cleaned. Some of these blades would have different levels of accumulated contaminants or dirt on their surface. The impact of these contaminants or dirt on the thermosonic results remains uncertain. The most important thing to be understood is the probability of false indications (PFI) due to surface contaminant. This study should involve the use of both cracked and crack-free turbine blades in the dirty condition. Anecdotal evidence from the several inspections carried out in this project has shown that crack-free blades with loose dirt can generate a heat signal of similar amplitude to the heat signal from a crack. An alternative methodology would be to use POD specimens coated with ‘representative dirt’.

7.4.2.2 Effect of component geometry on thermosonic inspection

High levels of acoustic excitation necessary to detect cracks may give false indications on the thin sections of a turbine blade. Results from thermosonic tests carried out during this project, but not reported in this Thesis, have shown crack-free thin sections of a blade generating similar or higher levels of heating compared to a crack. This could potentially lead to serviceable blades being scrapped at the screening phase. A more detailed investigation to determine the scale of this problem and also a potential solution to mitigate this issue are required.

7.4.3 Simulation of full-field vibrational response of a turbine blade

This Thesis only demonstrated the methodology of using vibration measurements and FEA for simulating the full-field vibrational response of a turbine blade under thermosonic excitation. Further work is required to understand how the simulated results can be used to evaluate the areas of a blade that have vibrational energy below or above the crack detection threshold. However, this can only be achieved by first completing calibration tests on a set of turbine blades to determine a threshold vibrational energy (i.e. EI or A^2) required to detect a crack of interest.

Appendix A

Input excitation function

B26_1

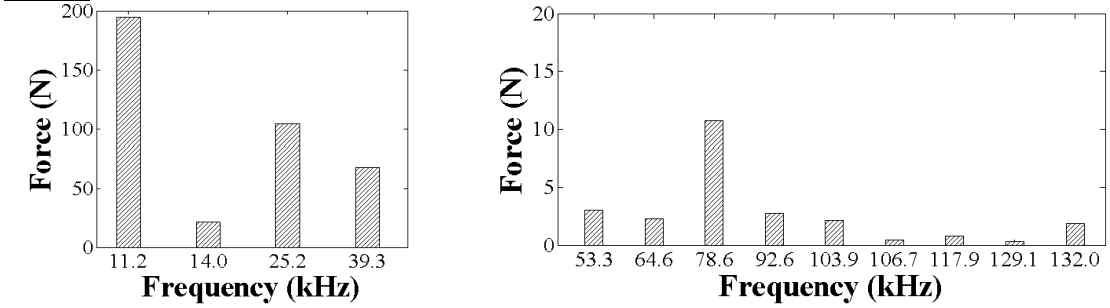

Figure C.1 Input excitation function for test B26_1 (a1) shows the first four modes and (a2), the remaining nine modes. The y-axis of (a1) is 10 times that of (a2).

B26_2

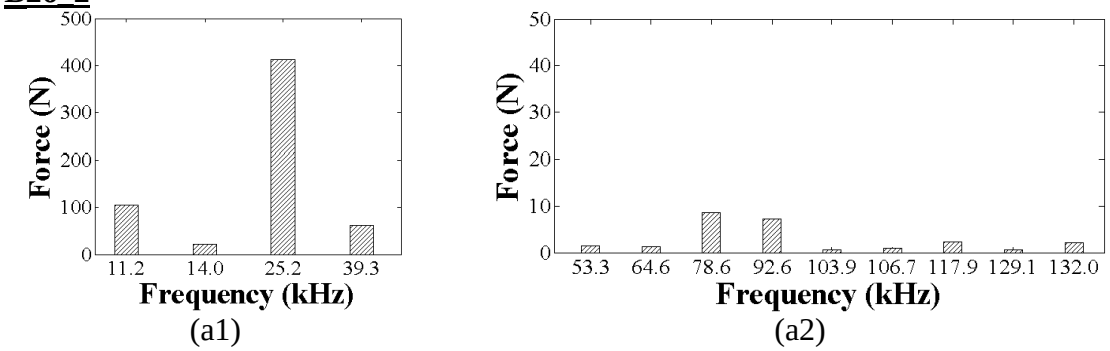

Figure C.2 Input excitation function for test B26_2 (a1) shows the first four modes and (a2), the remaining nine modes. The y-axis of (a1) is 10 times that of (a2).

B10

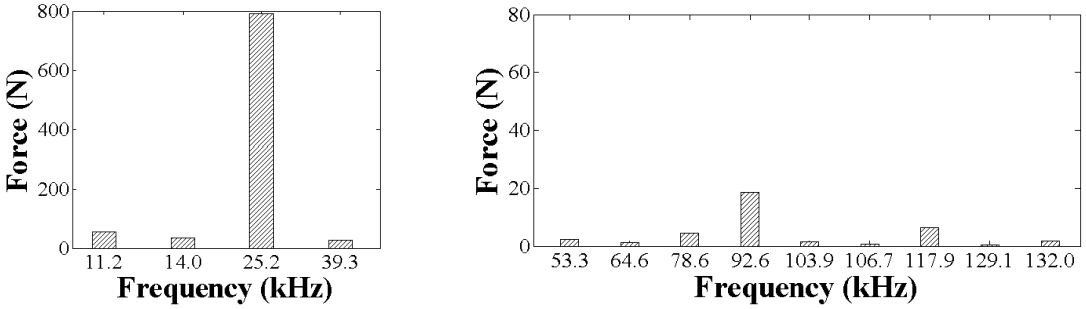

Figure C.3 Input excitation function for test B10. (a1) shows the first four modes and (a2), the remaining nine modes. The y-axis of (a1) is 10 times that of (a2).

B01

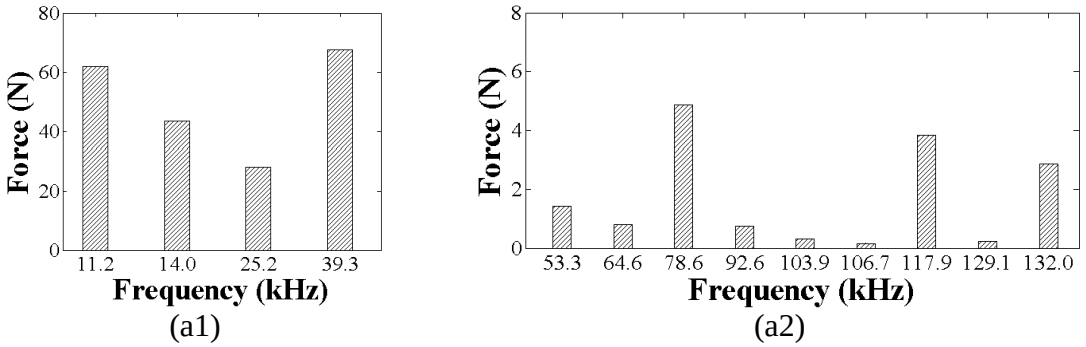

Figure C.4 Input excitation function for test B01. (a1) shows the first four modes and (a2), the remaining nine modes. The y-axis of (a1) is 10 times that of (a2).

B18_1

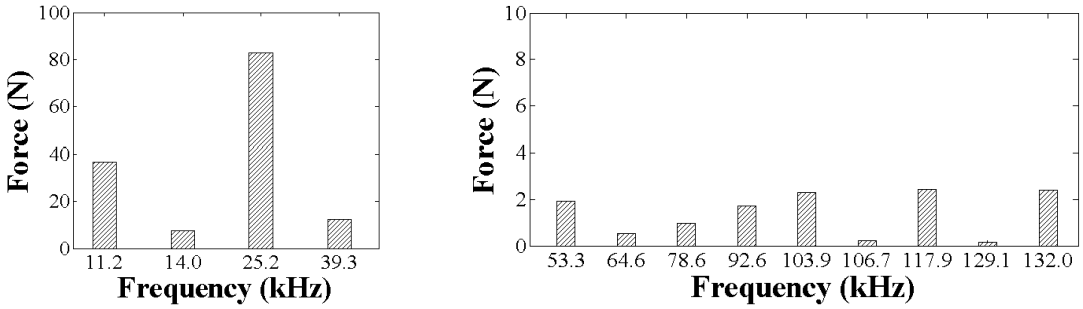

Figure C.5 Input excitation function for test B18_1. (a1) shows the first four modes and (a2), the remaining nine modes. The y-axis of (a1) is 10 times that of (a2).

B18_2

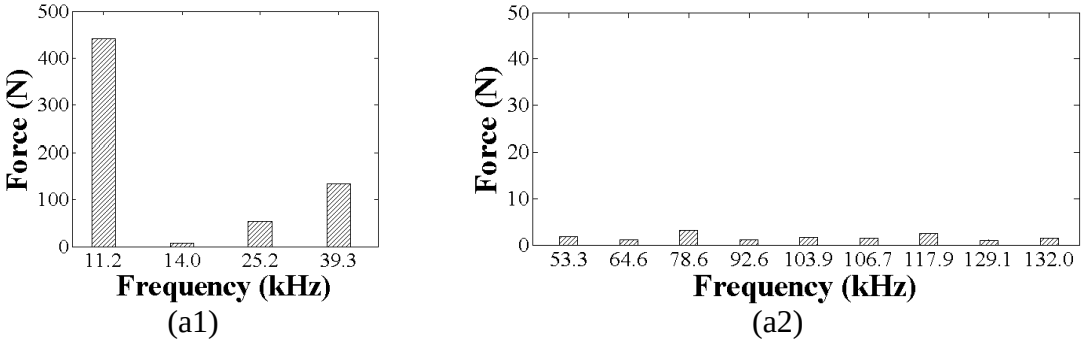

Figure C.6 Input excitation function for test B18_2. (a1) shows the first four modes and (a2), the remaining nine modes. The y-axis of (a1) is 10 times that of (a2).

B48

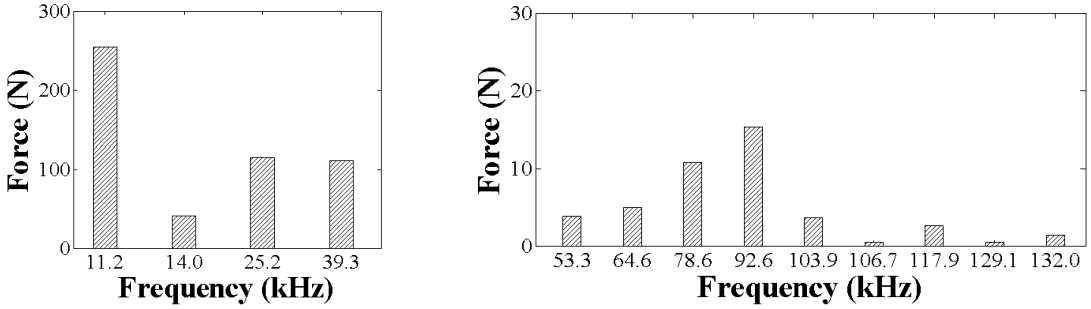

Figure C.7 Input excitation function for test B48. (a1) shows the first four modes and (a2), the remaining nine modes. The y-axis of (a1) is 10 times that of (a2).

B50_2

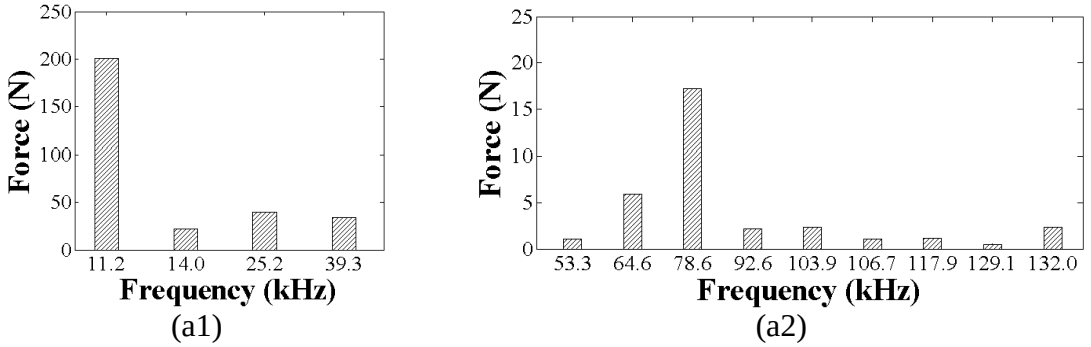

Figure C.8 Input excitation function for test B50_2. (a1) shows the first four modes and (a2), the remaining nine modes. The y-axis of (a1) is 10 times that of (a2).

Appendix B

Comparison of simulated and FE frequency response

B26_1

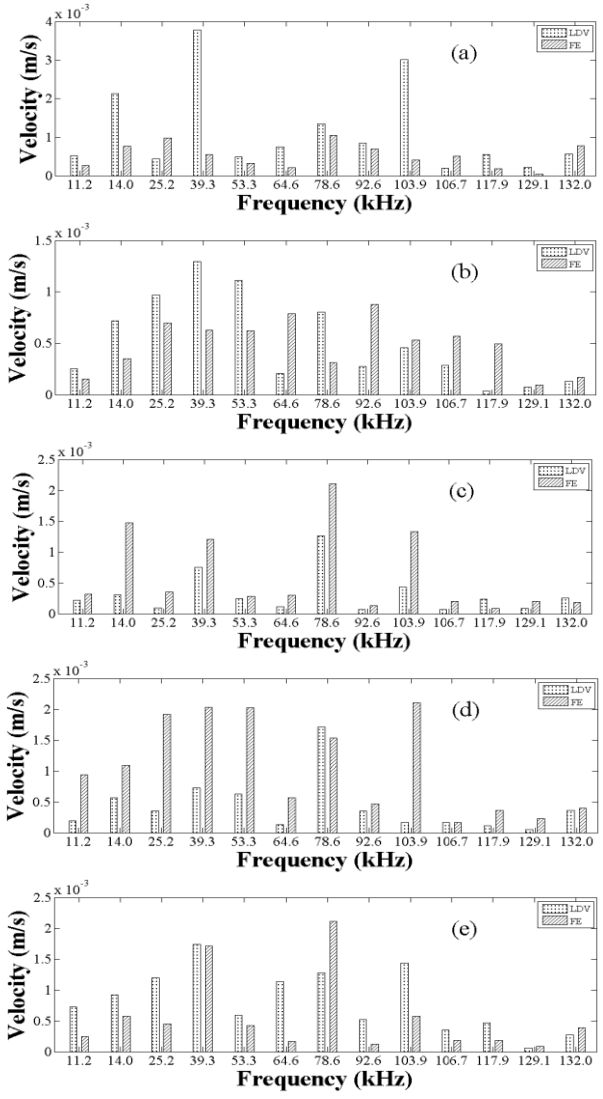

Figure D.1 Comparison of measured frequency response and FE frequency response for B26_1 (a) Mid aerofoil (b) Under platform (c) Shroud (d) Trailing edge (e) Leading edge.

B26_2

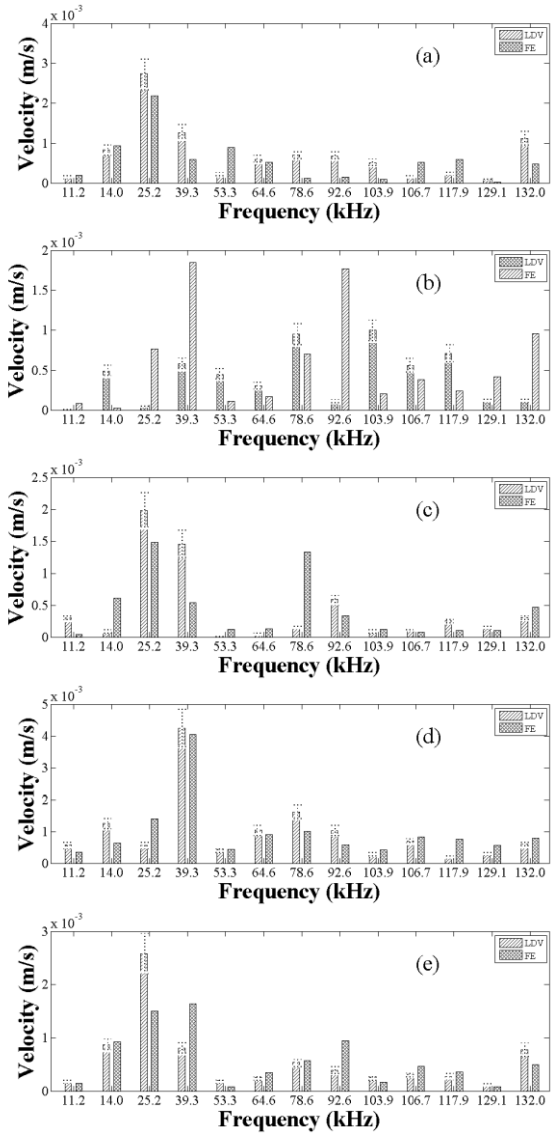

Figure D.2 Comparison of measured frequency response and FE frequency response for B26_2 (a) Mid aerofoil (b) Under platform (c) Shroud (d) Trailing edge (e) Leading edge.

B10

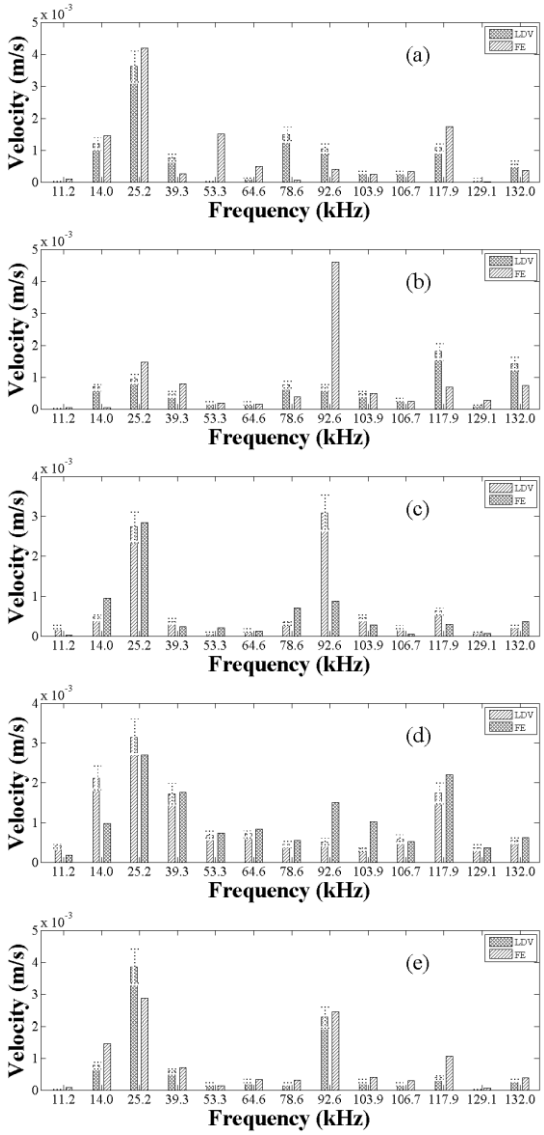

Figure D.3 Comparison of measured frequency response and FE frequency response for B10 (a) Mid aerofoil (b) Under platform (c) Shroud (d) Trailing edge (e) Leading edge.

B01

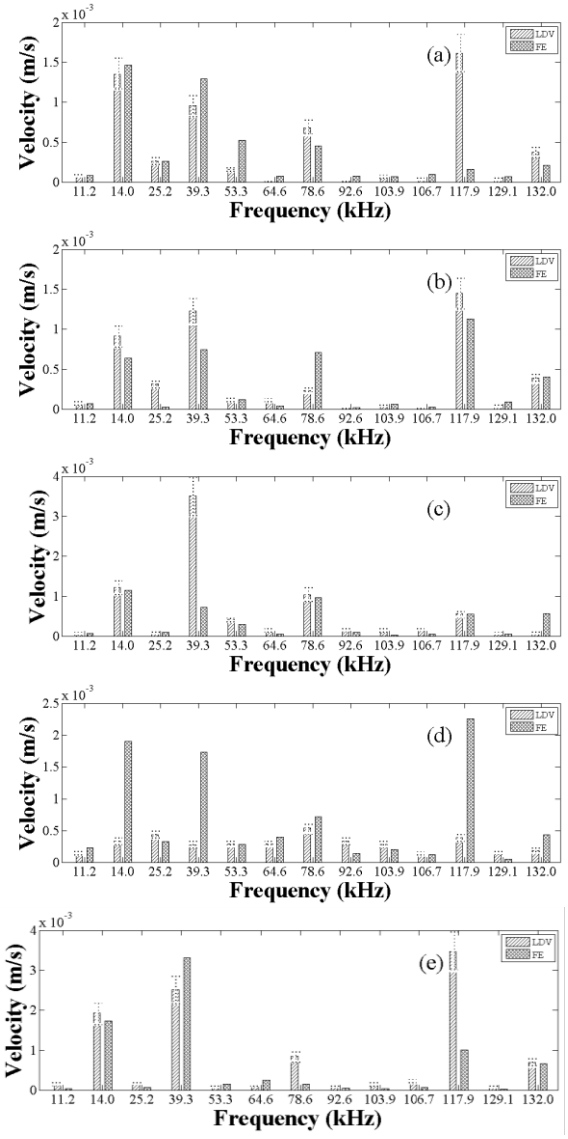

Figure D.4 Comparison of measured frequency response and FE frequency response for B01 (a) Mid aerofoil (b) Under platform (c) Shroud (d) Trailing edge (e) Leading edge.

B18_2

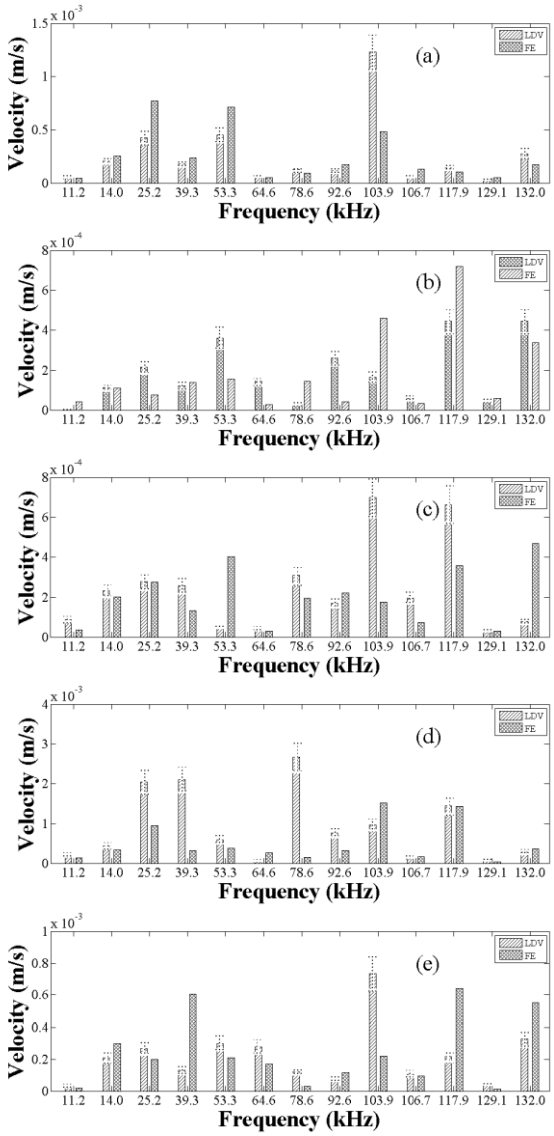

Figure D.5 Comparison of measured frequency response and FE frequency response for B18_2 (a) Mid aerofoil (b) Under platform (c) Shroud (d) Trailing edge (e) Leading edge.

B18_1

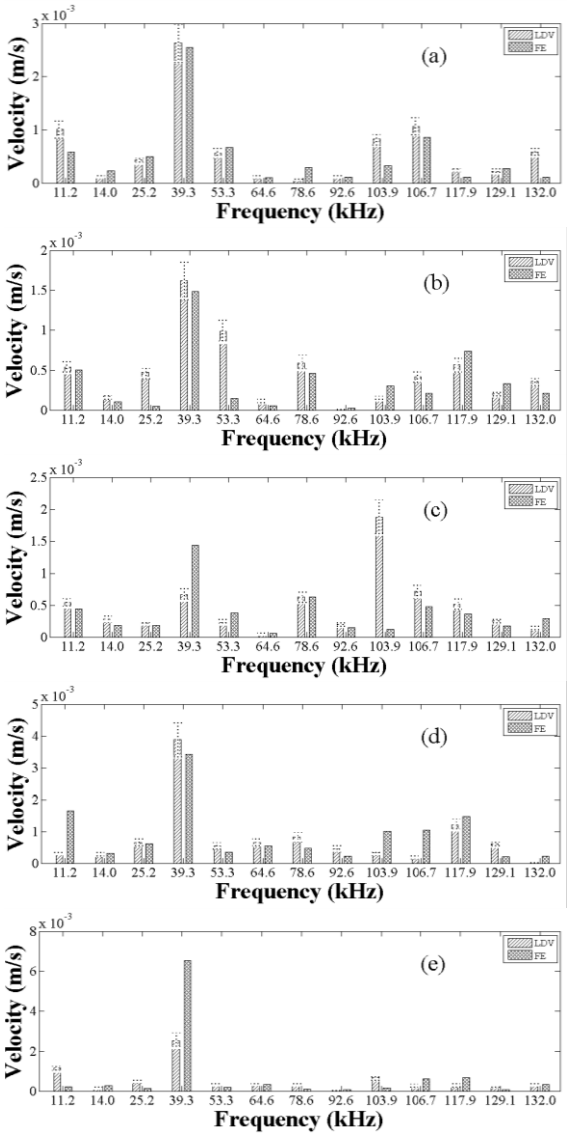

Figure D.6 Comparison of measured frequency response and FE frequency response for B18_1 (a) Mid aerofoil (b) Under platform (c) Shroud (d) Trailing edge (e) Leading edge.

B48

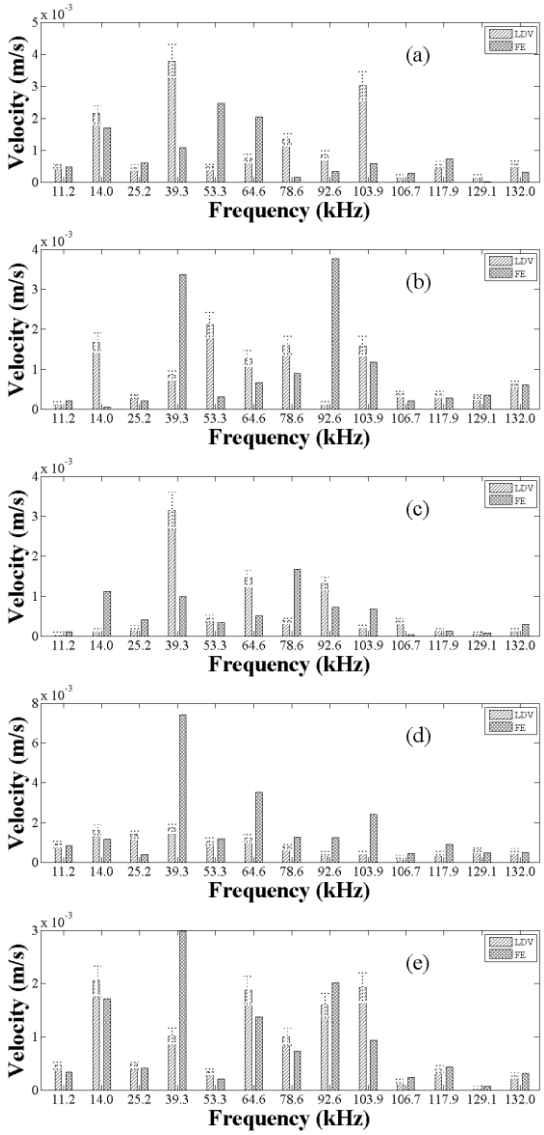

Figure D.7 Comparison of measured frequency response and FE frequency response for B48 (a) Mid aerofoil (b) Under platform (c) Shroud (d) Trailing edge (e) Leading edge.

B50_2

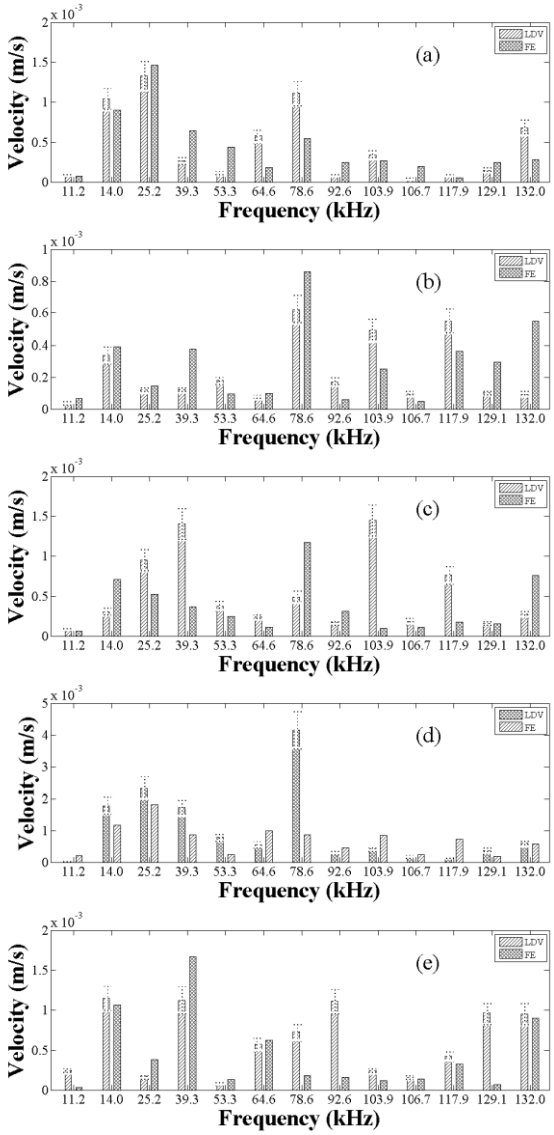

Figure D.8 Comparison of measured frequency response and FE frequency response for B50_2 (a) Mid aerofoil (b) Under platform (c) Shroud (d) Trailing edge (e) Leading edge.

Appendix C

Map of vibrational energy on FE model

B26_1

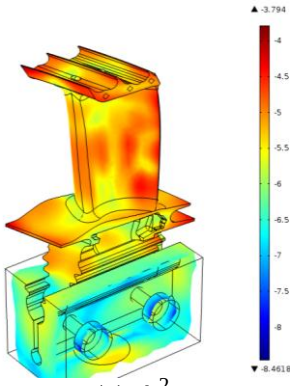

(a) A^2

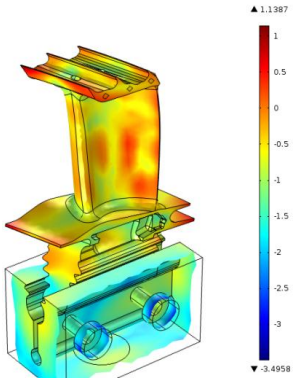

(b) Energy Index (EI)

Figure E.1 Computed full-field vibrational energy on the blade (concave side) for test B26_1.

B26_2

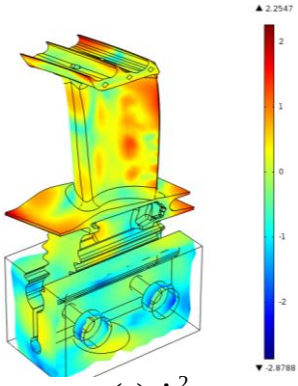

(a) A^2

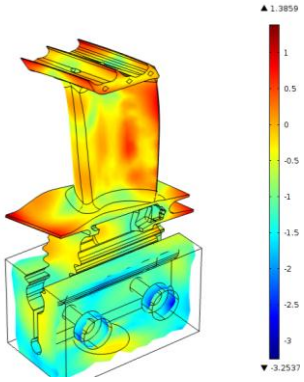

(b) Energy Index (EI)

Figure E.2 Computed full-field vibrational energy on the blade (concave side) for test B26_2.

B10

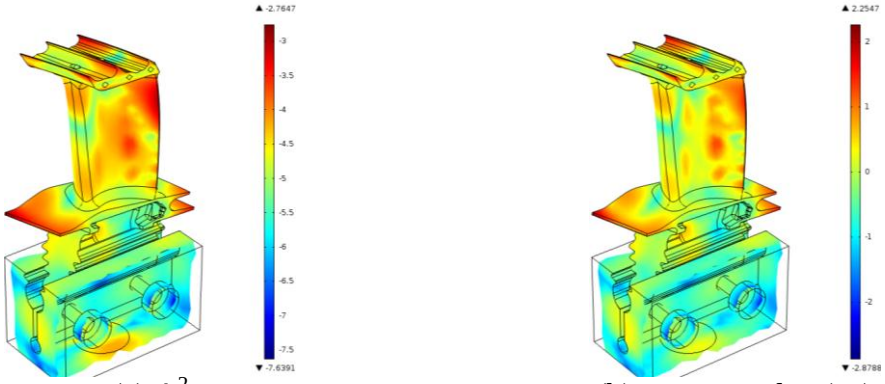

(a) A^2 (b) Energy Index (EI)

Figure E.3 Computed full-field vibrational energy on the blade (concave side) for test B10.

B01

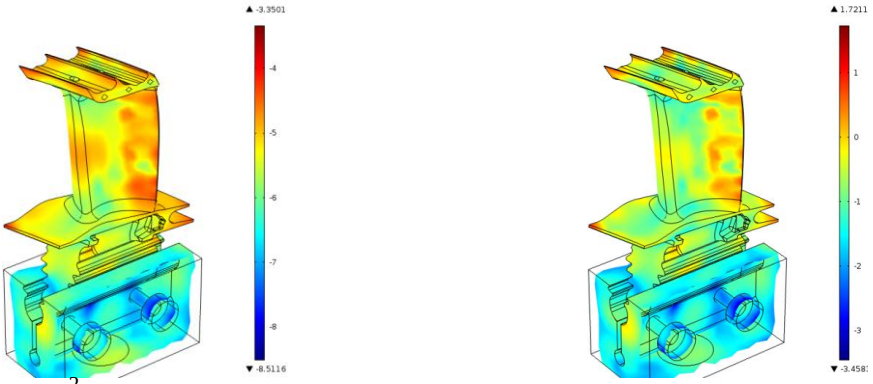

(a) A^2 (b) Energy Index (EI)

Figure E.4 Computed full-field vibrational energy on the blade (concave side) for test B01.

B18_2

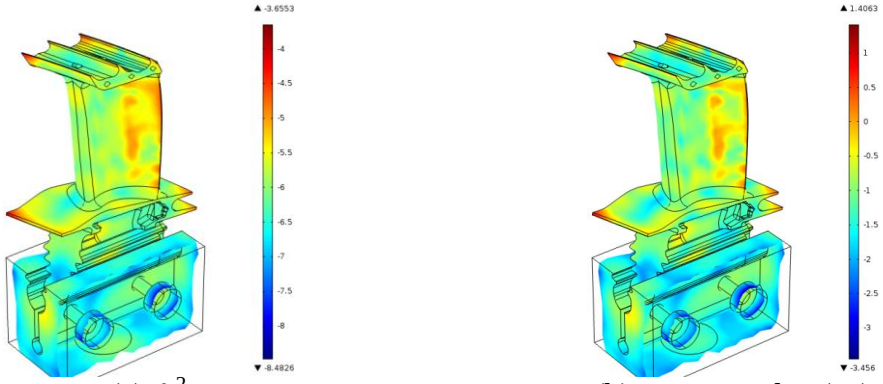

(a) A^2 (b) Energy Index (EI)

Figure E.5 Computed full-field vibrational energy on the blade (concave side) for test B18_2.

B18_1

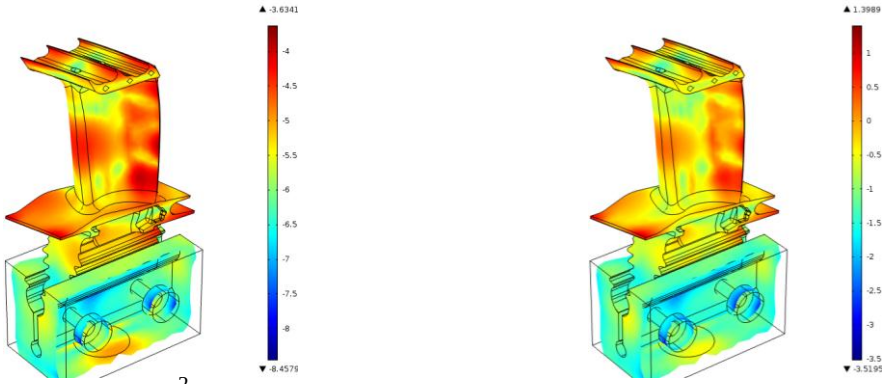

(a) A^2 (b) Energy Index (EI)

Figure E.6 Computed full-field vibrational energy on the blade (concave side) for test B18_1.

B48

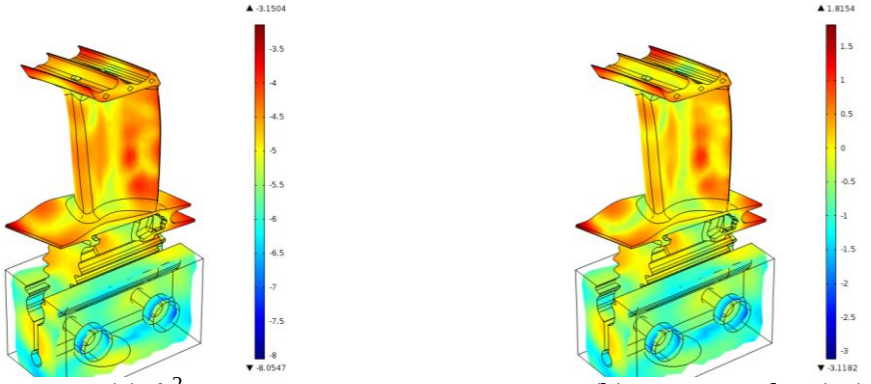

(a) A^2 (b) Energy Index (EI)

Figure E.7 Computed full-field vibrational energy on the blade (concave side) for test B48.

B50_2

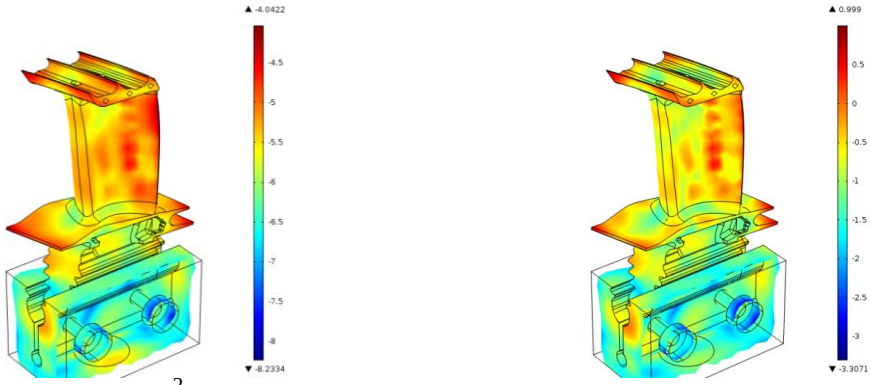

(a) A^2 (b) Energy Index (EI)

Figure E.8 Computed full-field vibrational energy on the blade (concave side) for test B50_2.

Bibliography

1. Rolls-Royce, *The Jet Engine*, 2005: Rolls-Royce Technical Publications.
2. A.S.f.T.a. Materials, "Standard Practice for Liquid Penetrant Testing", 2005, ASTM.
3. S. International, "Flourescent Penetrant Inspection, Aircraft and Engine Component Maintenance", 2009.
4. G. Harvey and J. Jones, "Small turbine blade inspection using laser strain techniques". Insight, 2009. 51(3).
5. K. Skuse, "Dirty blade CT inspection trial", Internal Report, 2007, Rolls-Royce plc - Bristol.
6. M. Morbidini, B.Y. Kang, and P. Cawley, "Improved Reliability of Sonic Infrared Testing". Materials Evaluation, 2009. 67(10): p. 1193-1202.
7. N.P. Avdelidis, D.P. Almond, A. Dobbinson, and B.C. Hawtin, "Pulsed thermography: philosophy, qualitative and quantitative analysis on certain aircraft applications". Insight, 2006. 48(5): p. 286 - 289.
8. Y.Y. Hung, Y.S. Chen, S.P. Ng, L. Liu, Y.H. Huang, B.L. Luk, R.W.L. Ip, C.M.L. Wu, and P.S. Chung, "Review and comparison of shearography and active thermography for nondestructive evaluation". Materials Science & Engineering R-Reports, 2009. 64(5-6): p. 73-112.
9. X.P.V. Maldague, P. Cielo, D. Poussart, and P. Emerson, "Thermographic nondestructive evaluation (NDE) of turbine blades: Methods and image processing". Industirial Metrology, 1990. 1(2): p. 139 - 153.

10. B. Weekes, "Investigation of Infrared Thermography NDE Techniques for Use in Power Station Environments", Ph.D. Thesis, Department of Mechanical Engineering, 2011, Imperial College London.

11. C. Ibarra-Castanedo, M. Genest, S. Guibert, J.M. Piau, X.P.V. Maldague, and A. Bendada, "Inspection of aerospace materials by pulsed thermography, lock-in thermography and vibrothermography: A comparative study - art. no. 654116". Thermosense XXIX, 2007. 6541: p. 54116-54116.

12. T. Li, D.P. Almond, and D.A.S. Rees, "Crack imaging by scanning pulsed laser spot thermography". NDT & E International, 2011. 44(2): p. 216-225.

13. K. Chatterjee, S. Tuli, S.G. Pickering, and D.P. Almond, "A comparison of the pulsed, lock-in and frequency modulated thermography nondestructive evaluation techniques". NDT & E International, 2011. 44(7): p. 655-667.

14. B. Weekes, P. Cawley, D.P. Almond, and T. Li. "The Effect of Crack Opening on Thermosonics and Laser-spot Thermography". in Review of Progress in Quantitative Nondestructive Evaluation, Vols 29a and 29b. 2010.

15. G. Zenzinger, J. Bamberg, M. Dumm, and P. Nutz, *Crack detection using EddyTherm*, in *Review of Progress in Quantitative Nondestructive Evaluation, Vols 24A and 24B*, D.O.C.D.E. Thompson, Editor 2005. p. 1646-1653.

16. I.Z. Abidin, G.Y. Tian, J. Wilson, S. Yang, and D. Almond, "Quantitative evaluation of angular defects by pulse deddy current thermography". NDT & E International, 2010. 43: p. 537 - 546.

17. G. Zenzinger, J. Bamberg, M. Dumm, and P. Nutz. "Crack Detection Using EddyTherm". in Review of Progress in Quantitative Nondestructive Evaluation. 2005.

18. L.D. Favro, X.Y. Han, Z. Ouyang, G. Sun, H. Sui, and R.L. Thomas, "Infrared imaging of defects heated by a sonic pulse". Review of Scientific Instruments, 2000. 71(6): p. 2418-2421.

19. L.D. Favro, R.L. Thomas, X. Han, Z. Ouyang, G. Newaz, and D. Gentile, "Sonic infrared imaging of fatigue cracks". International Journal of Fatigue, 2001. 23(1): p. 471-476.

20. E. Henneke, K. Reifsnider, and W. Stinchcomb, "Thermography - an NDI method for damage detection". Journal of Metals, 1979. 31(9): p. 11 - 15.

21. E. Henneke, K. Reifsnider, and W. Stinchcomb, "Vibrothermography: Investigation, development and applications of a new nondestructive evaluation technique", 1986, US Army Research Office.

22. R. Mignogna, R. Green, J. Duke, E. Henneke, and K. Reifsnider, "Thermographic investigations of high-power ultrasonic heating in materials". Ultrasonics, 1981. 19(4): p. 159 - 163.

23. C.J. Pye and R. Adams, "“Detection of damage in fiber reinforced plastics using thermal fields generated during resonant vibration". NDT & E International, 1981. 14(3): p. 111 - 118.

24. C.J. Pye and R.D. Adams, "Heat emission from damaged composite materials and its use in non-destructive testing". Journal of Physics D-Applied Physics, 1981. 14(5): p. 927-941.

25. J. Renshaw, "The mechanics of defect detection in vibrothermography", Ph.D. 2009, Iowa State University.

26. R. Thomas, D.F. Lawrence, H. Xiaoyan, O. Zhong, and S. Gang, "Infrared imaging of ultrasonically excited subsurface defects in materials", 2001: United States.

27. L.D. Favro, X.Y. Han, O.Y. Zhong, G. Sun, and R.L. Thomas, "Sonic IR imaging of cracks and delaminations". Analytical Sciences, 2001. 17: p. 451-453.

28. X. Han, L.D. Favro, and R.L. Thomas, "Sonic IR imaging and vibration pattern studies of cracks in an engine disk". Review of Progress in Quantitative Nondestructive Evaluation, Vols 22a and 22b, 2003. 20: p. 513-516.

29. X. Han, L.D. Favro, and R.L. Thomas, "Recent developments in sonic ir imaging". Review of Progress in Quantitative Nondestructive Evaluation, Vols 22a and 22b, 2003. 20: p. 500-504.

30. X. Han, L.D. Favro, and R.L. Thomas, "Sonic IR Imaging of delaminations and disbonds in composites". Journal of Applied Physics, 2011. 44(3).

31. X. Han and R. Yu, "Studying the effect of coupling materials in sonic IR Imaging". Sensors and Smart Structures Technologies for Civil, Mechanical, and Aerospace Systems 2007, Pts 1 and 2, 2007. 6529: p. U989-U994.

32. X.Y. Han, A.S. Ajanaballi, Z. Ahmed, W. Li, G.M. Newaz, L.D. Favro, and R.L. Thomas, "Finite-element modeling of sonic IR imaging of cracks in aluminum and titanium alloys". Review of Progress in Quantitative Nondestructive Evaluation, Vol 27a and 27b, 2008. 975: p. 483-490.

33. X.Y. Han, L.D. Favro, Z. Ouyang, and R.L. Thomas, "Recent developments in thermosonic crack detection". Review of Progress in Quantitative Nondestructive Evaluation, Vols 21a & B, 2002. 615: p. 552-557.

34. X.Y. Han, L.D. Favro, Z. Ouyang, and R.L. Thomas, "Thermosonics: Detecting cracks and adhesion defects using ultrasonic excitation and infrared imaging". Journal of Adhesion, 2001. 76(2): p. 151-162.

35. X.Y. Han, M.S. Islam, L.D. Favro, G.M. Newaz, and R.L. Thomas, "Simulation of sonic IR imaging of cracks in metals with finite element models". Review of Progress in Quantitative Nondestructive Evaluation, Vols 25A and 25B, 2006. 820: p. 544-549.

36. X.Y. Han, M.S. Islam, G. Newaz, L.D. Favro, and R.L. Thomas, "Finite-element modeling of acoustic chaos to sonic infrared imaging". Journal of Applied Physics, 2005. 98.

37. X.Y. Han, M.S. Islam, G. Newaz, L.D. Favro, and R.L. Thomas, "Finite element modeling of the heating of cracks during sonic infrared imaging". Journal of Applied Physics, 2006. 99(7).

38. X.Y. Han, M.S. Islam, G.M. Newaz, L.D. Favro, and R.L. Thomas, "Further development of the simulation of sonic IR imaging of cracks in metals with finite-element models". Review of Progress in Quantitative Nondestructive Evaluation, Vols 26A and 26B, 2007. 894: p. 471-477.

39. X.Y. Han, W. Li, Z. Zeng, L.D. Favro, G.M. Newaz, and R.L. Thomas, "Study of the effect of geometry in sonic IR imaging". Review of Progress in Quantitative Nondestructive Evaluation, Vols 24A and 24B, 2005. 760: p. 637-641.

40. X.Y. Han, W. Li, Z. Zeng, L.D. Favro, and R.L. Thomas, "Acoustic chaos and sonic infrared imaging". Applied Physics Letters, 2002. 81(17): p. 3188-3190.

41. X.Y. Han, V. Loggins, Z. Zeng, L.D. Favro, and R.L. Thomas, "Mechanical model for the generation of acoustic chaos in sonic infrared imaging". Applied Physics Letters, 2004. 85(8): p. 1332-1334.

42. X.Y. Han, J.P. Lu, M.S. Islam, W. Li, Z. Zeng, L.D. Favro, G. Newaz, and R.L. Thomas, "Sonic infrared imaging NDE". Smart Structures and Materials 2005: Sensors and Smart Structures Technologies for Civil, Mechanical, and Aerospace, Pts 1 and 2, 2005. 5765: p. 142-147.

43. X.Y. Han, J.P. Lu, S. Islam, W. Li, Z. Zeng, N. Kashyap, E. Yitamben, L.D. Favro, G.M. Newaz, and R.L. Thomas, "Developing sonic IR imaging NDE for aircraft structures". Review of Progress in Quantitative Nondestructive Evaluation, Vols 24A and 24B, 2005. 760: p. 632-636.

44. X.Y. Han, Y.Y. Song, and G. Godfrey, "Investigation of non-linear effects of coupling materials in sonic IR imaging - art. no. 69320N". Sensors and Smart Structures Technologies for Civil, Mechanical, and Aerospace Systems 2008, Pts 1 and 2, 2008. 6932: p. N9320-N9320.

45. X.Y. Han, Z. Zeng, W. Li, M.S. Islam, J.P. Lu, V. Loggins, E. Yitamben, L.D. Favro, G. Newaz, and R.L. Thomas, "Acoustic chaos for enhanced detectability of cracks by sonic infrared imaging". Journal of Applied Physics, 2004. 95(7): p. 3792-3797.

46. X.Y. Han, Z. Zeng, W. Li, S. Islam, J.P. Lu, V. Loggins, L.D. Favro, G.M. Newaz, and R.L. Thomas, "Importance of acoustic chaos in sonic IR imaging NDE". Review of Progress in Quantitative Nondestructive Evaluation, Vols 23a and 23b, 2004. 23: p. 496-500.

47. H.P. Lu, X.Y. Han, G. Newaz, L.D. Favro, and R.L. Thomas, "Study of the effect of crack closure in Sonic Infrared Imaging". Nondestructive Testing and Evaluation, 2007. 22(2-3): p. 127-135.

48. A. Mian, X.Y. Han, S. Islam, and G. Newaz, "Fatigue damage detection in graphite/epoxy composites using sonic infrared imaging technique". Composites Science and Technology, 2004. 64(5): p. 657-666.

49. A. Mian, G. Newaz, X.Y. Han, T. Mahmood, and C. Saha, "Response of sub-surface fatigue damage under sonic load - a computational study". Composites Science and Technology, 2004. 64(9): p. 1115-1122.

50. Y.Y. Song, G. Godfrey, and X. Han. "What role a coupling material could play in sonic IR imaging ". in Review of Quantitative Nondestructive Evaluation 2009. American Institute of Physics.

51. R.L. Thomas, X. Han, L.D. Favro, and G. Newaz. "Infrared Imaging of Defects in Materials with Chaotic Sonic Excitation". in IEEE Ultrasonics Symposium. 2010.

52. J. Renshaw, S.D. Holland, and D.J. Barnard, "Viscous material-filled synthetic defects for vibrothermography". Ndt & E International, 2009. 42(8): p. 753-756.

53. S.D. Holland, C. Uhl, and J. Renshaw, "Vibrothermographic Crack Heating: A Function of Vibration and Crack Size ". Review of Progress in Quantitative Nondestructive Evaluation, 2009. 1096: p. 489 - 494.

54. J. Renshaw, S.D. Holland, R.B. Thompson, and J. Anderegg, "Vibration-induced tribological damage to fracture surfaces via vibrothermography". International Journal of Fatigue, 2011. 33: p. 849-857.

55. S.D. Holland, C. Uhl, and J. Renshaw, "Toward a viable strategy for estimating vibrothermographic probability of detection". Review of Progress in Quantitative Nondestructive Evaluation, Vol 27a and 27b, 2008. 975: p. 491-497.

56. J. Renshaw, S.D. Holland, R.B. Thompson, and D.J. Eisenmann, "Synthetic Defects for Vibrothermography". Review of Progress in Quantitative Nondestructive Evaluation, Vols 29a and 29b, 2010. 1211: p. 498-504.

57. M. Li, S.D. Holland, and W.Q. Meeker, "'Statistical methods for automatic crack detection based on vibrothermography sequence-of-images data' by M. Li, S. D. Holland and W. Q. Meeker: Rejoinder". Applied Stochastic Models in Business and Industry, 2010. 26(5): p. 509-512.

58. J. Renshaw, J.C. Chen, S.D. Holland, and R.B. Thompson, "The sources of heat generation in vibrothermography". NDT & E International, 2011. 44(8): p. 736 - 739.

59. M. Li, S.D. Holland, and W.Q. Meeker, "Quantitative Multi-Inspection-Site Comparison of Probability of Detection for Vibrothermography Nondestructive Evaluation Data". Journal of Nondestructive Evaluation, 2011. 30(3): p. 172-178.

60. S.D. Holland, C. Uhl, Z. Ouyang, T. Bantel, M. Li, W.Q. Meeker, J. Lively, L. Brasche, and D. Eisenmann, "Quantifying the vibrothermographic effect". NDT & E International, 2011. (Currently in press but available online).

61. S.D. Holland and J. Renshaw, "Physics-based image enhancement for infrared thermography". NDT & E International, 2010. 43(5): p. 440-445.

62. J. Renshaw, S.D. Holland, and R.B. Thompson, "Measurement of crack opening stresses and crack closure stress profiles from heat generation in vibrating cracks". Applied Physics Letters, 2008. 93(8): p. 081914.

63. J. Renshaw and S.D. Holland, "Full-field vibration measurement for vibrothermography". Review of Progress in Quantitative Nondestructive Evaluation, Vol 27a and 27b, 2008. 975: p. 498-503.

64. W.J. Zhang, S.D. Holland, and J. Renshaw, "Frequency dependence of vibrothermography". Review of Progress in Quantitative Nondestructive Evaluation, Vols 29a and 29b, 2010. 1211: p. 505-509.

65. S.D. Holland. "First measurements from a new broadband vibrothermography measurement system". in Review of Progress in Quantitative Nondestructive Evaluation, Vols 26A and 26B. 2007.

66. J. Renshaw, S.D. Holland, R.B. Thompson, and C. Uhl, "The Effect of Crack Closure on Heat Generation in Vibrothermography". Review of Progress in Quantitative Nondestructive Evaluation, Vols 28a and 28b, 2009. 1096: p. 473-480.

67. M. Li, S.D. Holland, and W.Q. Meeker, "Automatic Crack Detection Algorithm For Vibrothermography Sequence-of-Images Data". Review of Progress in Quantitative Nondestructive Evaluation, Vols 29a and 29b, 2010. 1211: p. 1919-1926.

68. M. Morbidini and P. Cawley. "Reliable crack detection in Thermosonics NDE". in Review of Progress in Quantitative Nondestructive Evaluation, Vol 27a and 27b. 2008.

69. M. Morbidini, P. Cawley, T.J. Barden, D.P. Almond, and P. Duffour, "The relationship between crack damping, vibration amplitude and temperature rise in thermosonics NDT". Review of Progress in Quantitative Nondestructive Evaluation, Vols 26A and 26B, 2007. 894: p. 492-499.

70. M. Morbidini, P. Cawley, T. Barden, D. Almond, and P. Duffour, "Prediction of the thermosonic signal from fatigue cracks in metals using vibration damping measurements". Journal of Applied Physics, 2006. 100(10).

71. M. Morbidini, P. Cawley, T.J. Barden, D.P. Almond, and P. Duffour, "A new approach for the prediction of the thermosonic signal from vibration records". Review of Progress in Quantitative Nondestructive Evaluation, Vols 25A and 25B, 2006. 820: p. 558-565.

72. B. Kang and P. Cawley, "Multi-mode excitation system for thermosonic testing of turbine blades". Review of Progress in Quantitative Nondestructive Evaluation, Vol 27a and 27b, 2008. 975: p. 520-527.

73. B. Kang and P. Cawley, "Low power PZT exciter for thermosonics". Review of Progress in Quantitative Nondestructive Evaluation, Vols 26A and 26B, 2007. 894: p. 484-491.

74. M. Morbidini and P. Cawley, "The detectability of cracks using sonic IR". Journal of Applied Physics, 2009. 105(9).

75. M. Morbidini and P. Cawley, "A calibration procedure for sonic infrared nondestructive evaluation". Journal of Applied Physics, 2009. 106(2): p. 023504.

76. B. Weekes, P. Cawley, and D. Almond. "The effects of crack opening and coatings on the detection capability of thermosonics ". 2011. Review of Progress in Quantitatibe Nondestructive Evaluation.

77. T.J. Barden, D.P. Almond, S.G. Pickering, M. Morbidini, and P. Cawley, "Detection of impact damage in CFRP composites by thermosonics". Nondestructive Testing and Evaluation, 2007. 22: p. 71-82.

78. U. Polimeno and D.P. Almond. "A Compact Thermosonic Inspection System for the Inspection of Composites". in ICCM-17 - 17th International Conference on Composite Materials. 2009. Vancover: International Committee on Composite Materials.

79. T.J. Barden, D.P. Almond, M. Morbidini, and P. Cawley, "Advances in thermosonics for detecting impact damage in CFRP composites". Insight, 2006. 48(2): p. 90-93.

80. C. Homma, M. Rothenfusser, J. Baumann, and R. Shannon, "Study of the heat generation mechanism in acoustic thermography". Review of Progress in Quantitative Nondestructive Evaluation, Vols 25A and 25B, 2006. 820: p. 566-573.

81. X. Han, "Acoustic chaos for enhanced detectability of cracks by sonic infrared imaging". Journal of Applied Physics, 2004. 95(7): p. 3792.

82. M. Rothenfusser and C. Homma, "Acoustic thermography: Vibrational modes of cracks and the mechanism of heat generation". Review of Progress in Quantitative Nondestructive Evaluation, Vols 24A and 24B, 2005. 760: p. 624-631.

83. A.T. Kelly and N. Rajic. "Interference Fit Fastener Inspection using Sonic Thermography". in 5th Australasian Congress on Applied Mechanics, ACAM 2007. 2007. Brisbane, Australia.

84. D.P. Almond, T. Li, D.A.S. Rees, B. Weekes, J. Wilson, and G.Y. Tian. "Recent Developments in Thermographic NDE in the UK". in Proceedings of the National Seminar & Exhibition on Non-Destructive Evaluation. 2009.

85. B.Y. Kang, "Excitation Method for Thermosonic Non-Destructive Testing", Ph.D. 2008, PhD, Imperial College London.

86. M. Rothenfusser, C. Homma, P.J. Zombo, P.D. Vona, and R.E. SHAnnon, "Method for calibrating and enhancing flaw detection of an acoustic thermography system", 2006, Siemens Power Generation, Inc.: United States.

87. F.R. Ruhge, "Focused Investigation for the Application of Sonic IR NDE Methods for the Detection of Service Induced Defects on Critical Rotating Components", March 2010, Federal Aviation Administration, Rolls-Royce, Siemens, Sandia National Laboratories Wayne State University etc.

88. J.C. Chen, J. Kephart, K. Lick, and W.T. Riddell, "Crack growth induced by sonic IR inspection". Nondestructive Testing and Evaluation, 2007. 22(2): p. 83-92.

89. W. Hassan, C. Homma, Z. Wen, F. Vensel, and B. Hogan, "Detection of tight fatigue cracks at the root of dampers in fan blades using sonic IR inspection: A feasibility demonstration". Review of Progress in Quantitative Nondestructive Evaluation, Vols 26A and 26B, 2007. 894: p. 455-462.

90. W.O. Miller. "An evaluation of Sonic IR for NDE at Lawrence Livermore National Laboratory". in Thermosense Xxiii. 2001.

91. D. Mayton, F. Spencer, and C. Alvarez. "Characterizing the effects of sonic IR variables on turbine disk inspection using a design of experiments approach". in Review of Progress in Quantitative Nondestructive Evaluation. 2005.

92. Y. Guo and F.R. Ruhge. "Comparison of detection capability for acoustic thermography, visual inspection and fluorescent penetrant inspection on gas turbine components". in Review of Quantitative Nondestructive Evaluation 2009. American Institute of Physics.

93. G. Bolu, A. Gachagan, G. Pierce, and G. Harvey, "Reliable thermosonic inspection of aero engine turbine blades". Insight, 2010. 52(9): p. 488-493.

94. I. Perez and W.R. Davis. "Optimizing the thermosonics signal". in Review of Progress in Quantitative Nondestructive Evaluation, Vols 22a and 22b. 2003.

95. J. DiMambro, D. Ashbaugh, D. Nelson, and F. Spencer. "Sonic Infrared imaging and flourescent penetrant inspection probability of detction comparison". in Review of Progress in Quantitative Nondestructive Evaluation. 2007.

96. Mian and A., "Fatigue damage detection in graphite/epoxy composites using sonic infrared imaging technique". Composites Science and Technology, 2004. 64(5): p. 657-666.

97. M. Morbidini, "A comparison of the vibro-modulation and thermosonic NDT techniques", Ph.D. 2007, PhD, Imperial College London.

98. D. Mayton and E. Lindgren, "Nondestructive Evaluation Technology Initiatives I: Advanced Thermosonic Methods (Sonic-IR)", 2003, Science Applications International Corporation.

99. K. Lick, C.H. Wong, and J.C. Chen. "Determination of the minimum energy required for sonic-ir detection". 2007. Review of Progress in Quantitative Nondestructive Evaluation.

100. D. Mayton, "Nondestructive Evaluation Technology Initiatives II: Whole Field Turbine Disk Inspection", 2007, Science Applications International Corporation.

101. J. DiMambro, D. Ashbaugh, X. Han, L.D. Favro, J.P. Lu, Z. Zeng, W. Li, G. Newaz, and R.L. Thomas. "The Potential of Sonic IR to Inspect Aircraft Components Traditionally Inspected with Fluorescent Penetrant and or Magnetic Particle Inspection". in Quantitative Nondestructive Evaluation. 2006.

102. F. Mabrouki, M. Thomas, M. Genest, and A. Fahr, "Frictional heating model for efficient use of vibrothermography". NDT & E International, 2009. 42(5): p. 345-352.

103. P.J. Zombo and R. Shannon, "Advanced NDE systems for Flexible Operation and Maintenance of Gas Turbine Components", 2006, Siemens Energy.

104. G. Georgiou, "Probability of detection (PoD) curves: Derivation, applications and limitations", 2006.

105. S.M. Shepard, T. Ahmed, and J.R. Lhota, "Experimental considerations in vibrothermography". Thermosense Xxvi, 2004. 5405: p. 332-335.

106. " Sonotronic Ultrasonic Technology UK, Sonotronic USG400-40 welding system.".

107. S.G. Pickering and D.P. Almond, "An evaluation of the performance of an uncooled microbolometer array infrared camera for transient thermography NDE". Nondestructive Testing and Evaluation, 2007. 22(2): p. 63-70.

108. J. Zalameda and W. Winfreee, "Investigation of Uncooled Microbolometer Focal Plane Array Infrared Camera for Quantitative Thermography". Journal of Nondestructive Evaluation, 2005. 24(1).

109. A.L. Bovik, *Handbook of Image and Video Processing*2000: Academic Press.

110. G. De Angelis, M. Meo, D.P. ALmond, S.G. Pickering, and U. Polimeno, "Impact Damage Detection in a Stiffened Composite Wing Panel Using Digital

Shearography and Thermosonics". Key Engineering Materials, 2011. 471 - 472: p. 904 - 909.

111. E. Grimberg, "Radiometry Using An Uncooled Microbolometer Detector", 2008, Opgal Ltd: United States.

112. X. Han, W. Li, Z. Zeng, L.D. Favro, and R.L. Thomas, "Acoustic chaos and sonic infrared imaging". Applied Physics Letters, 2002. 81(17): p. 3188.

113. K.A. Tsoi, K. Yousif, N. Rajic, and I. Powlesland. "Optimisation of sonic thermographic inspection". in Nondestructive Characterization for Composite Materials, Aerospace Engineering, Civil Infrastructure and Homeland Security. 2009.

114. C.J. Uhl, "Relating crack heating to vibration for vibrothermography", Ph.D. 2008, Iowa State University.

115. P. Cawley, N. Sarsentis, and C. Homma, "A quick method for the measurement of structural damping". Mechanical Systems and Signal Processing, 1988. 2: p. 39 - 47.

116. D.J. Ewins, *Modal Testing: theory, practice and application*. 2nd ed2000: Research Studies Press Ltd.

117. S.D. Panteliou and A.D. Dimarogonas, "Damping associated with porosity and crack in solids". Theoretical and Applied Fracture Mechanics, 2000. 34(3): p. 217-223.

118. G.R.A.S.S.a. Vibration, " Data Sheet: Type 40DP pressure microphone".

119. J. Eargle, *The Microphone Book: From mono to stereo to surround - a guide to microphone design and application*. 2nd ed2004: Focal Press.

120. L.E. Drain, *The Laser Doppler Technique*1980: New York: John Wiley & Sons.

121. M.R. Spiegel, J.J. Schiller, and R.A. Srinivasan, *Probability and Statistics*. 3rd ed2009: McGraw-Hill.

122. T. Urdan, *Statistics in Plain English*. 2nd ed2005: Lawerence Erlbaum Associates.

123. H.D. Young, *Statistical Treatment of Experimental Data*1962: McGraw-Hill.

124. S.L. Jackson, *Research Methods and Statistics: A Critical Thinking Approach*. 4th ed2011: CENGAGE Learning Custom Publishing.

125. X.Y. Han, "Frequency dependence of the thermosonic effect". Review of Scientific Instruments, 2003. 74(1): p. 414-416.

126. C.J. Uhl, Holland, S. D., Renshaw, J. . "Vibrothermographic crack heating: a function of vibration and crack size". in Review of Progress in Quantitative Nondestructive Evaluation. 2009.

127. A.P. Bovsunovsky, "The mechanisms of energy dissipation in the non-propagating fatigue cracks in metallic materials". Engineering Fracture Mechanics, 2004. 71(16-17): p. 2271-2281.

128. R.D. Adams and A.L. Percival, "Measurement of the strain-dependent damping of metals in axial vibration". Journal of Physics D-Applied Physics, 1969. 2(2): p. 1693 -1704.

129. C.W. de Silva, *Vibration: Fundamentals and Practice*1999: CRC Publisher.

130. J.O. Rawlings, S.G. Pantula, and D.A. Dickey, *Applied Regression Analysis: A Research Tool*1998: Springer-Verlag New York.

131. R.D. Adams, P. Cawley, C.J. Pye, and B.J. Stone, "A Vibration Technique for Non-destructively Assessing Integrity of Structures". Journal of Mechanical Engineering Science, 1978. 20(2): p. 93-100.

132. COMSOL, *Comsol Multiphysics, Structural Mechanics Module*. Version 4.2a ed2011.

133. O.C. Zienkiewicz and R.L. Taylor, *The Finite Element method*. Vol. 1 2000: Butterworth-Heinemann.

134. C.J.L. Lane, A.K. Dunhill, B.W. Drinkwater, and P.D. Wilcox, "The inspection of anisotropic single-crystal components using a 2-D ultrasonic array". IEEE Transactions on Ultrasonics, Ferroelectrics, and Frequency Control, 2010. 57(12): p. 2742 - 2752

135. M.A. Hopcroft, W.D. Nix, and T.W. Kenny, "What is the Young's Modulus of Silicon?". Journal of Microelectromechanical Systems, 2010. 19(2): p. 229 - 238

136. C.J.L. Lane, "The Development of a 2D Ultrasonic Array Inspection for Single Crystal Turbine Blades ", Ph.D. Thesis, Department of Mechanical Engineering, 2011, University of Bristol.

137. G. Harvey, "An investigation into the simulation and measurement of high intensity ultrasonic systems", Ph.D. Thesis, Centre for Ultrasonic Engineering, 2008, University of Strathclyde.